A METHOD FOR WAVEFORM INVERSION OF BODY-WAVE SEISMOGRAMS

Thesis by

George Robert Mellman

In Partial Fulfillment of the Requirements

for the Degree of

Doctor of Philosophy

California Institute of Technology

Pasadena, California

1979

(Submitted October 13, 1978)

ACKNOWLEDGMENTS

I have a confession to make. I am a compulsive acknowledgment reader. Many are the times I've picked up a thesis in which I've had absolutely no interest just to read the acknowledgments. And you, gentle reader, did you just sort of stop at this page on your way through the thesis? Or is this page really your only interest? ("I just want to see what that turkey said about me.")

In either case, I would like to take this opportunity to thank those of you who, through long hours of discussion, helped make this work possible. My thanks also to those of you whose patience and encouragement have finally led to its completion. And, finally, my deepest thanks to those of you who have helped make life as a graduate student a bit more bearable.

This work was supported, in part, by National Science Foundation Grant EAR76-06619, by the Advanced Research Projects Agency of the Department of Defense under Contract F44620-72-C-0078, and by the Office of Naval Research under Contract NR083-399.

ABSTRACT

An iterative inversion method has been developed for the determination of velocity-depth structure and the estimation of seismic source parameters using the waveforms of far-field body-wave seismograms. The inversion is accomplished by minimizing an error function that expresses the difference between data and synthetic seismogram. This error function is constructed to be insensitive to absolute amplitudes and travel-times, and is thus a measure of waveform errors only.

In the case where the source is known and the velocity-depth function is to be determined, the Modified First Motion method is used to express changes in the error function in terms of changes in the model parameters relative to some starting model. An approximate inverse is derived for this expression, which determines the model perturbation that minimizes the error function. Stability is provided through the inclusion of specific non-linear terms in the inverse. As an example of the application of the inversion technique, the fine structure of the crust-mantle transition is examined, using data from a Bering Sea refraction profile.

In the case where earth structure is assumed known and the source parameters are to be determined, the source is represented as a small number of point shear dislocations. Using an inversion method quite similar to the one used for the earth structure problem, estimates are obtained of relative seismic moment, depth, fault orientation, source time function, and relative location for each point dislocation. The inversion method developed is applied to the study of the Borrego Mountain earthquake.

TABLE OF CONTENTS

Chapter 1

INTRODUCTION

Body-wave seismograms have proved quite useful throughout the history of seismology in the study of both earth structure and earthquake sources. The approach most often adopted in such studies has been to extract a small number of parameters from each seismogram and to then use these parameters, gathered from a large number of seismograms, to estimate earth structure or source parameters. Examples of this approach include travel time and $\frac{dT}{d\Delta}$ inversions and absolute amplitude studies applied to the case of earth structure problems, and first motion fault plane determinations, magnitude determinations and corner frequency-moment estimates applied to source problems.

Reducing a body-wave seismogram to a small number of parameters certainly makes the data easier to deal with. Unfortunately, much of the information content of the seismic waveform is lost in this manner. One method of retaining much of the information contained in the seismograms is to find models which give rise to synthetic seismograms that match the observed data waveforms. While some notable successes have been achieved through such studies, the trial and error modeling procedure used generally proves to be both time consuming and expensive. Due largely to the complexity and non-linearity of the forward problems, the inversion methods that have been so successful in other areas of geophysics have not to date been applied to the problems of matching waveforms for body-wave seismograms. In this thesis, we present an iterative method of inverting far-field body-waveform data to obtain model parameters. The method is applicable

to both the estimation of velocity-depth structure and to the estimation of source parameters.

In order for an iterative inversion method to be of practical value, it is usually necessary to have a fast and accurate method for the solution of the forward problem. For the problem of estimating velocity-depth structure, this means that an efficient means of solving the wave propagation problem in vertically inhomogeneous media is needed. One such method, the Modified First Motion approximation (MFM) is presented in Chapter 2. The MFM method is a series of approximations to the Cagniard-de Hoop method (de Hoop, 1960). As such, it is a generalized ray method which requires a plane layered velocity-depth model. Several comparisons between MFM and the full Cagniard-de Hoop method are presented which demonstrate the accuracy and speed of MFM.

In Chapter 3 we develop an iterative method of estimating velocity-depth structure using waveform data. The first step in this process is to determine an error function that is sensitive only to errors in waveform. Using the methods developed in Chapter 2, changes in this error function are related to changes in a starting velocity-depth function. An approximate expression is then derived which determines the model changes that minimize the error function. This expression makes explicit use of non-linear terms in the forward relationship between error function perturbations and model perturbations in order to stabilize the inversion procedure.

Applications of this inversion method to both synthetic and real data are presented in Chapter 4. In the synthetic case, it is

shown that for a starting model that produces seismograms that are markedly different from the "data" seismograms, the inversion procedure is capable of returning to the "data" model. The inversion method is then applied to real data taken from a refraction profile conducted in the Bering Sea. Using several different starting models, the fine structure of the crust-mantle transition in this region is investigated.

In Chapter 5, we modify the inversion method of Chapter 3 to solve the problem of estimating source parameters using teleseismic body-waves. This method, together with auxillary data, is then used in Chapter 6 to study the Borrego Mountain earthquake.

It should be noted that several chapters of this thesis have been previously published. Chapter 2 was published as Mellman and Helmberger (1978). Chapter 6 was published as Burdick and Mellman (1976).

Chapter 2

A MODIFIED FIRST MOTION APPROXIMATION FOR THE SYNTHESIS OF BODY-WAVE SEISMOGRAMS

INTRODUCTION

Body wave synthetic seismograms have been extensively used in recent years to study a wide variety of earthquake source and earth structure problems. Two methods have primarily been used for the calculation of synthetic seismograms, the reflectivity method of Fuchs and Muller (Fuchs and Muller, 1971) and the Cagniard-de Hoop method (de Hoop, 1960). The principal drawback of both of these methods is that they require relatively long, expensive computer programs. Recently Wiggins (1976) and Chapman (1976) have independently developed a first motion method which greatly reduces the computer time needed for the generation of synthetic seismograms, but appears to be somewhat restrictive in application to geophysical problems.

First motion approximations have been known in geophysics for a number of years (Gilbert and Knopoff, 1961). While they provide a great deal of insight, they have until recently proved to be of little use in the calculation of synthetic seismograms. This paper presents a modification of the standard Cagniard-De Hoop first motion approximation that allows for rapid calculation of synthetic seismograms for a wide variety of problems. This Modified First Motion method (MFM) retains the advantages of physical insight provided by the Cagniard-de Hoop method, while requiring significantly less computation and hence computer time. In addition, the method

is compatible with the standard Cagniard-de Hoop method, so that significant savings may be realized even in cases where MFM is not entirely applicable.

CLASSICAL FIRST MOTION APPROXIMATION

We take as our starting point the Cagniard-de Hoop high frequency approximation for displacement potential of a generalized ray reflected from the n^{th} interface in a layered elastic stack (Helmberger, 1968).

$$\phi(t) = \psi(t) * 1/\sqrt{t} * S'(t)$$
$$\psi(t) = \mathrm{Im}\left[\sqrt{2p/r}\ \ 1/\pi\eta_1\ R_n(p)\ T(p)\ dp/dt\right] \tag{2.1}$$

where $R_n(p)$ is the complex generalized plane wave reflection coefficient for the n-1, n layer interface; $T(p) \equiv \Pi_i\ T_i(p)$ is the product of plane wave transmission coefficients, $S'(t)$ is the derivative of the source time function, r is the range, and p is the ray parameter. The relationship between p and t for a given generalized ray is:

$$t = pr + \sum_{i=1}^{n-1} 2h_i\ \eta_i,\ \mathrm{Im}\left(t(p)\right) = 0 \tag{2.2}$$

where h_i is the thickness of the i^{th} layer, c_i is the elastic velocity in the i^{th} layer and $\eta_i = (1/c_i^2 - p^2)^{1/2}$.

The contour defined by equation (2.2) leaves the real p axis at p_0 such that $\frac{dt}{dp}(p_0) = 0$, corresponding to the ray parameter and arrival time t_o of the geometric ray. If $p_0 > 1/c_n \equiv p_c$, then the

reflection coefficient $R_n(p)$ becomes complex for $p > p_c$ and a head wave is present. In this case the head wave is the first arrival, at a time $t_c < t_0$.

It is convenient, at this point, to restrict our discussion to fluid models, since the expression for $R_n(p)$ is simple in this case. It should be noted, however, that the approximations that are developed may be readily applied to solid elastic models as well.

In the classical first motion approximation, we attempt to approximate ψ by approximating the most rapidly varying quantities in ψ near $p = p_c$ and p_0, while considering all other quantities to be constant. In the neighborhood of p_c, the most rapidly varying quantity is η_n. Since, by definition $\eta_n = (p + 1/c_n)^{1/2} (1/c_n - p)^{1/2}$, and in the neighborhood of p_c, $p - p_c \approx (t - t_c) \frac{dp}{dt} (p_c)$ we have

$$\eta_n \approx -i \sqrt{2/c_n} (t - t_c)^{1/2} (dp/dt (p_c))^{1/2} \tag{2.3}$$

For a fluid, we have

$$R_n (p) = \frac{\eta_{n-1} - \delta\eta_n}{\eta_{n-1} + \delta\eta_n} \tag{2.4}$$

and

$$\text{Im } (R_n) = \frac{-2\delta \text{ Im } \eta_n \eta_{n-1}}{|\delta\eta_n|^2 + |\eta_{n-1}|^2} \tag{2.5}$$

where

$$\delta = \frac{\rho_{n-1}}{\rho_n}$$

Since $|\eta_n| << |\eta_{n-1}|$ in the neighborhood of t_c we have

$$\text{Im } R_n(t) \approx 2i\delta \frac{\eta_n}{\eta_{n-1}} \quad \text{and} \tag{2.6}$$

$$\psi(t) \approx \frac{2}{\pi\eta_1} \delta\sqrt{2/c_n} \left(dp/dt\ (p_c)\right)^{3/2} \sqrt{2p_c/r}\ (t - t_c)^{1/2} \tag{2.7}$$

If we now assume a step function source, and, recognizing that $\left(\frac{dt}{dp}(p_c)\right) \equiv L$ is the distance traveled in the refractor, we find

$$\phi(t) = \frac{4\delta}{\eta_1(p_c)} \frac{1}{c_n\sqrt{rL^3}} (t-t_c) \qquad t_c < t \tag{2.8}$$

Thus, the time dependence of the headwave is the integral of the source time function.

In the neighborhood of t_o, the most rapidly varying quantity is dp/dt. Using a Taylor series for t and keeping only the first nonzero term, we have

$$t - t_0 \approx 1/2(p - p_0)^2 \frac{d^2t}{dp^2}(p_0) \tag{2.9}$$

and solving for $p - p_0$ and differentiating

$$\frac{dp}{dt} \approx \frac{1}{(t - t_0)^{1/2} (2\, d^2t/dp^2)^{1/2}} = \frac{1}{(t_0 - t)^{1/2} (2|d^2t/dp^2|)^{1/2}} \tag{2.10}$$

since $d^2t/dp^2\ (p_0) < 0$.

This gives us

$$\psi(t) \approx \sqrt{p_0/r} \frac{1}{\pi\eta_1} \text{Im}\left(R(p_0)\right) T(p_0) \left|\frac{d^2t}{dp^2}\right|^{-1/2} (t_0 - t)^{-1/2},\ t < t_0 \tag{2.11a}$$

$$\psi(t) \approx \sqrt{p_0/r} \frac{1}{\pi\eta_1} \text{Re}\left(R(p_0)\right) T(p_0) \left|\frac{d^2t}{dp^2}\right|^{-1/2} (t - t_0)^{-1/2},\ t > t_0 \tag{2.11b}$$

Convolution with $1/\sqrt{t}$ assuming a step function source, gives, for (11a)

$$\psi(t) = -\sqrt{p_0/r}\,\frac{1}{\pi\eta_1(p_0)}\,\mathrm{Im}(R_n(p_0))\;T(P_0)\left|\frac{d^2t}{dp^2}\right|^{-1/2}\ell n\,\frac{|t_0 - t|}{2t_0} \quad (2.12a)$$

and for (11b)

$$\psi(t) = \sqrt{p_0/r}\,\frac{1}{\eta_1(p_0)}\,\mathrm{Re}(R_n(p_0))\;T(p_0)\;\left|\frac{d^2t}{dp^2}\right|^{-1/2} H(t - t_0), \quad (2.12b)$$

where H(t) is the Heaviside function.

The expression (2.12a) contains the log singularity that characterizes a critical reflection and (2.12b) is the step response obtained from geometric optics. For $p_0 > 1/c_n$, the total response is given by 2.12b. Thus, the first motion approximation always gives the source time function for pre-critical reflections. Rather abruptly, at ranges where $p_0 < 1/c_n$, there develops an additional critical reflection term, given by (2.12a), which, due to the singularity at t_0, dominates the response. For ranges where $p_0 >> 1/c_n$, the integral of the time function given by (2.8) becomes the dominant feature.

Some of the problems associated with the standard first motion approximations may be seen from the profile of generalized rays in figure 2.1. As may be seen from 2.1a, even precritical generalized rays exhibit appreciable differences in shape from the step function predicted by the first motion approximations. Further problems are present for critical reflections where p_0 is near p_c, since there is no mechanism in the first motion approximations for joining the two approximations used for $t < t_0$. To do this, we must modify the approximations used to obtain a single expression that agrees with

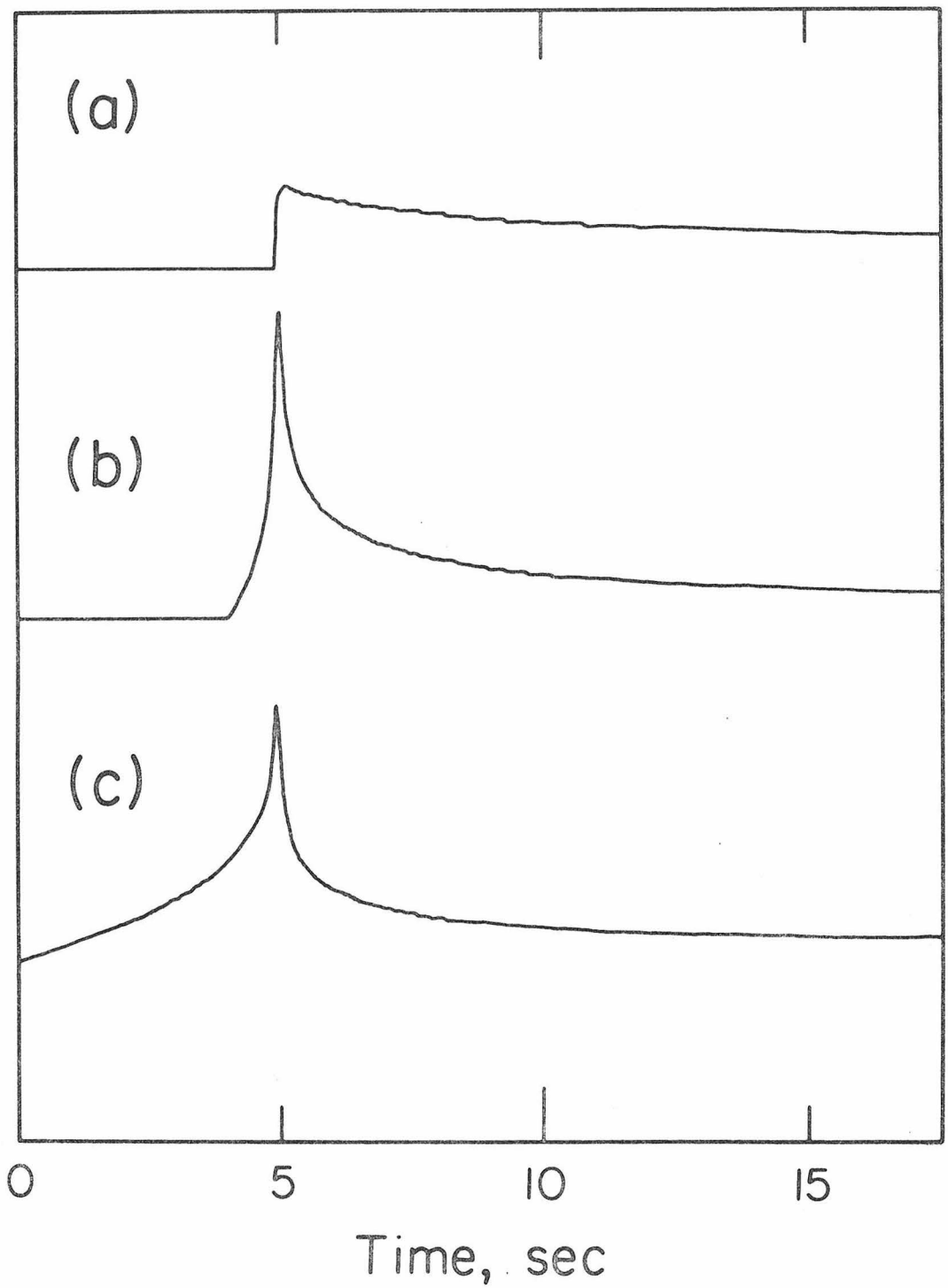

Figure 2.1. Profile of step function responses for a fluid interface illustrating typical waveforms for (a) near vertical reflection, (b) near critical reflection, (c) well developed refraction.

the standard expressions for ψ near t_0 and t_c, but is valid for all $t_c < t < t_0$.

THE MODIFIED FIRST MOTION APPROXIMATIONS

We wish to find an approximation which will preserve first motion behavior of ψ in the neighborhood of t_0 and t_c and vary continuously in between. In addition, we wish to do this in such a way that little or no information other than that used for the standard first motion approximation is needed.

It will again be convenient to consider the head wave and reflected wave portions of ψ separately. For the head wave portion, where $t < t_0$, we will modify the standard first motion approximations for η_n and dp/dt by the addition of higher order terms that leave the standard approximations unchanged in the neighborhood of the original expansion point, but also give the correct values of $\eta_n(t_0)$ and dp/dt (t_c). In addition, it will be necessary to develop approximate expressions for η_{n-1} and T(p). All other quantities will be considered to be constant.

We start with the approximate expression for dp/dt given by (2.10)

$$dp/dt \approx \left(2\left|\frac{d^2t}{dp^2}\right|\right)^{-1/2} (t_0 - t)^{-1/2}. \tag{2.10}$$

We note that addition of terms of the form $a_\alpha(t_0 - t)^m$ where $m \geq 0$ have no effect on the behavior of dp/dt in the neighborhood of t_0. Thus, we may generate the desired approximation by addition of such terms to (2.10) and appropriate choice of constants. The simplest such approximation is

$$dp/dt = \left(2\left|\frac{d^2t}{dp^2}(p_0)\right|\right)^{-1/2}\left[(t_0 - t)^{-1/2} + a_\alpha\right]$$
$$a_\alpha = \frac{dp}{dt}(p_c)\left(2\left|\frac{d^2t}{dp^2}(p_0)\right|\right)^{1/2} - (t_0 - t_c)^{-1/2} \tag{2.13}$$

which also preserves the monotone increasing behavior of dp/dt.

Similarly, we may modify equation (2.3),

$$\eta_n \approx -i\left(2/c_n\ dp/dt(p_c)\right)^{1/2}(t - t_c)^{1/2} \tag{2.3}$$

by the addition of terms of the form $a_n (t - t_c)^m$, $m \geq 1$, without changing the behavior of η_n in the neighborhood of p_c. Thus we have

$$\eta_n \approx -i\left(2/c_n\ dp/dt(p_c)\right)^{1/2}(t - t_c)^{1/2}\left[1 + (t - t_c)a_n\right] \tag{2.14}$$
$$a_n = \left[|\eta_n(p_0)|\left(2/c_n\ dp/dt(p_c)\right)^{-1/2}(t_0 - t_c)^{-1/2} - 1\right]/(t_0 - t_c)$$

which preserves the behavior of $\eta_n(p_c)$, as well as the value of $\eta_n(p_0)$.

In order to accurately approximate Im (R_n) over the entire range $t_c < t < t_0$, it is necessary to have an approximation for η_{n-1}, as well as η_n. One method of obtaining such an approximation is to integrate the approximation for dp/dt given in (2.13) to obtain an explicit expression for p in terms of t. We may then substitute this expression into the expression for η_{n-1} to obtain an explicit expression for η_{n-1} in terms of t. As this expression is somewhat cumbersome, however, we use a further approximation of this expression, namely

$$\eta_{n-1} \approx a_p(t_p - t)^{1/2} \tag{2.15}$$

where a_p and t_p are chosen such that the values of $\eta_{n-1}(t_c)$ and $\eta_{n-1}(t_0)$ are preserved.

For $t_c < t < t_0$ we have from (2.1) and (2.5)

$$\psi = \frac{1}{\pi\eta_1}\sqrt{p/r}\;\; T(p)\,\frac{-2\delta \mathrm{Im}(\eta_{n-1}\,\eta_n)}{|\eta_{n-1}|^2+\delta^2|\eta_n|^2}\,dp/dt. \tag{2.16}$$

Replacing dp/dt, η_n and η_{n-1} with their approximate time domain expressions and replacing all other terms by their values at p_0, we obtain an explicit time domain expression for ψ.

If $p_0 \approx 1/c_{n-1}$, then the assumption that T(p) is constant is violated. In this case, using $T(p_0)$ gives much too small a value for the head wave. Instead, we used a value of p where Im $(R_n(p))$ has a maximum, since this is the region from which the greatest contribution to the head wave will arise. Thus we evaluate T(p) at $p = \min\left(p_0, \sqrt{(1/c^2_{n-1} + \delta^2/c^2_n)/(1+\delta^2)}\right)$ and then make the assumption that T(p) is constant.

If $(t_0 - t_c)$ is not large compared to the time point spacing, then the expressions that we have developed will fail to give a good approximation of Ψ. In this case, the area under ψ, rather than the actual shape of ψ, is important. We may thus determine $\int_{t_c}^{t_0}\psi dt$, and replace ψ with a convenient functional form having the appropriate area. For simplicity a triangle may be used, starting at t_c and having its maximum at t_0. To determine the area, we note that

$$I \equiv \int_{t_c}^{t_0}\psi dt = \int_{t_c}^{t_0}\frac{1}{\pi\eta_1}\sqrt{2p/r}\;\; T(p)\,\frac{2\delta\eta_{n-1}|\mathrm{Im}\;\eta_n|}{|\eta_{n-1}|^2+\delta^2|\eta_n|^2}\,dp/dt\;dt$$

$$= \int_{p_c}^{p_0}\frac{1}{\pi\eta_I}\sqrt{2p/r}\;T(p)\,\frac{2\delta\eta_{n-1}|\mathrm{Im}\;\eta_n|}{|\eta_{n-1}|^2+|\delta\eta_n|^2}\,dp$$

Making the approximation that $\eta_i \approx \sqrt{2/c_i}\ (1/c_i - p)^{1/2}$, we have

$$I \approx \frac{4\delta}{\pi\eta_1(p_0)} \sqrt{2p_0/r}\ T(p_0) \frac{1}{\sqrt{c_n c_{n-1}}} \int_{p_c}^{p_0} (p - 1/c_n)^{1/2}\ (1/c_{n-1} - p)^{1/2}\ dp$$

$$= \frac{4\delta}{\pi\eta_1(p_0)} \sqrt{2p_0/r}\ T(p_0) \frac{1}{\sqrt{c_n c_{n-1}}} \left[1/4(2p_0 - 1/c_{n-1} - p_c)\ \sqrt{(1/c_1 - p_0)(p_0 - p_c)}\right.$$

$$\left. + \pi/16(1/c_{n-1} - p_c)^2 - 1/8(1/c_{n-1} - p_c)^2\ \sin^{-1}\left(\frac{(1/c_{n-1} + p_c - 2p_0)}{1/c_{n-1} - p_c}\right)\right] \qquad (2.17)$$

For $t > t_0$, we retain the first motion approximation (2.10) for dp/dt. We do not, however, maintain the assumption that R_n is constant. Instead, we use the approximate contour, given by

$$t - t_0 \approx 1/2(p - p_0)^2 \frac{d^2t}{dp^2} + 1/6(p - p_0)^3 \frac{d^3t}{dp^3}\ . \qquad (2.18)$$

Using the second term on the right hand side of (2.18) as a perturbation, we obtain

$$p - p_0 \approx \frac{i\sqrt{2}\ \sqrt{t - t_0}}{\sqrt{\left|\frac{d^2t}{dp^2}\ (p_0)\right|}}\ (1 - ia_c(t - t_0)^{1/2}) \qquad (2.19)$$

$$a_c = \frac{\sqrt{2}}{6} \frac{\frac{d^3t}{dp^3}\ (p_0)}{\left(\left|\frac{d^2t}{dp^2}\ (p_0)\right|\right)^{3/2}}$$

Using this approximate contour, we may evaluate $\left(\text{Re}\ R_n(t)\right)$ for several values of t and then use interpolation to find $\left(\text{Re}\ R_n(t)\right)$ for other values of t. We then have

$$\psi \approx \sqrt{p_0/r}\ \frac{1}{\pi\eta_1(p_0)}\ \text{Re}(R_n(t))\ T(p_0) \left|\frac{d^2t}{dp^2}\ (p_0)\right|^{-1/2} (t - t_0)^{-1/2}\ t > t_0 \qquad (2.20)$$

We now have a complete time domain description of ψ, which may be convolved with $1/\sqrt{t}$ and source terms using fast Fourier transform techniques.

It should be noted that the primary limiting factor to the validity of the modified first motion approximations is the approximate contour (2.19). Where the reflected portion of the generalized ray is unimportant or if the contour has relatively little structure, the approximations will remain valid. Where the contour bends over quickly or has significant structure, as in tunneling problems, or where exact determination of the contour is important, as in the treatment of surface waves, a better approximation of the contour must be employed.

TESTS OF THE MODIFIED FIRST MOTION APPROXIMATION

It has become almost traditional (Helmberger, 1973; Chapman, 1974) to test generalized ray theory programs by attempting to compute the step function response for a homogeneous fluid whole space using an earth flattening transformation. We begin with a homogeneous fluid whole space, with wave velocity of 6 km/sec. On this space, we impose a spherical coordinate system. We choose our source and receiver to lie at a distance of 6371 km from the origin, separated by an angular distance of 70°. The sphere is divided into 25 km thick spherical layers, and the earth flattening approximation is applied, giving a layered, flat, equivalent model. This process is illustrated in Figure 2.2. The response for this model is then computed using only first order reflections.

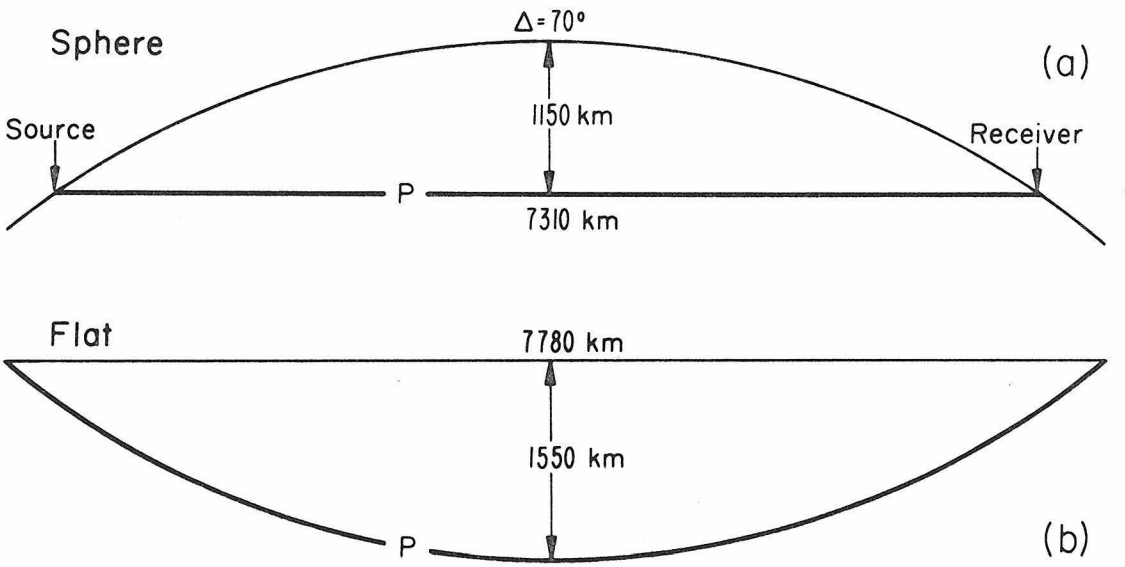

Figure 2.2. The earth flattening approximation used for the test problem of a point source in a homogeneous wholespace.

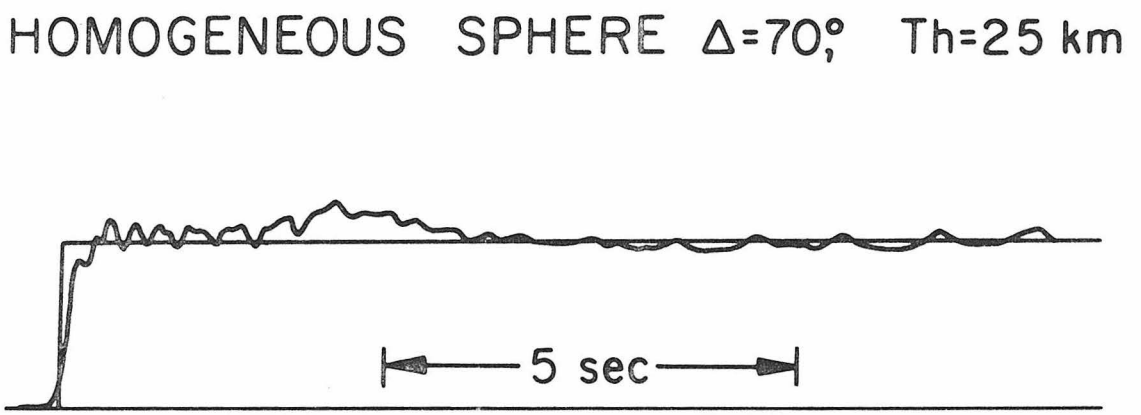

Figure 2.3. Comparison of the exact response for a point source in a homogeneous fluid and the MFM response for the equivalent earth flattened model using only first reflections.

The homogeneous wholespace problem is an extremely good test of a generalized ray method, since the final response is a rather delicate superposition of a large number of first order generalized rays. These include precritical reflections, critical reflections and postcritical refractions.

A comparison of the MFM solution and the exact solution is given in Figure 2.3. As may be seen, excellent agreement is obtained. The "graininess" of the MFM solution is an artifact of the layering approximation, not of the MFM method itself, since the similar effect occurs for the full Cagniard-de Hoop method.

It is instructive, at this point, to examine the ray response for several representative generalized rays from the wholespace problem. Figure 2.4 presents a comparison of four such rays computed using MFM with the same rays computed using the full Cagniard-de Hoop method. The ray number identifying each ray is the layer, from the top of the model, in which the reflection occurred. Ray 13 represents a well developed refraction, ray 40 represents a case where the refraction and critical reflection strongly interact, ray 52 represents a case in which $t_0 - t_c$ is comparable to the time spacing used to compute the ray, and ray 62 represents a precritical reflection. In all cases, good agreement is obtained between the two methods.

Further insight into the operation of MFM may be gained by examining in detail the approximations for η_n, η_{n-1}, and $\mathrm{Im}(R_n)$ used in computing rays 40 and 13. Comparisons of the approximate and actual values of these quantities is given in Figures 2.5 and 2.6. As may be seen, all quantities exhibit considerable structure not accounted

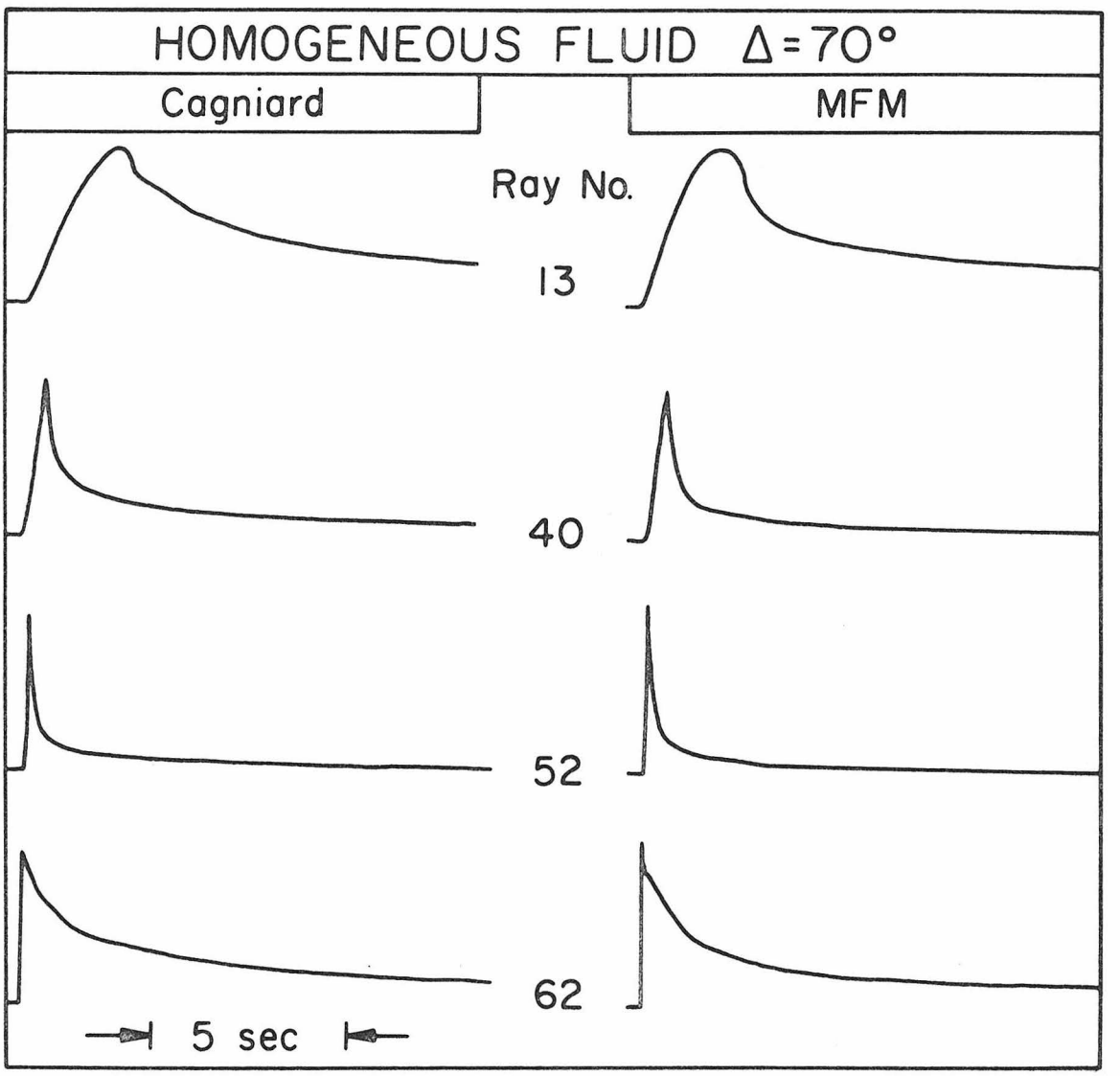

Figure 2.4. Comparison of MFM and full Cagniard for representative generalized rays from the earth flattened homogeneous fluid problem. Ray number refers to the layer from which the generalized ray was reflected. Layer thickness is 25 km before earth flattening is applied. Corresponding MFM and Cagniard rays are to same scale.

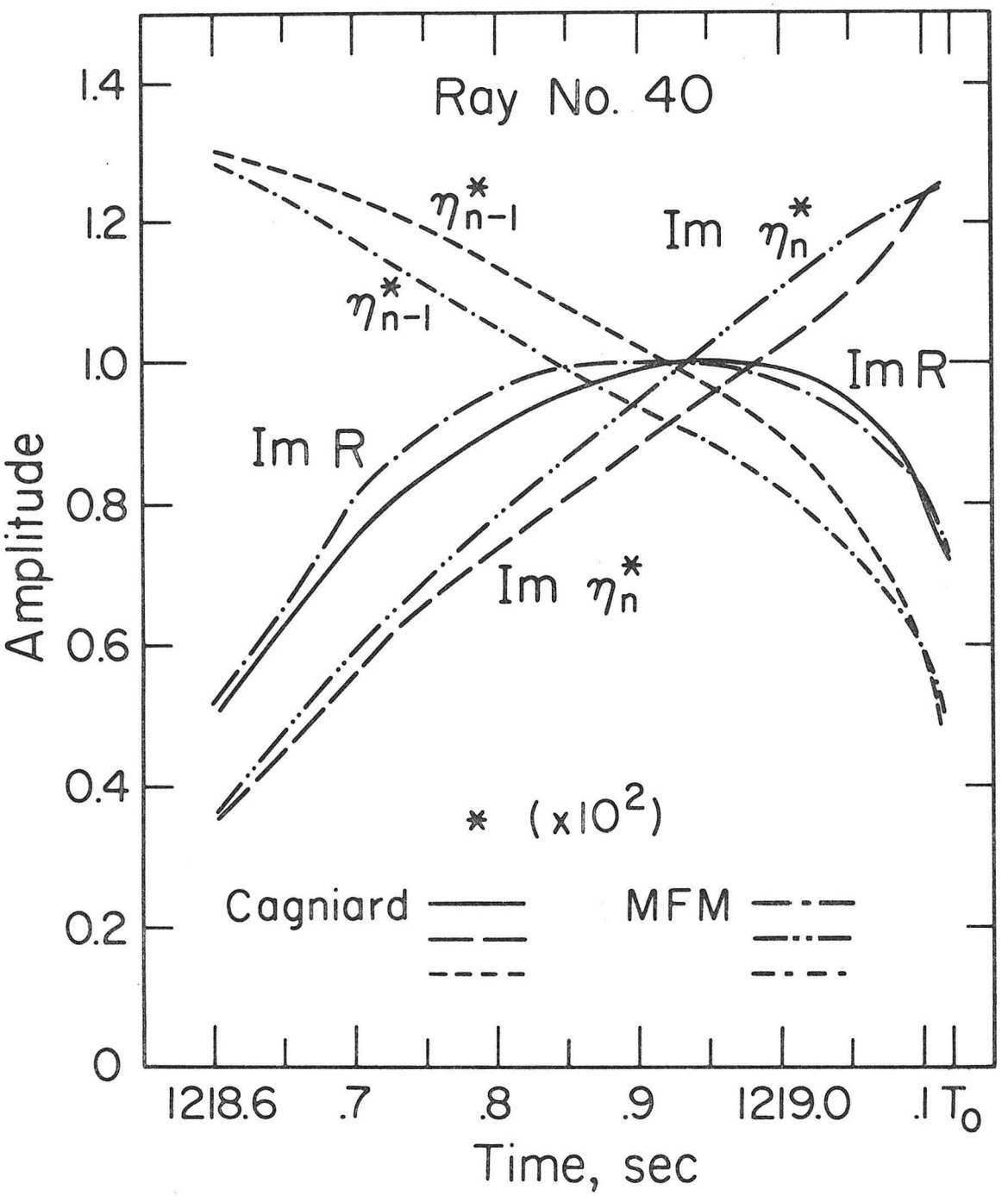

Figure 2.5. Comparison of several quantities critical to head wave portion of Ray 40 for MFM and full Cagniard.

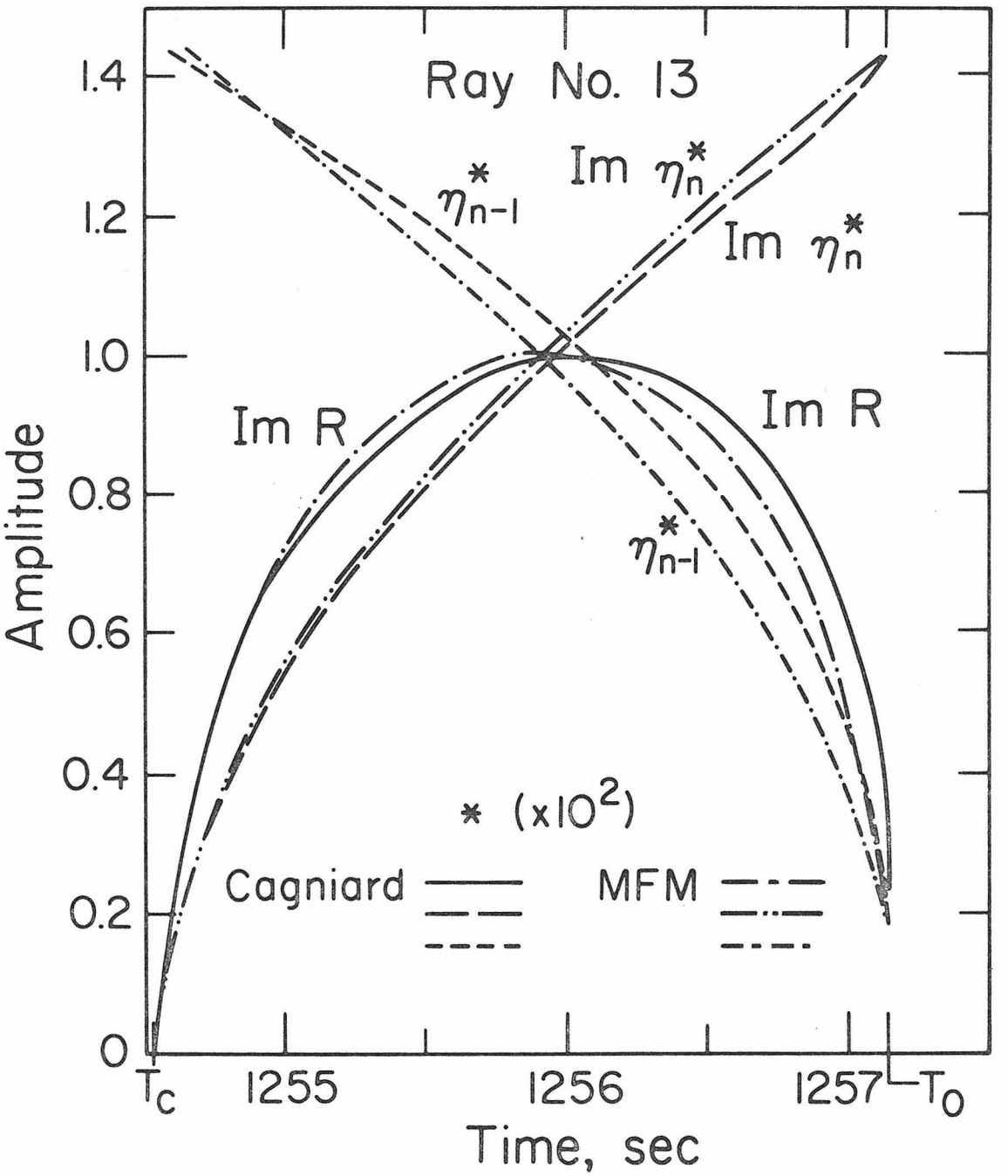

Figure 2.6. Comparison of several quantities critical to head wave portion of Ray 13 for MFM and full Cagniard.

for by standard first motion approximations. In particular, the nearly linear behavior of η_n near p_0 and the non-constant behavior of η_{n-1} are not predicted by the standard first motion approximations. However, using MFM good agreement is obtained.

Further comparisons of MFM and Cagniard-de Hoop have been made for the model shown in Figure 2.7. This model may be viewed as presenting a somewhat simplified ocean sub-bottom. The size of the density contrast was chosen so that in the long period limit the amplitude of the reflections from the velocity gradient and from the density contrast will be equal for a source to receiver distance of 3 km.

Step function responses were obtained using both Cagniard-de Hoop and MFM for a profile of 8 distances which cover the development of the triplication. Synthetic seismograms were generated by convolving step responses with a system function previously used by Helmberger (1976) in oceanic studies. This function contains instrument and filter functions, as well as the source time function. In order to study frequency dependent effects, and thus investigate the behavior of MFM over a relatively large frequency range, a number of system functions were derived from the original system function by either compression or expansion of the time axis. In this manner, system functions with peaks at 1, .5, .25 and .12 sec. periods were obtained.

Results of synthetic seismogram calculations for this model are shown in Figure 2.8. The same scale is used in the profiles generated using Cagniard and MFM. Hence, amplitudes in Figures 2.8a and 2.8b are directly comparable. Comparisons of corresponding

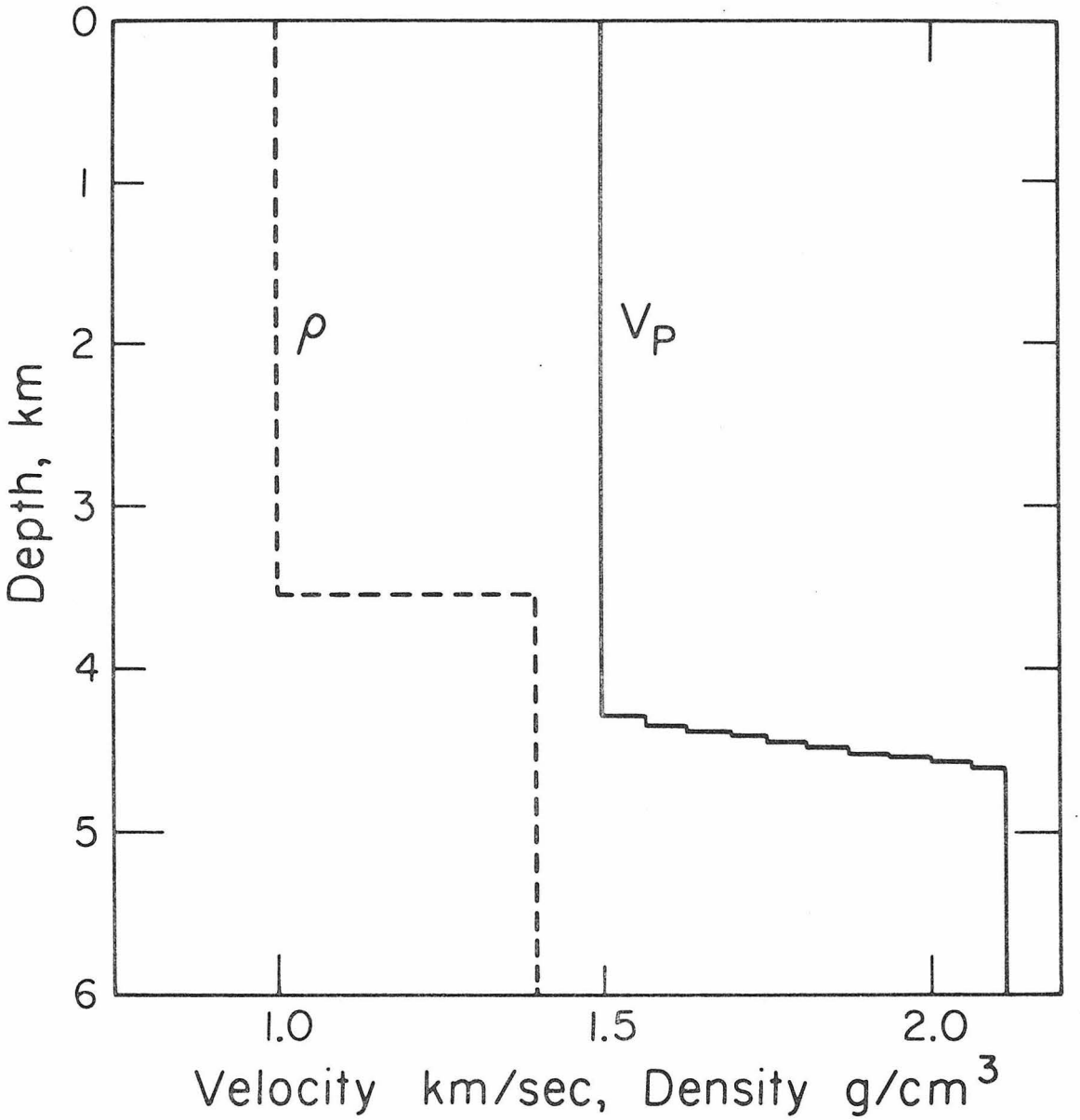

Figure 2.7. Velocity and density model for a simplified oceanic sub-bottom.

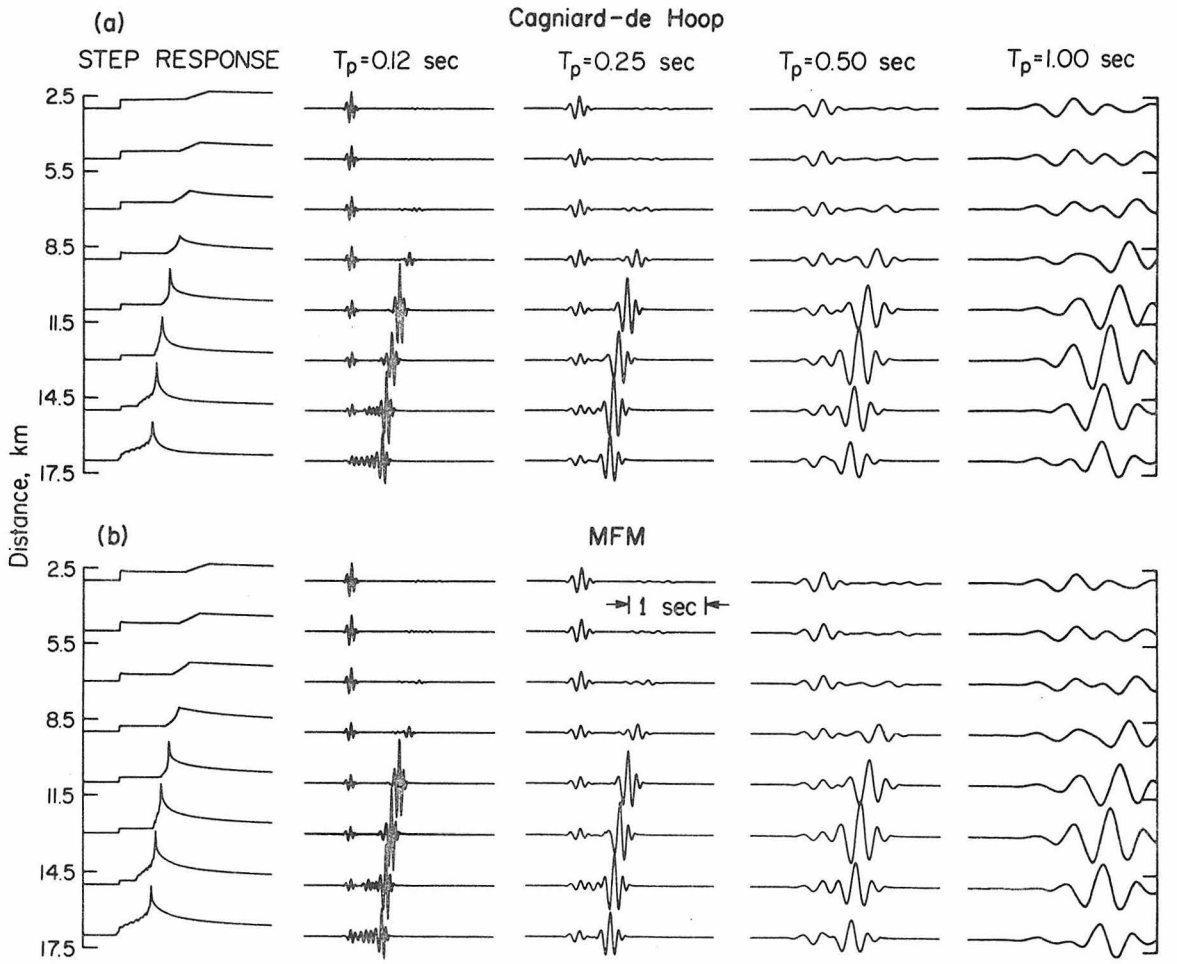

Figure 2.8. Comparison of synthetic seismograms generated using Cagniard-De Hoop (2.8a) and MFM (2.8b). Synthetics were produced using both methods for ranges of 3, 5, 7, 9, 11, 13, 15, and 17 km and for system functions with peak periods T_p of .12, .25, .5 and 1 sec. The same scale is used in all synthetics, in this figure so that amplitudes are directly comparable.

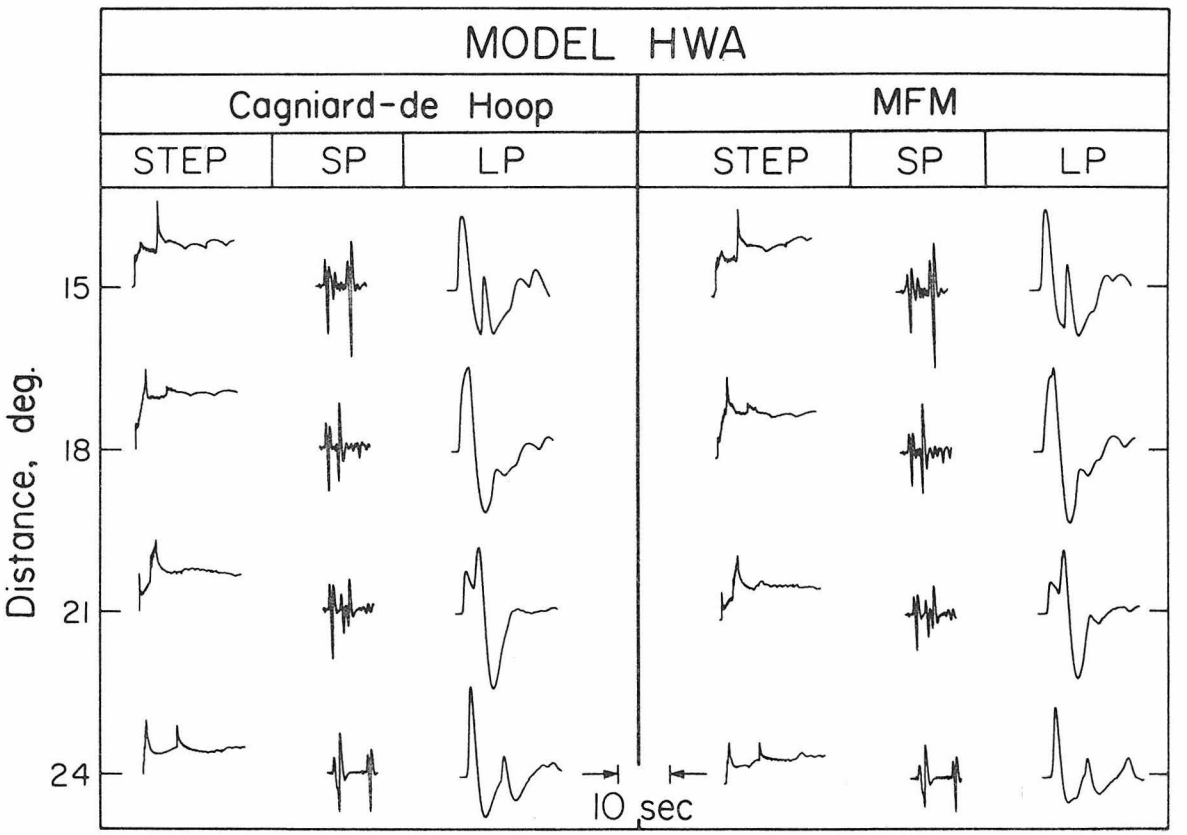

Figure 2.9. Comparison of synthetic seismograms for upper mantle model HWA. Synthetics were produced for ranges of 15, 18, 21, and 24°. Step function and short and long period WWSSN seismograms are shown. Short and long period seismograms assume a delta function point source and a Futterman Q operator with T/Q = 1 sec. Instrumental gain has been scaled for ease of presentation, but scale remains the same throughout the figure so that amplitudes may be directly compared.

CONCLUSION

A series of modifications to the Cagniard-de Hoop first motion approximations have been developed. These approximations provide explicit time domain expressions for quantities used in calculating generalized rays, resulting in a significant saving in computer time. Tests performed for a homogeneous earth, for an oceanic sub-bottom triplication, and for an upper mantle triplication indicate that MFM will be useful for the calculation of synthetic seismograms in a wide variety of geophysically interesting problems.

Chapter 3

THE INVERSE PROBLEM FOR DETERMINATION OF EARTH STRUCTURE

INTRODUCTION

To date, formal inversion of body wave data has been largely restricted to travel time inversion. Amplitude and waveform studies have, for the most part, been done using trial and error methods. In general, travel time data lacks the ability to resolve relatively fine, but important, details of a model, such as the thickness of transition zones. While amplitude and waveform studies can provide such detail, the trial and error methods that have been used to date have been both costly and time consuming. In addition, such methods provide relatively little information on resolution, although the difficulties encountered in fitting waveforms usually convince the people involved in such studies that the model is quite tightly constrained. The inversion procedure presented below provides a method for finding perturbations to a starting model that improve the fit of synthetic seismograms to waveform data. This method also, to some extent, provides a means of exploring the constraints imposed by the waveform data on specific model features.

In general, the methods used in solving the forward wave propagation problem are sufficiently complicated, and the available data sufficiently noisy and sparse, that an exact inversion is probably not practical. Instead, we wish to develop an iterative linear or quasi-linear method which fits available data in a least squares sense. Such methods have been used in geophysics on a number of problems,

including studies of normal modes (Backus and Gilbert, 1967), travel times (Johnson and Gilbert, 1972), electrical conductivity (Parker, 1970), and plate tectonics (Minster et al., 1974).

Besides immunity to instabilities caused by noise, iterative least squares inversions have the advantage of providing a simple means of incorporating data from other data sets. Thus, waveform inversion may be used to "fine tune" a model which has been obtained through other means. This would not, in general, be possible with an "exact" inversion method.

THE CHOICE OF ERROR FUNCTION

It is often observed that waveforms will show good station to station coherence even when absolute travel times or absolute amplitudes show significant scatter. For this reason, we would like to separate the information about wave shape from absolute amplitude and travel time information. Since we are performing a least squares inversion, absolute travel time and amplitude data may be included explicitly, in a least squares sense, or implicitly through choice of starting model.

In order to separate errors in waveform from travel time and amplitude errors, we consider the error function

$$d_i = 1 - \frac{\max(f_i * s_i)}{\left((f_i * f_i)(0)\right)^{\frac{1}{2}} \left((s_i * s_i)(0)\right)^{\frac{1}{2}}} \tag{3.1}$$

where f_i is the i^{th} data seismogram, s_i is the i^{th} synthetic seismogram and

$$(f*s)(\tau) \equiv \int f(t)s(t+\tau)dt = \int f(t-\tau)s(t)dt$$

is the cross-correlation function of f and s.

We note that, since

$$\left((f_i*f_i(0)\right)^{\frac{1}{2}} = \left(\int f_i^{\,2}(t)dt\right)^{1/2}$$

we may rewrite (3.1) as

$$d_i = 1 - \max\,(\hat{f}_i*\hat{s}_i) \tag{3.2}$$

where $\hat{f}_i(t) = \dfrac{f_i(t)}{\left(\int f_i^{\,2}(t)dt\right)^{\frac{1}{2}}}$ $\qquad$ $\hat{s}_i(t) = \dfrac{s_i(t)}{\left(\int s_i^{\,2}(t)dt\right)^{\frac{1}{2}}}$

The normalization of f_i and s_i makes d_i insensitive to the absolute amplitudes of f and s_i. By choosing the maximum of the correlation function, we allow f_i and s_i to optimally align themselves in time, thus making d_i insensitive to absolute travel time. The function d_i has zero as its minimum which is achieved only when

$$f_i(t) = \text{const} \cdot s_i\,(t + \tau_i)$$

In fact, if we consider

$$\int\left(\hat{f}_i(t)-\hat{s}_i(t+\tau_i)\right)^2dt = \int\hat{f}_i^{\,2}(t)dt+\int\hat{s}_i^{\,2}(t)dt-2\int\hat{f}_i(t)\hat{s}_i(t+\tau_i)dt$$

we find, if τ_i is chosen as the optimal lag time

$$\int\left(\hat{f}_i(t) - \hat{s}_i(t+\tau_i)\right)^2dt = 2d_i \tag{3.3}$$

Thus, d_i is one-half of the squared error between the normalized

time shifted data and synthetics. Hence, to minimize the difference in waveform between a set of synthetic and data seismograms, we need merely minimize the objective function

$$d = \sum_i d_i^2$$

THE RELATIONSHIP OF CHANGES IN THE SYNTHETIC SEISMOGRAMS TO CHANGES IN THE ERROR FUNCTION

We now consider the change in the function d_i for some small change in the synthetic s_i. From the definition of d_i, we have

$$d_i+\delta d_i = 1 - \frac{\max f_i \star (s_i+\delta s_i)}{\left(f_i \star f_i(0)\right)^{1/2}\left((s_i+\delta s_i)\star(s_i+\delta s_i)(0)\right)^{1/2}} \tag{3.4}$$

$$\text{or} \quad d_i+\delta d_i = 1 - \frac{\left(f_i(t-\tau_i-\delta\tau_i)\star s_i(t)\right)(0)+\left(f_i(t-\tau_i-\delta\tau_i)\star \delta s_i(t)\right)(0)}{\left(f_i \star f_i(0)\right)^{1/2}\left((s_i\star s_i)(0)+2(s_i\star\delta s_i)(0)+(\delta s_i\star\delta s_i)(0)\right)^{1/2}}$$

where τ_i is the lag that maximizes $f_i \star s_i$ and $\tau_i+\delta\tau_i$ is the lag that maximizes $f_i\star(s_i+\delta s_i)$.

If we assume that $(s_i\star s_i)(0) >> 2(s_i\star\delta s_i)(0)+(\delta s_i\star\delta s_i)(0)$ we may expand the denominator of equation (3.4) in a Taylor series and obtain, to first order

$$d_i+\delta d_i \simeq 1 - \left(\hat{f}_i(t-\tau_i-\delta\tau_i)\star\hat{s}_i(t)\right)(0)\left[\,1 - \left(\hat{s}_i(t)\star\delta\hat{s}_i(t)\right)(0) - 1/2\left(\delta\hat{s}_i(t)\star\delta\hat{s}_i(t)\right)(0)\,\right] + \left(\hat{f}_i(t-\tau_i-\delta\tau_i)\star\delta\hat{s}_i(t)\right)(0) \tag{3.5}$$

where $\delta\hat{s}_i = \dfrac{\delta s_i}{\left((s_i * s_i)(0)\right)^{1/2}}$, and f_i, s_i are as in equation (3.2). If we now approximate

$$f_i(t-\tau_i-\delta\tau_i) \approx f_i(t-\tau_i) - \frac{\partial f_i(t-\tau_i)}{\partial t}\delta\tau_i + 1/2\,\frac{\partial^2 f_i(t-\tau_i)}{\partial t^2}\,\delta\tau_i{}^2$$

we find

$$\begin{aligned} d_i+\delta d_i \approx 1 &- \left(\hat{f}_i(t-\tau_i)*\hat{s}_i(t)\right)(0) - \left(\left(\hat{f}_i(t-\tau_i)-c_i s_i(t)\right)*\delta\hat{s}_i\right)(0) \\ &+ 1/2c_i\left(\delta\hat{s}_i*\delta\hat{s}_i\right)(0) - 1/2\,\frac{\partial^2}{\partial^2 t}\left(\hat{f}_i(t-\tau_i)*\hat{s}_i(t)\right)(0)(\delta\tau_i)^2 \\ &+ \left(\frac{\partial\hat{f}_i(t-\tau_i)}{\partial t} * s_i(t)\right)(0)(\delta\tau_i) \end{aligned} \tag{3.6}$$

where $c_i = \int \hat{f}_i(t-\tau_i)\hat{s}_i(t)dt$.

Here we have used the fact that

$$\frac{\partial}{\partial t}\left(\hat{f}_i(t-\tau_i)*\hat{s}_i(t)\right)(0) = 0 \qquad \text{and}$$

$$\frac{\partial}{\partial t}(a*b) = \frac{\partial}{\partial t}*b = a*\frac{\partial b}{\partial t}$$

Subtracting equation (3.2) from equation (3.6), we find

$$\begin{aligned} \delta d_i \approx &- \left(\left(\hat{f}_i(t-\tau_i)-c_i\hat{s}_i(t)\right)*\delta\hat{s}_i\right)(0) + 1/2c_i\left(\delta\hat{s}_i*\delta\hat{s}_i\right)(0) \\ &- 1/2\,\frac{\partial^2}{\partial t^2}\left(\hat{f}_i(t-\tau_i)*\hat{s}_i\right)(0)(\delta\tau_i)^2 \\ &+ \left(\frac{\partial f_i}{\partial t}(t-\tau_i)*\delta\hat{s}_i(t)\right)(0)(\delta\tau_i) \end{aligned} \tag{3.7}$$

The first term on the r.h.s. of equation (3.7) is the only linear term in $\delta\hat{s}$ and $\delta\tau$. If max $\left(\hat{f}_i * \delta\hat{s}_i\right)$ and $\left(\hat{s}_i * \delta\hat{s}_i\right)(0)$ are small compared to max $\left(\hat{f}_i * \hat{s}_i\right)$ and $\left(\hat{s}_i * \hat{s}_i\right)(0)$, we may feel justified in ignoring higher powers and products of these terms. The term $(\delta\hat{s} * \delta\hat{s})(0)$, however, while of order $(\delta\hat{s}_i)^2$, is not necessarily small compared to $\left(\hat{s}_i * \delta\hat{s}_i\right)(0)$ (0) or $\left(\hat{f}_i * \delta\hat{s}_i\right)(\tau_i)$. In particular, consider a perturbation $\delta\hat{s}_i$ that consists of an arrival at a time where $\hat{s}_i(t)$ and $\hat{f}_i(t-\tau_i)$ have no arrivals. Then, for an arbitrarily large $\delta\hat{s}_i$, we have $\left(\hat{s}_i * \delta\hat{s}_i\right)(0)$ $= \left(\hat{f}_i * \delta\hat{s}_i\right)(-\tau_i) = 0$, and the entire effect of the perturbation is contained in the $\left(\delta\hat{s}_i * \delta\hat{s}_i\right)(0)$ and higher order terms. This situation arises in particular at the onset of a triplication, and inclusion of the non-linear second term in equation (3.7) is important in these circumstances to stabilize the inversion. Similarly, the third and fourth terms of equation (3.7) is important in these circumstances to stabilize the inversion. Similarly, the third and fourth terms of equation (3.7) are important, even though of order $(\delta\tau_i)^2$ and $(\delta\tau_i)(\delta\hat{s}_i)$ and hence non-linear, in that they are the lowest order terms that describe the change in time alignment of the perturbed synthetic and the data seismogram.

THE RELATIONSHIP OF CHANGES IN THE MODEL TO CHANGES IN THE ERROR FUNCTION

In the previous section, we related changes in d_i to changes in the synthetic seismogram, s_i, and the optimal time lag between synthetic and observed seismograms, τ_i. We must now determine the relationship between model changes and changes in the synthetic seismogram. In order to do this, we must first choose a method for

solution of the forward wave propagation problem. The method that will be used is the Modified First Motion approximation to Cagniard-de Hoop, discussed in Chapter 2.

Since we are using a modification of the Cagniard-de Hoop method, it is necessary to specify the model as a stack of homogeneous plane layers. The synthetic seismogram s_i may be written as

$$s_i = I(t) * \sum_j \phi_{ij}(t) \tag{3.8}$$

where I (t) is the effective source function, containing the far field source time function, the attenuation operator, the effects of near source and near receiver structure and the derivatives needed to convert the displacement potential response to a step function input to the displacement response for a delta function input. ϕ_{ij} is the j^{th} generalized ray in the infinite sum of rays. For a number of problems it is sufficient to consider only the first reflections, and we will for simplicity restrict ourselves to such problems. To further simplify the problem, we will restrict ourselves to fluid models. We may thus take ϕ_{ij} to be the displacement potential response for a step function in time of a generalized ray which reflects once off the top of the j^{th} layer. From (2.1), we may write

$$\phi_{ij}(t) = \psi_{ij}(t) * 1/\sqrt{t} \tag{3.9}$$

$$\psi_{ij}(t) = \mathrm{Im}\sqrt{2p/r}\ \frac{1}{\pi\eta_1} R_j(p) T(p) \frac{dp}{dt}$$

where * denotes convolution, $\eta_k = \left(\frac{1}{c_k^2} - p^2\right)^{1/2}$, c_k is the velocity of

the k^{th} layer, r is the source to receiver distance, $R_j(p)$ is the generalized plane wave reflection coefficient for the j-1, j^{th} layer interface and p is the generalized ray parameter, which is related to t by

$$t = pr + 2 \sum_{k=1}^{j=1} h_k \eta_k, \quad \text{Im } (t) = 0 \tag{3.10}$$

with h_k the thickness of the k^{th} layer.

Using the fact that for arbitrary functions x(t), y(t), z(t)

$$x*(y*z) = (x*y)*z = (x*z)*y$$

we may rewrite equation (3.7) as

$$\begin{aligned} \delta d_i \simeq & -\left(\left(\left(I(t)*1/\sqrt{t}\right)*\left(\hat{f}_i(t-\tau_i)-c_i\hat{s}_i(t)\right)\right)*\sum_j \delta\hat{\psi}_{ij}(t)\right)(0) \\ & + 1/2c_i\left(\left(\left(I(t)*1/\sqrt{t}\right)*\left(I(t)*1/\sqrt{t}\right)\right)*\left(\sum_j \delta\hat{\psi}_{ij}(t)*\sum_j \delta\hat{\psi}_{ij}(t)\right)\right)(0) \\ & - 1/2\,\frac{\partial^2}{\partial t^2}\left(\hat{f}_i(t-\tau_i)*\hat{s}_i\right)(0)(\delta\tau_i)^2 + \left(\left(\left(I(t)*1/\sqrt{t}\right)* \right.\right. \\ & \left.\left.\frac{\partial \hat{f}_i}{\partial t}(t-\tau_i)\right)*\left(\sum_j \delta\hat{\psi}_{ij}(t)\right)\right)(0)\delta\tau_i \end{aligned} \tag{3.11}$$

where $\delta\hat{\psi}_{ij} = \dfrac{\delta\psi_{ij}}{(s_i*s_i)(0)^{1/2}}$ is the normalized change in ψ_{ij}.

We must now find a relationship between model changes δm and changes in the generalized rays, $\delta\psi_{ij}$. To do this, we first consider the model parameterization we will use and the form of the model perturbations that we will allow.

Changes in the velocity depth function for a plane layered model may take the form of either changes in layer velocities or changes

in layer thicknesses. If no low velocity zone is present, or if the maximum lid velocity and minimum velocity in the low velocity zone are specified, then we may approximate any velocity-depth function satisfying these constraints by changing layer thicknesses only.

The main reason for wishing to vary only the layer thicknesses is the relative simplicity of derivatives with respect to layer thickness as opposed to the velocity derivatives. In addition, by using uniform velocity changes between adjacent layers we may attempt to minimize errors in waveforms caused by using the Modified First Motion approximations and by ignoring multiple reflections. The disadvantage of varying only layer thickness is that, in general, more layers will be needed in order to effectively make the inverse problem underdetermined than if layer velocities had been allowed to vary. The range of models that may be realized through variation of layer thickness is also somewhat restrictive in that low velocity zones cannot be introduced unless they were present in the original model.

In computing the change $\delta\psi_{ij}$ for some change δh_k in the thickness of the k^{th} layer it is convenient, as was done in Chapter 2, to consider the refracted and reflected portions of $\psi_{ij}(t)$ separately. Let ψ^c_{ij} be the head wave portion of ψ_{ij}, ψ^0_{ij} be the reflected portion, t^c_{ij} be the time of the onset of the head wave, and t^0_{ij} be the time of the onset of the reflection. We first consider the head wave.

For any change in layer thickness only, p^c_{ij}, the ray parameter corresponding to the onset of the headwave, remains unchanged.

Further, from (2.17) we know that the functional form of $\bar{\psi}^c_{ij}(p) \equiv \psi^c_{ij}(p)\frac{dp}{dt}$ is independent of layer thickness. Thus, the area under $\bar{\psi}^c_{ij}(p)$ in the interval $[p, p+\delta p]$ remains constant. Changes $\delta\psi^c_{ij}$ caused by changes δh_k in the model are a result of changes in the ray parameter corresponding to reflection, p^0_{ij}, and of changes in the t-p relationship for that ray.

For an arbitrary smooth function x(t), we may approximate the change δI_{ijk} in $I_{ij} = \left(x(t)\star\psi^c_{ij}(t)\right)(0)$ caused by a change in p^0_{ij} induced by a change δh_k in thickness of the k^{th} layer by

$$\delta I_{ijk} \approx \left(\bar{\psi}^c_{ij}(p^0_{ij})\ \delta p^0_{ij}\right) \cdot x(t^0_{ij})$$

From Paper I we know that p^0_{ij} is a solution of $\frac{dt_{ij}}{dp} \equiv r_i - 2\sum_m \frac{h_m p}{\eta_m} = 0$.

Thus, to first order we have

$$\delta p^0_{ij} = \frac{2p^0_{ij}}{\eta_k \frac{d^2 t_{ij}}{dp^2}(p^0_{ij})}\ \delta h_k \qquad k<j$$

$$= 0 \qquad k \geq j$$

and (3.13)

$$\delta I_{ijk} \approx \delta A^c_{ijk}\ x(t^0_{ij})\ \delta h_k \qquad k<j$$

$$= 0 \qquad k \geq j$$

where

$$\delta A^c_{ijk} = \frac{2p^0_{ij}\bar{\psi}^c_{ij}(p^0_{ij})}{\eta_k \frac{d^2 t_{ij}}{dp^2}(p^0_{ij})} = \frac{\left(2p^0_{ij}\right)^{3/2} T(p^0_{ij})\,\mathrm{Im}\,R_j(p^0_{ij})}{\pi\eta_1\eta_k r_i^{\frac{1}{2}} \frac{d^2 t_{ij}}{dp^2}(p^0_{ij})} \qquad (3.14)$$

For an arbitrary model change, we thus find

$$\delta I_{ij} \approx x(t^0_{ij}) \sum_{k=1}^{j-1} \delta A^c_{ijk}\, \delta h_k \tag{3.14}$$

In order to calculate the changes in I_{ij} caused by changes in the t-p relationship, we consider the contribution to the integral of a small time interval $[t,t+\delta t]$, corresponding to a small p interval $[p,p+\delta p]$. This may be approximated by

$$\int_t^{t+\delta t} x(t)\psi^c_{ij}(t)dt \approx x(t) \int_t^{t+\delta t} \psi^c_{ij}(t)dt = x(t) \int_p^{p+\delta p} \bar{\psi}^c_{ij}(p)dp$$

for x(t) smooth and δt and δp sufficiently small. For a perturbed model the same p interval maps into a time interval, say $[t', t'+\delta t']$. The contribution of this time interval to $I_{ij} + \delta I_{ij}$ is now

$$\int_{t'}^{t'+\delta t'} x(t')\bar{\psi}'_{ij}(t') \approx x(t')\int_p^{p+\delta p} \bar{\psi}^c_{ij}(p)dp$$

Letting $\delta p \to 0$, and thus $\delta \to 0$, we find

$$I_{ij} + \delta I_{ij} = \int_{t^c_{ij}}^{t^0_{ij}} x(t')\psi^c_{ij}(t)dt$$

where t' is, as above, the perturbed time calculated for the same p as the corresponding t. From equation (3.10), we find

$$t' = t + 2 \sum_{k=1}^{j-1} \eta_k \delta h_k$$

We thus find

$$I_{ij}+\delta I_{ij} = \int_{t_{ij}^c}^{t_{ij}^0} x(t+2\sum_{k=1}^{j-1} \eta_k \delta h_k)\ \psi_{ij}^c(t)\,dt \tag{3.15}$$

Expanding x in a Taylor series, we find

$$I_{ij} + \delta I_{ij} \approx I_{ij} + \int \frac{dx(t)}{dt}\ \psi_{ij}^c(t)\,\delta t_{ij}\,dt \tag{3.16}$$

where $\delta t_{ij} = 2\sum_{k=1}^{j-1} \eta_k\ \delta h_k$.

When $t_{ij}^0 - t_{ij}^c$ is small compared to the predominant period of x(t), we may further approximate equation (3.16) by

$$\delta I_{ij} \approx \overline{\frac{dx}{dt}}\ \delta t_{ij}^0\ A_{ij}^c \tag{3.17}$$

with $A_{ij}^c \equiv \int_{t_{ij}^c}^{t_{ij}^0} \psi_{ij}^c(t)\,dt$, $\delta t_{ij}^0 \equiv \delta t_{ij}(t_{ij}^0)$ and $\overline{\frac{dx}{dt}}$ is the average value of $\frac{dx}{dt}$ in $\left[t_{ij}^c, t_{ij}^0\right]$.

When the head wave duration is of the same order as or longer than the predominant instrument period, we may still obtain a reasonably good estimate of equation (3.16) by

$$\delta I_{ij} \approx \overline{\frac{dx}{dt}}\ \bar{\psi}_{ij}^{\,c}\ \overline{\delta t}\cdot(t_{ij}^0 - t_{ij}^c) = \overline{\frac{dx}{dt}}\ A_{ij}^c\ \overline{\delta t} \tag{3.18}$$

since $\eta_k(t)$, $\psi_{ij}^c > 0$ where again the bar indicates an average value. Where greater accuracy is desired, it is necessary to divide the head-wave into several parts and then use equation (3.18). This corresponds to a rectangle rule integration of equation (3.16).

The accuracy of equation (3.16) depends on the accuracy of using only the first term in the Taylor series expansion of x(t). Where time shifts caused by model perturbations approach the time scale on

which x(t) deviates from a straight line, information provided by equation (3.16) on the change of the total error function will clearly be inaccurate. The result will often be serious instabilities in the inverse problem. The problem may, however, be stabilized through use of the second order term. Since we wish to insure stability, we will use the second order term only when it increases the error function d. The result will generally be that the inverse problem will be somewhat overstabilized, which results in a slower convergence rate. This is usually far preferable to trying to deal with an understabilized problem.

Including the second term in equation (3.16), we get

$$\delta I_{ij} \simeq \int_{t_{ij}^c}^{t_{ij}^0} \frac{dx(t)}{dt}\, \psi_{ij}^c(t)\delta t_{ij}\, dt + 1/2 \int_{t_{ij}^c}^{t_{ij}^0} \frac{d^2x}{dt^2}\, \psi_{ij}^c(t)(\delta t_{ij})^2 dt \tag{3.19}$$

and for equation (3.18)

$$\delta I_{ij} \simeq \overline{\frac{dx}{dt}}\, A_{ij}^c\, \overline{\delta t} + 1/2\, \overline{\frac{d^2x}{dt^2}}\, A_{ij}^c\, \overline{(\delta t)}^2 \tag{3.20}$$

Combining the results for time shifts from equation (3.20) and amplitude changes from equation (3.14), we get, for the head wave

$$\delta I_{ij}^c \simeq x(t_{ij}^0) \sum_{k=1}^{j-1} \delta A_{ijk}^c \delta h_k + 2\overline{\frac{dx}{dt}}\, A_{ij}^c \sum_{k=1}^{j-1} \overline{\eta}_k \delta h_k$$

$$+2\, \overline{\frac{d^2x}{dt^2}}\, A_{ij}^c \sum_{k,m=1}^{j-1} \overline{\eta}_k \overline{\eta}_m \delta h_k \delta h_m \tag{3.21}$$

The treatment of the reflected portion of a generalized ray is similar to the treatment of the refracted portion. For rays where the Modified First Motion approximation is valid, we expect that the contribution of the reflected portion of the generalized ray, ψ^0_{ij}, to the final seismogram will be controlled largely by the arrival time, t^0_{ij} and the amplitude of ψ^0_{ij} in a small time interval following t^0_{ij}. Thus, we consider changes in ψ^0_{ij} to occur only in the interval $[t^0_{ij}, t^0_{ij}+\varepsilon]$ where ε is chosen to be less than the period of the instrument.

As was done for the refracted portion of the generalized ray, we wish to find the change in $I_{ij} = \int_{t^0_{ij}}^{\infty} x(t)\psi^0_{ij}(t)dt$ for some small model perturbation.

If we use the first motion approximation from Chapter 2, we have

$$\psi^0_{ij} \simeq \sqrt{\frac{p_o r}{\pi \eta_1}}\, T(p^0_{ij})\, \mathrm{Re}\left(R(p^0_{ij})\right) \left|\frac{d^2t}{dp^2}\right|^{-\frac{1}{2}} (t-t^0_{ij})^{-\frac{1}{2}} \qquad t>t^0_{ij} \tag{2.11}$$

A change in the model effects ψ^0_{ij} by changing both p^0_{ij} and t^0_{ij}. Since the most rapidly varying functions of p in equation (2.11) are $R_j(p)$ and $\frac{d^2t}{dp^2}$, we will neglect changes in other quantities. Thus, we have, for a change δh_k in thickness of the k^{th} layer, $k<j$,

$$\psi^0_{ij} + \delta\psi^0_{ij} \simeq \sqrt{\frac{p_o r}{\pi \eta_1}}\, T(p^0_{ij})\, (t-t^0_{ij}-\delta t^0_{ij})^{-\frac{1}{2}} \cdot \left[\mathrm{Re}\left(R(p^0_{ij}+\delta p^0_{ij})\right) \cdot \left|\frac{d^2t}{dp^2}(p^0_{ij}+\delta p^0_{ij}) - \frac{2\delta h_k}{c_k^2 \eta_k^3}\right|^{-\frac{1}{2}}\right] \tag{3.22}$$

Expanding $R_j(p^0_{ij} + \delta p^0_{ij})$ in a Taylor series about p^0_{ij} we find, for a fluid

$$R_j(p^0_{ij}+\delta p^0_{ij}) \approx R_j(p^0_{ij}) + \frac{2p^0_{ij}\rho}{\eta_{j-1}\eta_j}\left[R_j(p^0_{ij}) + \frac{(\rho^2-1)\eta_j^2}{(\eta_{j-1}+\rho\eta_j)^2}\right] \delta p^0_{ij} \tag{3.23}$$

where $\rho = \frac{\rho_{j-1}}{\rho_j}$. When $\rho \approx 1$ this reduces to

$$\begin{aligned} R_j(p^0_{ij} + \delta p^0_{ij}) &\approx R_j(p^0_{ij}) + \frac{2\rho p^0_{ij}}{\eta_{j-1}\eta_j} R_j(p^0_{ij})\delta p^0_{ij} \quad \text{and} \\ \operatorname{Re}\left(R_j(p^0_{ij}+\delta p^0_{ij})\right) &\approx \operatorname{Re}\left(R_j(p^0_{ij})\right) - \frac{4\rho^2 p^0_{ij}}{|\eta_{j-1}|^2+\rho^2|\eta_j|^2} \text{ if } p^0_{ij} > \frac{1}{c_j} \\ &\approx R_j(p^0_{ij}) + \frac{2\rho p^0_{ij}}{\eta_{j-1}\eta_j} R_j(p^0_{ij})\delta p^0_{ij} \text{ if } p^0_{ij} < \frac{1}{c_j} \end{aligned} \tag{3.24}$$

These expressions are well behaved except when p^0_{ij} approaches $\frac{1}{c_j}$ from the left. In this region we replace $\frac{\partial R}{\partial p}$ by a local average value. Thus

$$\operatorname{Re}\left(R_j(p^0_{ij}+\delta p^0_{ij})\right) \approx R_j(p^0_{ij}) + \frac{1-R\left(\frac{3}{2c_j} - \frac{1}{2c_{j-1}}\right)}{\frac{1}{2}\left(\frac{1}{c_{j-1}} - \frac{1}{2c_j}\right)} \delta p^0_{ij}$$

$$\text{if } \left(\frac{3}{2c_j} - \frac{1}{2c_{j-1}}\right) \le p^0_{ij} < \frac{1}{c_j}$$

The choice of the point $\frac{3}{2c_j} - \frac{1}{2c_{j-1}}$ as the point at which to begin using the average behavior of $R_j(p)$ is arbitrary, but appears to give reasonably good results in practice.

We may also expand the geometric spreading term

$$\left|\frac{d^2t}{dp^2}\,(p_{ij}^0+\delta p_{ij}^0) - 2\,\frac{\delta h_k}{c_k^2\eta_k^3}\right|^{-1/2} \approx \left|\frac{d^2t}{dp^2}\,(p_{ij}^0)\right|^{-1/2} - \frac{\delta h_k}{\eta_k^3 c_k^2\left|\frac{d^2t}{dp^2}\,(p_{ij}^0)\right|^{3/2}}$$

$$- \frac{\left|\frac{d^3t}{dp^3}\,(p_{ij}^0)\right|\delta p_{ij}^0}{2\left|\frac{d^2t}{dp^2}\,(p_{ij}^0)\right|^{3/2}} \tag{3.25}$$

Thus, to first order in δh, equation (3.22) becomes

$$\psi_{ij}^0+\delta\psi_{ij} \approx \frac{\sqrt{p/r}}{\pi\eta_1}\,T(p_{ij}^0)\left(t-t_{ij}^0-\delta t_{ij}^0\right)^{-1/2}\mathrm{Re}\left(R(p_{ij}^0)\right)\left|\frac{d^2t}{dp^2}\,(p_{ij}^0)\right|^{-1/2}\cdot$$

$$\left[1+\frac{1}{\mathrm{Re}\left(R(p_{ij}^0)\right)}\cdot\mathrm{Re}\left(\frac{dR}{dp}(p_{ij}^0)\right)\delta p_{ij}^0 - \frac{1/2\left|\frac{d^3t}{dp^3}(p_{ij}^0)\right|\delta p_{ij}^0+\frac{\delta h_k}{c_k\eta_k}}{\left|\frac{d^2t}{dp^2}(p_{ij}^0)\right|}\right] \tag{3.26}$$

with p_{ij}^0, δt_{ij}^0 as in equation (3.12) and equation (3.16) and $\mathrm{Re}(\frac{dR}{dp})$ as in equation (3.24). Written in this way, we see that to first order the change in ψ_{ij}^0 consists of a time shift of δt_{ij}^0 and an amplitude change given by the factor in square brackets in equation (3.26). Proceeding as we did in the case of the refraction, we find that the time shift gives us

$$\delta I_{ij} \approx \int_{t_{ij}^0}^{\infty}\frac{dx(t)}{dt}\,\psi_{ij}^0(t)\delta t_{ij}^0 dt + 1/2\int_{t_{ij}^0}^{\infty}\frac{d^2x(t)}{dt^2}\,\psi_{ij}^0(t)\left(\delta t_{ij}^0\right)^2 dt$$

$$\overline{\frac{dx(t^0)}{dt}}A_{ij}^0\;\delta t_{ij}^0 + 1/2\overline{\frac{d^2x(t^0)}{dt^2}}\;A_{ij}^0\;(\delta t_{ij}^0)^2 \tag{3.27}$$

where $A_{ij}^0 = \int_{t_{ij}^0}^{t_{ij}^0+\epsilon} \psi_{ij}^0(t)\,dt$, and $\overline{\frac{dx(t^0)}{dt}} = \frac{1}{\epsilon} \int_{t_{ij}^0}^{t_{ij}^0+\epsilon} \frac{dx}{dt}\,dt$

As in the refracted case, the second term in equation (3.27) is included only if it increases the error function d.

The amplitude change in equation (3.26) gives us

$$\delta I_{ij} \simeq \left[\frac{1}{\mathrm{Re}\left(R_j(p_{ij}^0)\right)} \cdot \mathrm{Re}\left(\frac{dR_j}{dp}(p_{ij}^0)\right) \delta p_{ij}^0 - \frac{\left|\frac{d^3t}{dp^3}(p_{ij}^0)\right| \delta p_{ij}^0 + \frac{2\delta h_k}{c_k^2 \eta_k^3}}{2\left|\frac{d^2t}{dp^2}(p_{ij}^0)\right|} \right] \tag{3.28}$$

$$\cdot \int_{t_{ij}^0}^{\infty} \psi_{ij}^0(t)x(t)\,dt \simeq \delta A_{ijk}^0 \overline{x(t^0)}\ \delta h_k$$

with

$$A_{ijk}^0 = \left[\frac{1}{\mathrm{Re}\left(R(p_{ij}^0)\right)} \cdot \mathrm{Re}\left(\frac{dR}{dp}(p_{ij}^0)\right) \cdot \frac{-2p_{ij}^0}{\eta_k \frac{d^2t}{dp^2}(p_{ij}^o)} \right. \tag{3.29}$$

$$\left. + \frac{\left|\frac{d^3t}{dp^3}(p_{ij}^0)\right| p_{ij}^0}{\eta_k \left|\frac{d^2t}{dp^2}(p_{ij}^0)\right|^2} - \frac{1}{\left|\frac{d^2t}{dp^2}(p_{ij}^0)\right| c_k^2 \eta_k^3} \right] \cdot \overline{x(t^0)}\ \delta h_k$$

Substituting for t_{ij}^0 and combining equation (3.27) and (3.28) we find that the total contribution of the reflected portion of the i, jth ray for a model change given by $\{\delta h_k\}$ is

$$\delta I^0_{ij} \approx \overline{x(t^0)} \sum_{k=1}^{j-1} \delta A^c_{ijk}\, \delta h_k + 2\, \overline{\frac{dx(t^0)}{dt}}\, A^o_{ij} \sum_{k=1}^{j-1} \eta_k \delta h_k \qquad (3.30)$$

$$+ 2\, \overline{\frac{d^2x(t^0)}{dt^2}}\, A^0_{ij} \sum_{k,m=1}^{j-1} \eta_k \eta_m \delta h_k \delta h_m$$

Combining equations (3.21) and (3.30) we find the total change in I_{ij}, δI^T_{ij} to be

$$\delta I^T_{ij} = \sum_{k=1}^{j=1} \left(x(t^0_{ij})\, A^0_{ijk} + \overline{x(t^0)}\, \delta A^0_{ijk} + 2\, \overline{\frac{dx}{dt}}\, A^c_{ij} + 2\, \overline{\frac{dx(t^0)}{dt}}\, A^0_{ij} \right) \delta h_k \qquad (3.31)$$

$$+ \sum_{k,m=1}^{j-1} \left(2\, \overline{\frac{d^2x}{dt^2}}\, A^c_{ij}\, \overline{\eta_k}\, \overline{\eta_m} + 2\, \overline{\frac{d^2x(t^0)}{dt^2}}\, A^0_{ij} \eta_k(p^0_{ij}) \eta_m(p^0_{ij}) \right) \delta h_k \delta h_m$$

We may now use equations (3.31) and (3.11) to find δd_1 in terms of δh_k and $\delta \tau_i$, thus finally relating the change in the error function to the change in model parameters. Keeping only terms up to second order, we find

$$\delta d_i \approx \sum_{k=1}^{n} \sum_{j=k+1}^{n} \left(F_i(t^0_{ij})\, \delta A^c_{ijk} + \overline{F_i(t^0)}\, \delta A^0_{ijk} + 2\, \overline{\frac{dF_i}{dt}}\, A^c_{ij} \overline{\eta}_k \right. \qquad (3.32)$$

$$\left. + 2\, \overline{\frac{d\overline{F}_i(t^0)}{dt^2}}\, A^c_{ij} \eta_k \right) \delta h_k + \sum_{k,m-1}^{n} \sum_{j=\max(k,m)+1}^{n} \left(2\, \frac{d^2F_i}{dt^2}\, A^c_{ij}\, \overline{\eta}_i\, \overline{\eta}_m \right.$$

$$\left. + 2\, A^0_{ij}\, \frac{d^2F(t^0)}{dt^2}\, \eta_k(p^0_{ij}) \eta_m(p^0_{ij}) \right) \delta h_k \delta h_m - \sum_{k,m=1}^{n} \sum_{j,\ell=\max(k,m)+1}^{n} \left[2 \left(A^c_{ij} + A^0_{ij} \right) \right.$$

$$\left(A^c_{i\ell}+A^0_{i\ell}\right)\cdot \frac{\partial^2 J}{\partial t^2}\,(t^0_{ij}-t^0_{i\ell})\eta_k(p^0_{ij})\eta_m(p^0_{i\ell}) - \tfrac{1}{2}J(t^0_{ij}-t^0_{i\ell})\cdot$$

$$\left(\delta A^c_{ijk}+\delta A^0_{ijk}\right)\cdot\left(\delta A^c_{i\ell m}+\delta A^0_{i\ell m}\right)\Big]\ \delta h_k \delta_k h_m$$

$$-\tfrac{1}{2}\frac{\partial^2}{\partial t^2}\left(\hat{f}_i(t-\tau_i)*\hat{s}_i(t)\right)(0)\left(\delta\tau_i\right)^2 + \sum_{k=1}^{n}\sum_{j=k+1}^{n}\left(G_i(t^0_{ij})\delta A^c_{ijk}\right.$$

$$\left. + \overline{G_i(t^0)}\ \delta A^0_{ijk} + 2\,\frac{\overline{dG_i}}{dt}\,A^c_{ijk}\,\bar{\eta}_k + 2\,\frac{dG_i(t^0)}{dt}\,A^0_{ij}\eta_k\right)\delta h_k \delta\tau_i$$

where

$$F_i(t) = \frac{1}{\left((s_i*s_i)(0)\right)^{\frac{1}{2}}}\left(I(t)*1/\sqrt{t}\right)*\left(\hat{f}_i(t-\tau_i) - c_i\hat{s}_i(t)\right)$$

$$J(t) = \frac{c_i}{(s_i*s_i)(0)}\left(I(t)*\frac{1}{\sqrt{t}}\right)*\left(I(t)*\frac{1}{\sqrt{t}}\right)$$

$$G_i(t) = \frac{1}{\left((s_i*s_i)(0)\right)^{\frac{1}{2}}}\qquad\left(I(t)*1/\sqrt{t}\right)*\frac{\partial\hat{f}_i}{\partial t}\,(t-\tau_i)$$

and n is the number of layers in the model. Collecting terms, we may rewrite equation (3.32) as

$$\delta d_i \approx B_{ik}\ \delta m_k + C_{ikm}\ \delta m_k\ \delta m_m \qquad (3.33)$$

with summation implied over repeated indices and where

$$B_{ik} = \sum_{j=k+1} \left(F_i(t^0_{ij})\ A^c_{ijk} + \overline{F_i(t^0)}\ A_{ijk} + 2\ \overline{\frac{dF_i}{dt}}\ A^c_{ij}\ \overline{\eta_k} \right.$$

$$\left. + 2\ \overline{\frac{dF_i(t^0)}{dt}}\ A^0{}_{ij}\eta_k(p^0_{ij}) \right) \qquad \text{if } k \leq n$$

$$= 0 \qquad \text{if } k > n$$

$$C_{ikm} = \sum_{j=\max(k,m)+1} \left(2\ \frac{d^2F_i}{dt^2}\ A^c_{ij}\eta_k\ \eta_m + 2\ \frac{d^2F_i(t^0)}{dt^2}\ A^0_{ij}\eta_k(p^0_{ij})\eta(p^0_{ij}) \right)$$

$$- \sum_{j,\ell=\max(k,m)+1} \left(2\left(A^c_{ij}+A^0_{ij}\right)\cdot\left(A^c_{i\ell}+A^0_{i\ell}\right)\frac{\partial^2 J}{\partial t^2}\ (t^0_{ij}-t^0_i)\eta_k(p^0_{ij})\eta_m(p^0_{i\ell}) \right.$$

$$\left. - 1/2\ J(t^0_{ij}-t_{i\ell})\cdot\left(\delta A^c_{ijk}+\delta A^0_{ijk}\right)\cdot\left(\delta A^c_{i\ell m}+\delta A_{i\ell m}\right) \right)$$

$$C_{ikm} = C_{imk} = \sum_{j=k+1}^{n} \left(G_i(t^0_{ij})\delta A^c_{ijk} + \overline{G_i(t^0)}\ \delta A^0_{ijk} + 2\ \frac{dG_i}{dt}\ A^c_{ij}\ \overline{\eta_k} \right.$$

$$\left. + 2\ \frac{dG_i(t^0)}{dt}\ A^0_{ij}\eta_k(p^0_{ij}) \right)\ \delta m_k \delta m_m \qquad \text{if } k \leq n,\ m = n+i$$

$$C_{ikm} = -1/2\ \frac{\partial^2}{\partial t^2}\ \left(f_i(t-\tau_i) * s_i(t)\right)\ (0)\delta m_k \delta m_m \qquad \text{if } k,m = n+i$$

$$C_{ikm} = 0 \qquad \text{otherwise}$$

and m is a vector containing changes of layer thickness and time lags, defined by

$$\delta m_k = \delta h_k \qquad \text{if } k \leq n$$

$$= \delta\tau_i \qquad \text{if } K = n+1$$

THE INVERSION PROCEDURE

We have obtained, in equation (3.33), an approximate quadratic expression for changes in the difference between synthetic and data waveforms in terms of changes in the model. The model changes consist not only of changes in layer thickness, but also of changes in the alignment in time of synthetic and data waveforms. We must now, using equation (3.33) find model changes that simultaneously minimize the errors in waveform, d_i, as defined by equation (3.2).

For the remainder of this chapter, we will use the summation convention for repeated indices. The problem we wish to solve is, given a starting model vector $\underset{\sim}{m}^0$ with an associated waveform error vector $\underset{\sim}{d}^0$, to find a model change $\underset{\sim}{\delta m}$ that minimizes the objective function

$$d \equiv (d_i^0 + \delta d_i)\ (d_i^0 + \delta d_i) \tag{3.34}$$

We do this by finding a $\underset{\sim}{\delta m}$ such that d is stationary,

$$\delta[(d_i^0 + \delta d_i)(d_i^0 + \delta d_i)] = 0 \tag{3.35}$$

Substituting equation (3.33) into equation (3.35) we find

$$\delta[(d_i^0 + B_{ij}\delta m_j + C_{ikm}\delta m_k \delta m_m)(d_i^0 + B_{ip}\delta m_p + C_{iqr}\delta m_q \delta m_r)]=0 \tag{3.36}$$

or, computing the first variation in equation (3.36)

$$(d_i^0 + B_{ij}\delta m_j + C_{ikm}\delta m_k \delta m_m)\ (B_{ip} + 2C_{iqp}\delta m_q) = 0 \tag{3.37}$$

This may be rewritten as

$$-B_{ip}d_i^0 = (B_{ij}B_{ip} + 2d_i^0C_{ijp} + 2B_{ij}C_{ikp}\delta m_k + B_{ip}C_{ijk}\delta m_k \qquad (3.38)$$

$$+ 2C_{ijk}\,C_{ipq}\,\delta m_k\,\delta m_q)\delta m_j$$

Keeping only the linear terms in δm in equation (3.38), we get the approximate solution

$$\delta m_j \simeq -(B_{ij}B_{ik} + 2d_i^0C_{ijk})^{\dagger}\,B_{\ell k}d_\ell^0 \qquad (3.39)$$

where $\dagger$ denotes a generalized inverse. The solution (equation 3.39) may be used to generate an iterative solution to equation (3.38), or $\underset{\sim}{m}^0+\delta\underset{\sim}{m}$ as obtained from equation (3.39) may be used directly as the next starting model for the iterative solution of the full problem. In practice, the latter choice has been used.

We note that equation (3.39) is just the Newton-Raphson solution of equation (3.37). This differs from the more usual linear least squares solution by the presence of the addition term $2d_i^0C_{ijk}$ in the inverse operator in equation (3.39). Due to the choice of non-linear information included in equations (3.7), (3.19) and (3.27) the matrix $2d_i^0C_{ijk}$ will be positive semi-definite. It thus serves the purpose of stabilizing the inversion procedure and reducing the size of the null space that would be present in the purely linear case. Thus, the non-linear terms in our formulation play a role similar to the damping terms in various damped least squares methods (Levenberg, 1944; Osborne, 1972), and to the "noise" term in the stochastic inversion of Jordan and Franklin (1971). The degree of stabilization

used is determined by the non-linear structure of the problem itself in our case, rather than by *à priori* estimates of rank or size of eigenvalues, as is done in damped least squares, or *à priori* estimates of a noise correlation function, as is done in the stochastic inverse. We may thus anticipate that the problems of slow convergence often encountered with damped least squares (Davies and Whiting, 1971) will not be as severe in the present case.

It should be noted that some degree of damping may still be necessary in computing a stable inverse in equation (3.39). That is, there may well be some model changes for which both waveforms and travel times of the data are insensitive. In particular, the thickness of layers at depths greater than the bottoming depth of the deepest penetrating ray included in the data set will be largely unconstrained, independent of any approximations used in the inversion. Inclusion of the damping term modifies equation (3.39) to

$$\delta m_j = -(B_{ij}\, B_{ik} + 2d_i^0\, C_{ijk} + \sigma\delta_{jk})^{-1}\, B_{\ell k} d_\ell^0. \qquad (3.40)$$

In general, the amount of damping necessary to stabilize equation (3.39) will be far less than that needed to stabilize the linear approximation.

One of the major advantages of a least squares formulation is the relative ease with which it may be modified to include additional types of data. We will briefly discuss two such modifications, the imposition of a correlation function to smooth model perturbations and the incorporation of absolute travel time data into the inversion.

Since it is desirable in general to overparameterize the

model, it may be desirable to impose a correlation function on the model perturbation in order to maintain the smoothness of the starting model in the final model. Let us call this correlation operator W. Then, letting $m'_i = W_{ji}\, m_j$, $B'_{ij} = W_{ik}W^{-1}_{\ell j}B_{k\ell}$, $C'_{ijk} = W_{ik}W^{-1}_{\ell j}C_{ik\ell}$ in equation (3.33) and proceeding as before, we find

$$\delta m'_m = -W_{mj}\ (B_{ij}B_{ik} + 2d_i C_{ijk})^{\dagger}B_{\ell k}d^0_\ell. \tag{3.41}$$

Thus, we see that imposing a correlation operator on the model perturbations is equivalent to smoothing the uncorrelated perturbations with the operator W.

Absolute travel times may be incorporated in the inversion through the lag times τ_i. Rather than using first arrival times of the data and synthetic seismograms to determine travel time errors, we use the lag time which maximizes the normalized correlation function. We thus use the time shift needed to maximize the correlation of data and synthetic seismograms as the error in travel time. Defining a new objective function

$$d' = d + \sum_i a_i \tau_i^2 \tag{3.42}$$

with a_i the weight assigned to the travel time error of the i^{th} synthetic and with d as in equation (3.34), we find

$$\delta d' = \delta d + \sum_i 2a_i\tau_i\delta\tau_i = 0 \tag{3.43}$$

Proceeding as we did with equation (3.38), we find

$$\delta m_j = -(B_{ij}B_{ik} + 2d^0_i C_{ijk} + E_{jk})^{\dagger}B_{\ell k}d^0_\ell \tag{3.44}$$

where $E_{ji} = a_{(i)}\tau_{(i)}$ if $j = k = n+i$

$= 0$ otherwise

and the parentheses in the subscript suppresses summation.

So far, we have treated the inverse problem as if the model space were completely unconstrained. Clearly, with our choice of model parameterization, this is not the case. It should not be permissible to have layers with thickness less than zero. The problem is how to ensure that the new model $\underset{\sim}{m}^0 + \delta\underset{\sim}{m}$ is feasible.

Our approach to this problem is to ignore the constraints until a non-feasible point is reached. When this occurs, we replace the non-feasible model by a nearby feasible model. This model may be generated by setting the thickness of the negative layer to some minimum value and reducing the thickness of the two adjacent layers each by one half the change applied to the negative layer. When the adjacent layer is too thin to accept the full reduction, it is reduced to the minimum thickness and the next layer in the stack is reduced in thickness by the remaining amount. Thus, by locally smoothing the model, we obtain a feasible model. By averaging in this manner, we attempt to preserve the travel times and dynamic behavior of generalized rays reflecting from interfaces outside the averaged region, thus minimizing changes in the predicted waveform error.

This method is similar to the "hemstitching" method of Roberts and Livers (1961), which uses projections perpendicular to the constraint boundary to generate a new feasible point. However, by minimizing the change in the predicted objective function as we have done, we can hopefully avoid the slowed convergence that "hemstitching" often entails.

DISCUSSION

Many of the characteristics of the inversion procedure presented in this paper are highly dependent on the use of the L_2 norm to determine the magnitude of the difference between normalized data and synthetic seismograms in equations (3.2) and (3.3). Through choice of the norm, we may control the relative importance of peak heights and peak widths, or, in other words, shape and amplitude. The L_2 norm provides sensitivity to both shape and amplitude, and is thus well suited to the study of situations where several arrivals strongly interact. It is thus well suited to the study of transition regions that give rise to triplications. Where zero crossing information is more important than the relative amplitude of individual peaks, as in the study of dispersive phenomena, use of an L_1 norm is probably more appropriate. Similarly, where individual arrivals are well separated and the shapes of individual arrivals is considered relatively less important as compared to relative arrival times and amplitudes, an L_p norm with $p > 2$ is more appropriate than L_2. In the limiting case, where arrivals are well separated and the only information in the waveform is relative arrival times and amplitudes, with no shape information, it is probable that a direct inversion for these two quantities, rather than a waveform inversion, is best.

Thus, while use of the inversion method presented in this paper with the L_2 norm is still applicable to these other problems, the L_2 norm is not necessarily sensitive only to those factors that are important in a given problem. Other factors, however, favor using the L_2 norm for waveform inversion.

The principal advantage of using L_2 is the relationship between the norm of the waveform error and the cross correlation function given in equation (3.3). By being able to use the properties of correlation functions, and through use of FFT's, the calculation of derivatives is made much faster and easier.

The use of the Modified First Motion approximation also helps to make the calculation of derivatives quite fast. Despite the complexity of equation (3.39), calculation of the necessary derivatives usually consists of a small number of matrix multiplications. Further, these matrices consist of quantities that are necessary for the MFM calculations of the waveforms for the starting model, together with the data and starting waveforms. As a result, the computer time needed for the calculation of all derivatives needed for equation (3.39) and the inversion of this equation for the models given in the next section was comparable to the time necessary for the calculation of the waveforms for the starting model.

The fact that the time required for the evaluation of the objective function is comparable to the time needed for the evaluation of all derivatives for a given model suggests that a full step method of inversion is essential for an efficient inversion procedure. Since experience with a linear waveform inversion for the determination of source parameters (Burdick and Mellman, 1975) showed that a full step method was impossible, and that convergence for even a partial step method was slow, it proved necessary to include the effects of non-linear terms on the second derivative matrix in equation (3.33). A

stabilized Newton-Raphson method thus becomes a logical choice as a method of solution, since this method makes full use of second derivative information.

A possible alternative method is to minimize $\sum_i d_i$ as given by equation (3.33) rather than constructing a least squares solution to equation (3.33). This could be done using any of a number of non-linear programming algorithms. It has the advantage of explicitly including the inequality constraints on the model, and may exhibit faster convergence than the least squares method.

In situations where primary reflections are not sufficient to produce accurate synthetic waveforms, it is a straightforward procedure to include important multiple reflections in the inversion procedure if the identity of these multiple reflections is known. Where it is not known, or where the number of rays that would have to be included is quite large, it may still be possible to obtain a solution by using a reflectivity algorithm (Fuchs and Muller, 1971) to generate derivatives. This is the equivalent of assuming that changes in the primary reflections give a good description of changes in the seismogram, even though the primary reflections themselves are not sufficient to generate an accurate seismogram. This would clearly be a costly method, and its convergence properties are not known at this time.

Where MFM is not accurate, it is possible to use the full Cagniard-de Hoop method to calculate derivatives. Alternatively, by discretizing the t-p curves, it is possible to use Disc Ray Theory (Wiggins, 1976; Chapman, 1976) to compute derivatives. In both cases, it is necessary to modify the form of the derivatives somewhat, in the Cagniard case

to account for changes in the de Hoop contour and in the Disc Ray case to accommodate a continuous model. The basic inversion method, however, remains the same. The necessary modifications will be the subject of a later work.

Chapter 4

APPLICATIONS - THE FINE STRUCTURE OF THE CRUST-MANTLE TRANSITION IN THE BERING SEA

As an example of the application of the inversion technique presented in Chapter 3, we examine the structure of the crust-mantle transition using a Bering Sea refraction profile previously studied by Shor (1964) and by Helmberger (1968, 1976). We will assume the sub-bottom and crustal model of Helmberger (1976), shown in Figure 4.1, which was determined using travel time, amplitude and waveform data, and allow only the depth and thickness of the transition region to vary. As a good mantle headwave is observed, the mantle velocity is tightly constrained and need not be included in the inversion.

In order to obtain the effective source and instrument functions, we make use of the last seismogram before the onset of the triplication, at a distance of 26.5 km. Since the delta function response of the medium at this distance, excluding free surface effects and water reverberations, is expected to be nearly a delta function, we may feel reasonable confident in using this seismogram as our effective source function for greater distances. This assumes that shot sizes at these distances are the same and that the effects of changes in takeoff angle for the distances in question are small. Thus, the synthetic seismograms consist of the delta response of the medium at the appropriate distance convolved with the effective source function derived from the 26.5 km record. This effective source function contains the instrument and source functions, as well as free surface effects, effects of near source and near receiver

structure, and attenuation effects.

As a first example, we consider a noise free synthetic problem. The "data" seismograms were generated using the model of Helmberger (1976) shown in Figure 4.1. The starting model is shown in Figure 4.2. For the starting model, we have increased the thickness of the transition zone to 3 km, as compared to 2 km for the "data" model, and decreased the depth of the onset of the transition region. The transition region was divided into five layers in both cases, and six ranges, covering the most of the triplication, were used.

The inversion method used on this problem did not include the ($\delta s * \delta s$) term in equation (3.5), but did contain all other non-linear terms. As a result, some instability existed and convergence was somewhat slow. Even so, a good fit to the "data" was obtained by the 25^{th} iteration.

The progression of waveforms as the inversion proceeded may be seen in Figure 4.3. As may be seen, the amplitudes of the second arrivals are much too small in the starting model at all ranges. These amplitudes were improved considerably in the early iterations. However, it was not until the later iterations that relative timing and amplitude information was "fine tuned" sufficiently to give really close agreement in the fine structure of the waveforms.

A comparison of the data, starting and final waveforms is given in Figure 4.4. As may be seen, agreement in waveform is rather poor between the starting model and the "data", even though the arrival times of the second arrivals are quite similar. Excellent agreement in waveform has been obtained between the "data" and iteration 25.

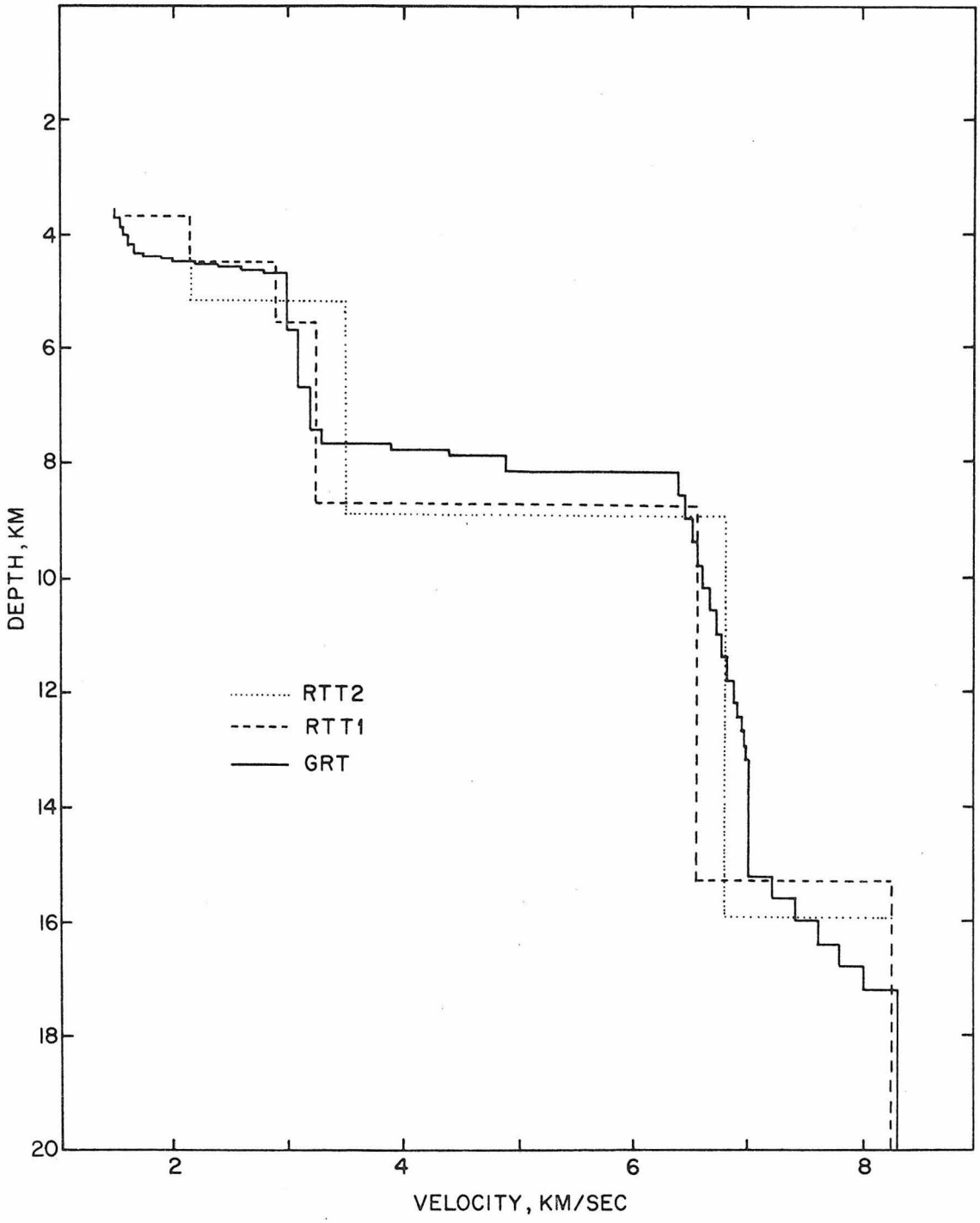

Figure 4.1. The crustal models of Helmberger (1976). The model GRT is based on travel time, amplitude, and waveform analysis. This crustal model is used in this study, with variations introduced in the depth and thickness of the crust-mantle transition region. Models RTT1 and RTT2 are based on travel times only.

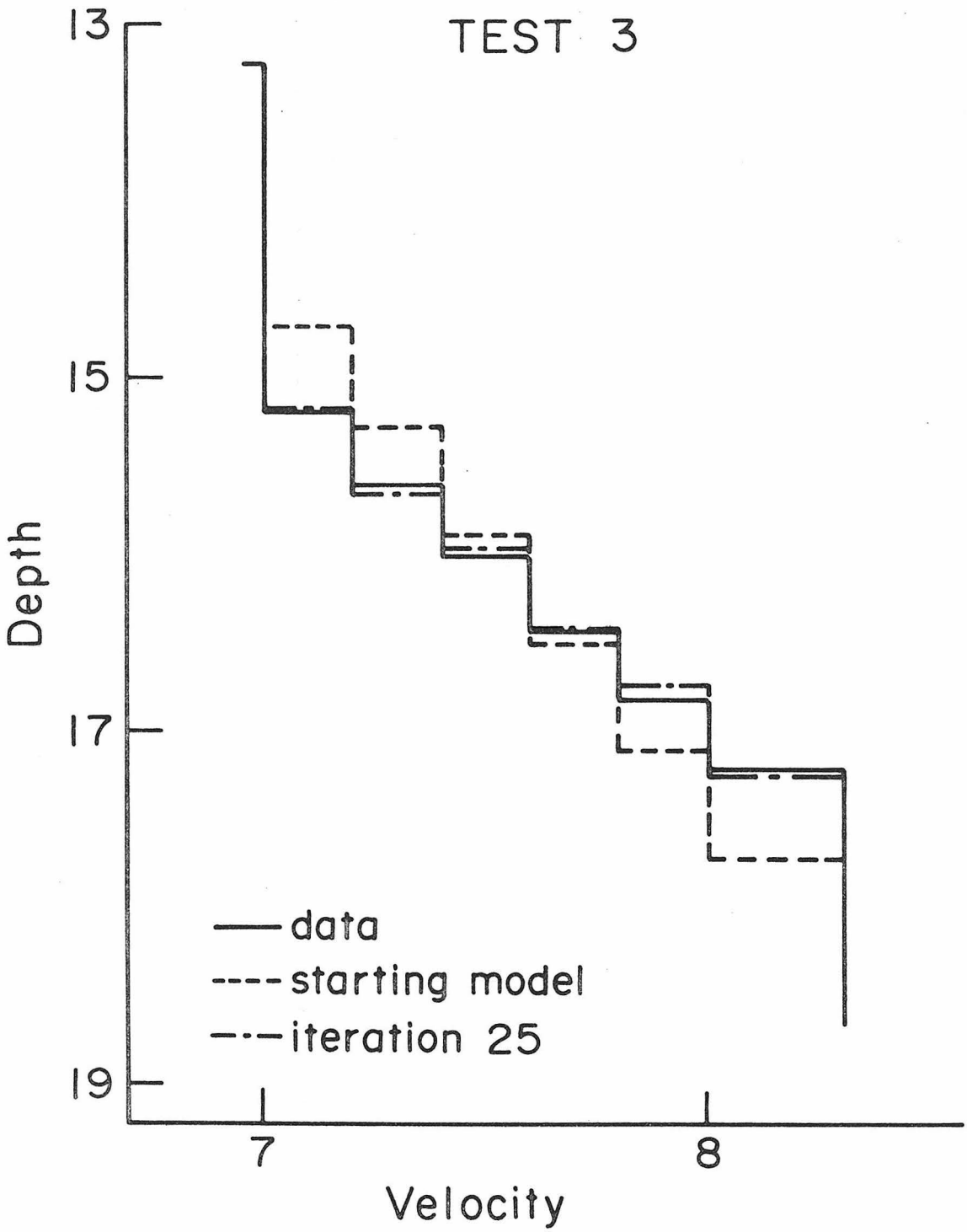

Figure 4.2. The structure of the transition region used in the test problem. Data seismograms were computed using the 2 km transition region. This is precisely the model GRT shown in Figure 1. The starting model used a 3 km transition zone. After 25 iterations, the model had returned to a good approximation of the starting model.

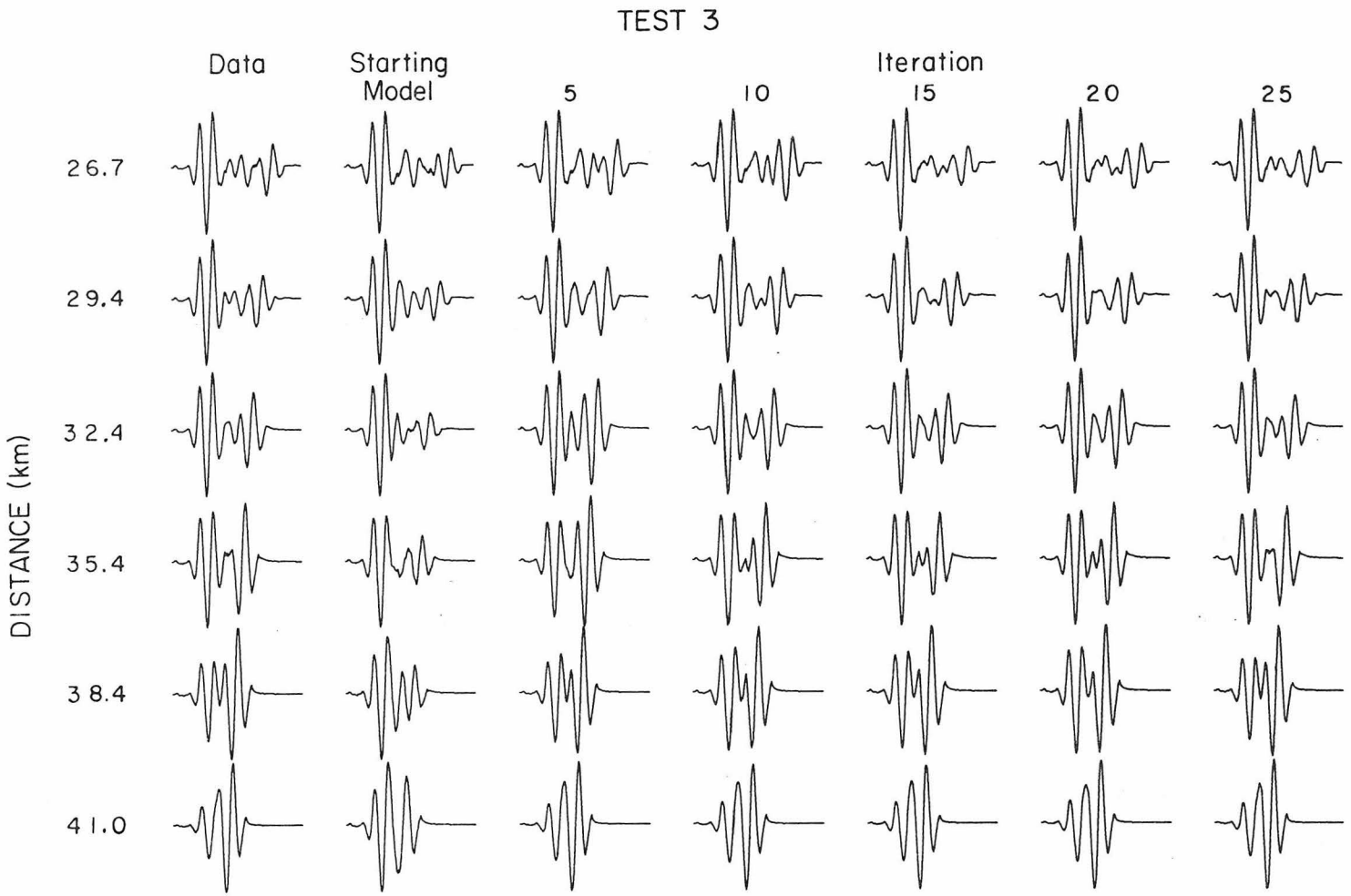

Figure 4.3. The progression of waveforms from starting model through iteration 25 for the test problem. Waveforms have been shown for each 5 iterations. Each waveform has been scaled independently to unit maximum amplitude.

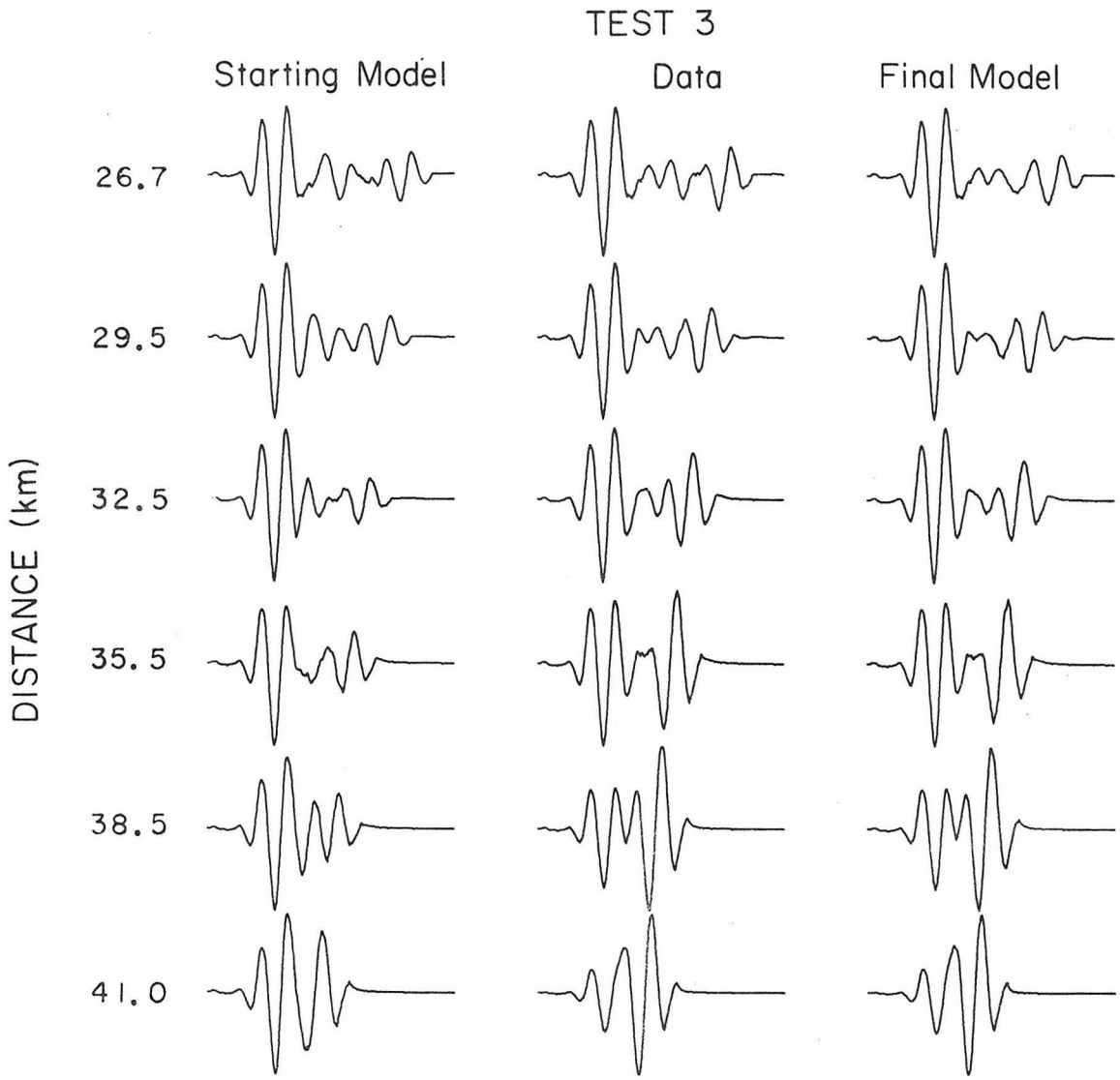

Figure 4.4. A comparison of the data, starting and final waveforms for the test problem.

As shown in Figure 4.2, the model has nearly returned to the "data" model.

Often, in working with real data, it is desirable to know the constraints that the data places on some model feature, rather than just knowing a single best-fitting model. Unfortunately, when the inverse problem is sufficiently non-linear to make an iterative method necessary, it is unlikely that the usual linear resolution analysis will be particularly meaningful. One possible means of determining model bounds is to use several extreme starting models which are known to bracket the acceptable model, where an acceptable model is one that produces an acceptable fit to waveform data. If the inversion procedure is overstabilized, then the first acceptable models generated by the inversion, together with the resolution matrices for those models, should provide a reasonably good idea of the bounds on the model feature in question. If, in fact, multiple iterations are required, it is probable that the model constraints are imposed primarily by the non-linearities in the problem. In this case, the set of first acceptable models itself probably provides a good idea of the bounds on the model.

This method was used to estimate the bounds on the thickness of the crust-mantle transition region for our Bering Sea profile. In this case, seismograms from five distances, again representing the onset of the triplication, were used. The starting models, down to the transition region, were once again the Helmberger (1976) model shown in Figure 4.1. Two starting models were used. The first of these, shown in Figure 4.5, contains a 3 km transition zone. The second,

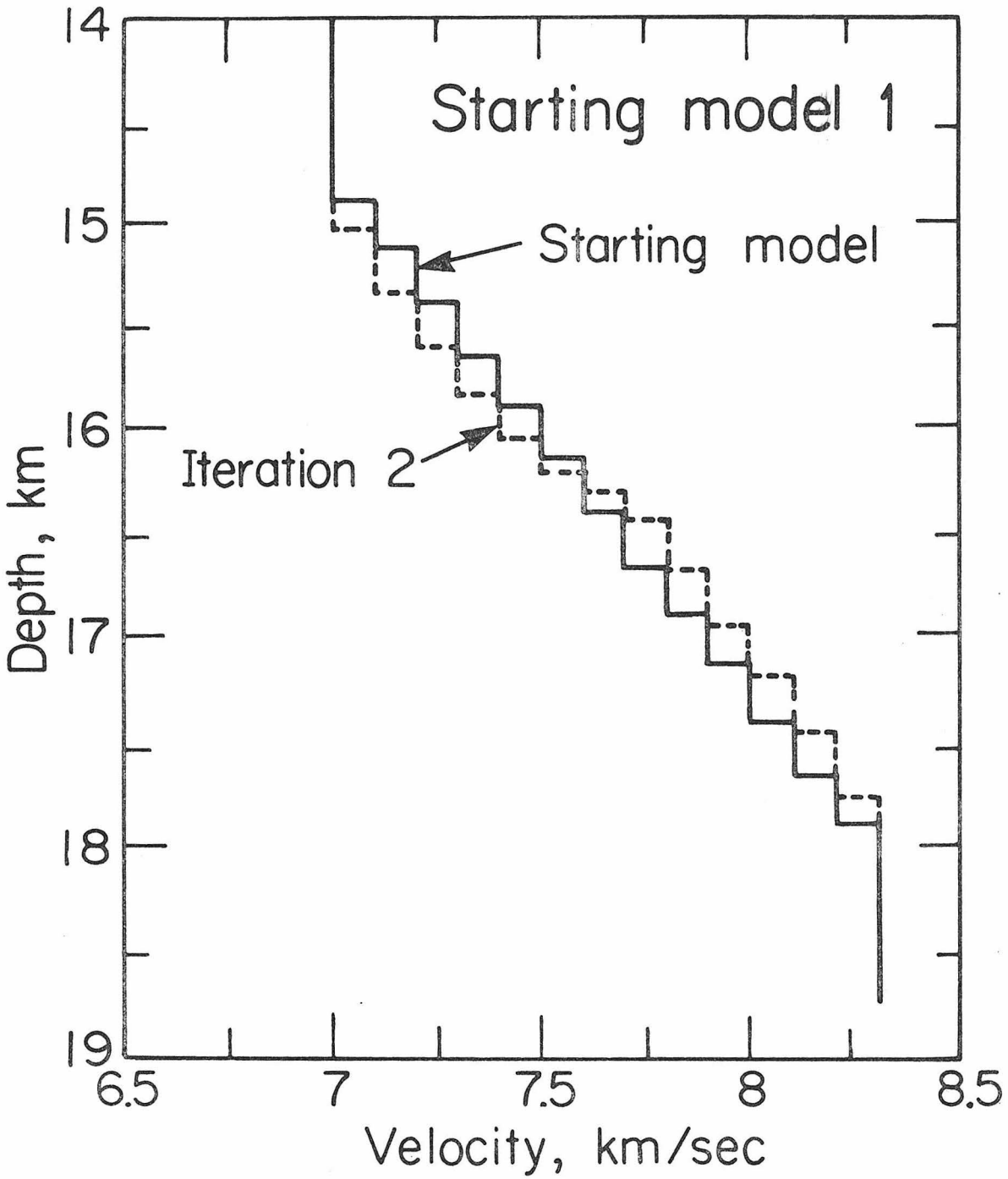

Figure 4.5. Starting model 1 and the resultant model after two iterations. The starting model has been chosen so that the transition region is too thick to fit the data.

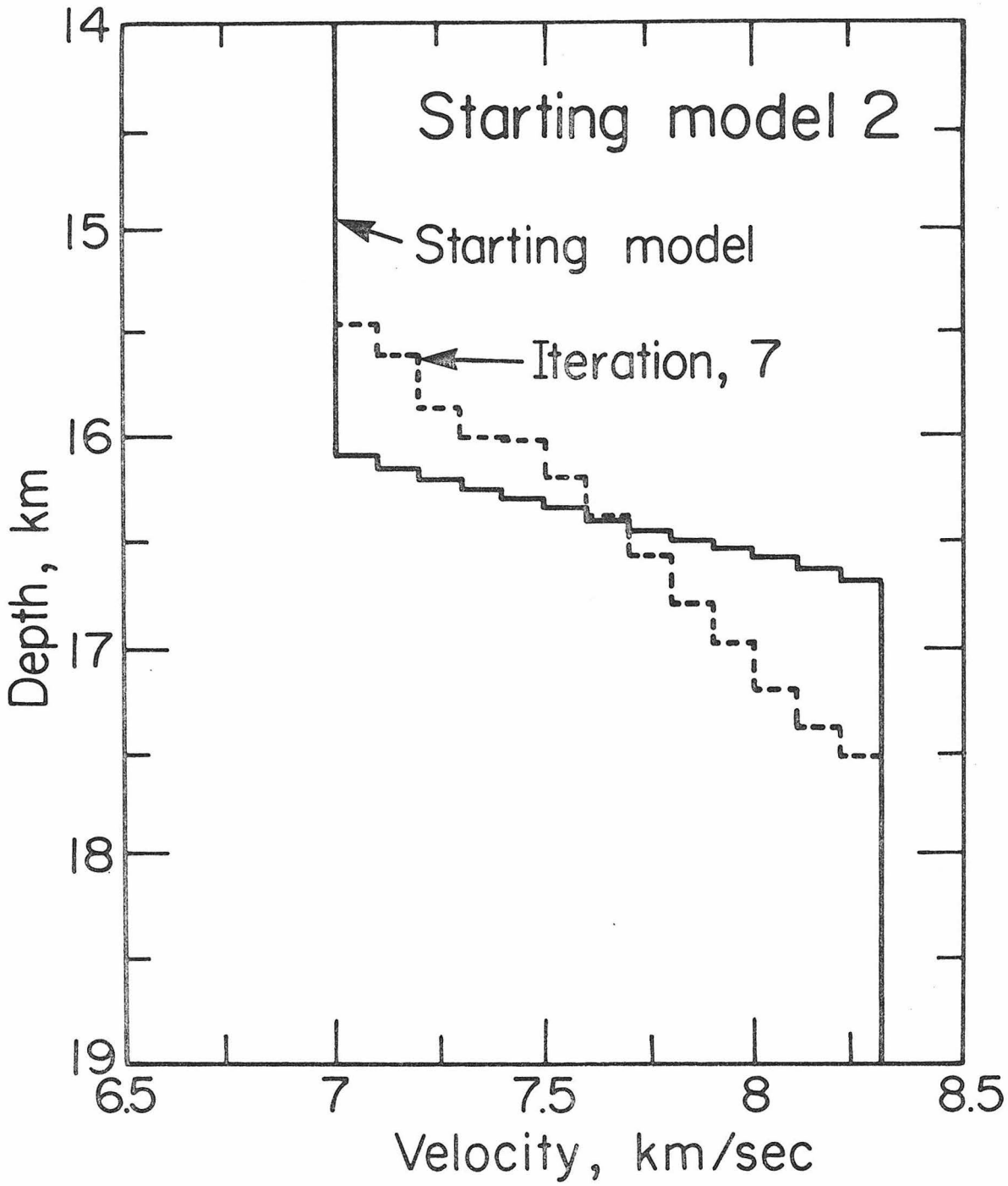

Figure 4.6. Starting model 2 and the resultant model after seven iterations. The starting model has been chosen to approximate model RTT1 in Figure 1.

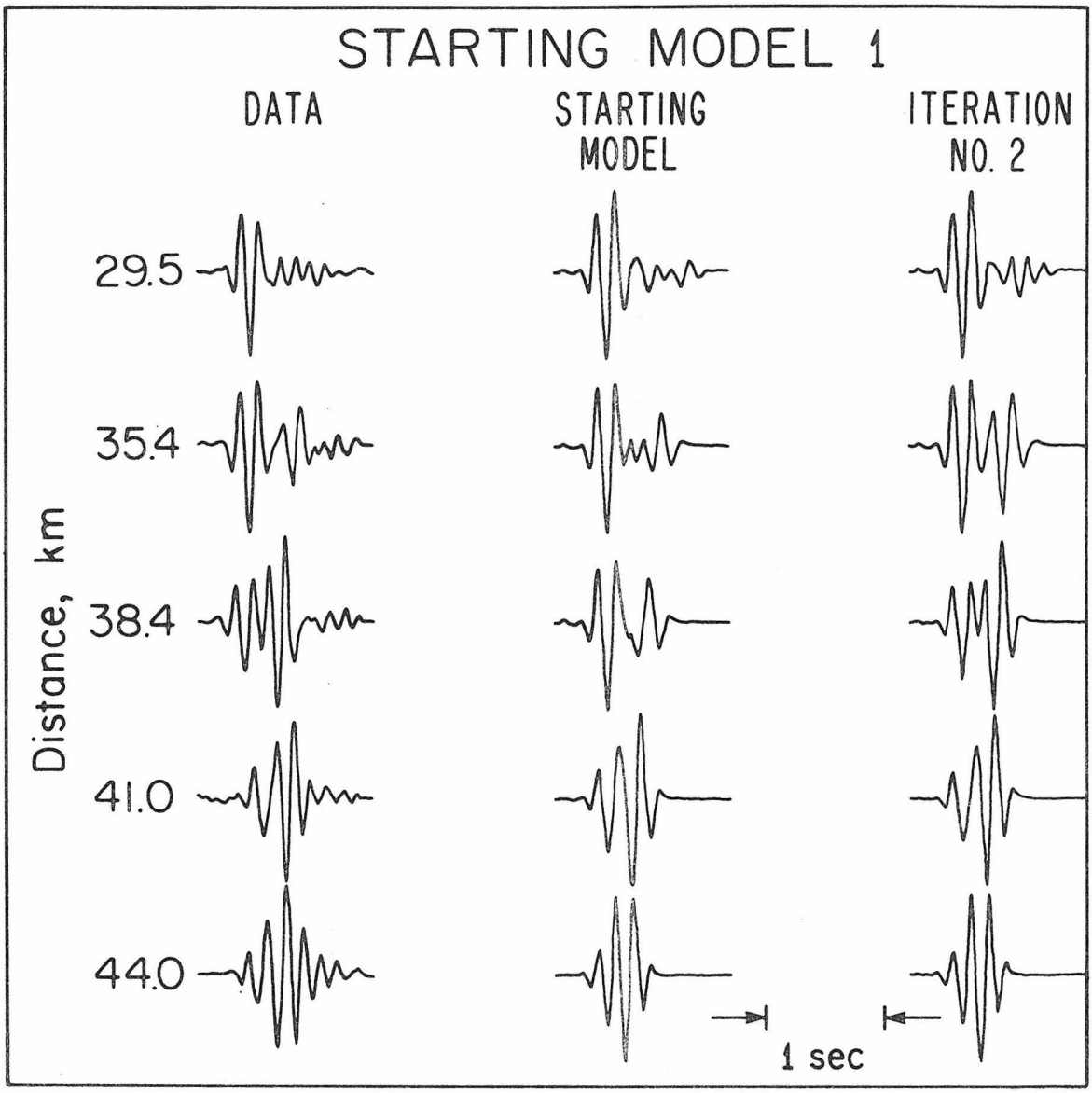

Figure 4.7. A comparison of the data, starting and final waveforms for starting model 1. All seismograms are independently scaled to unit maximum amplitude.

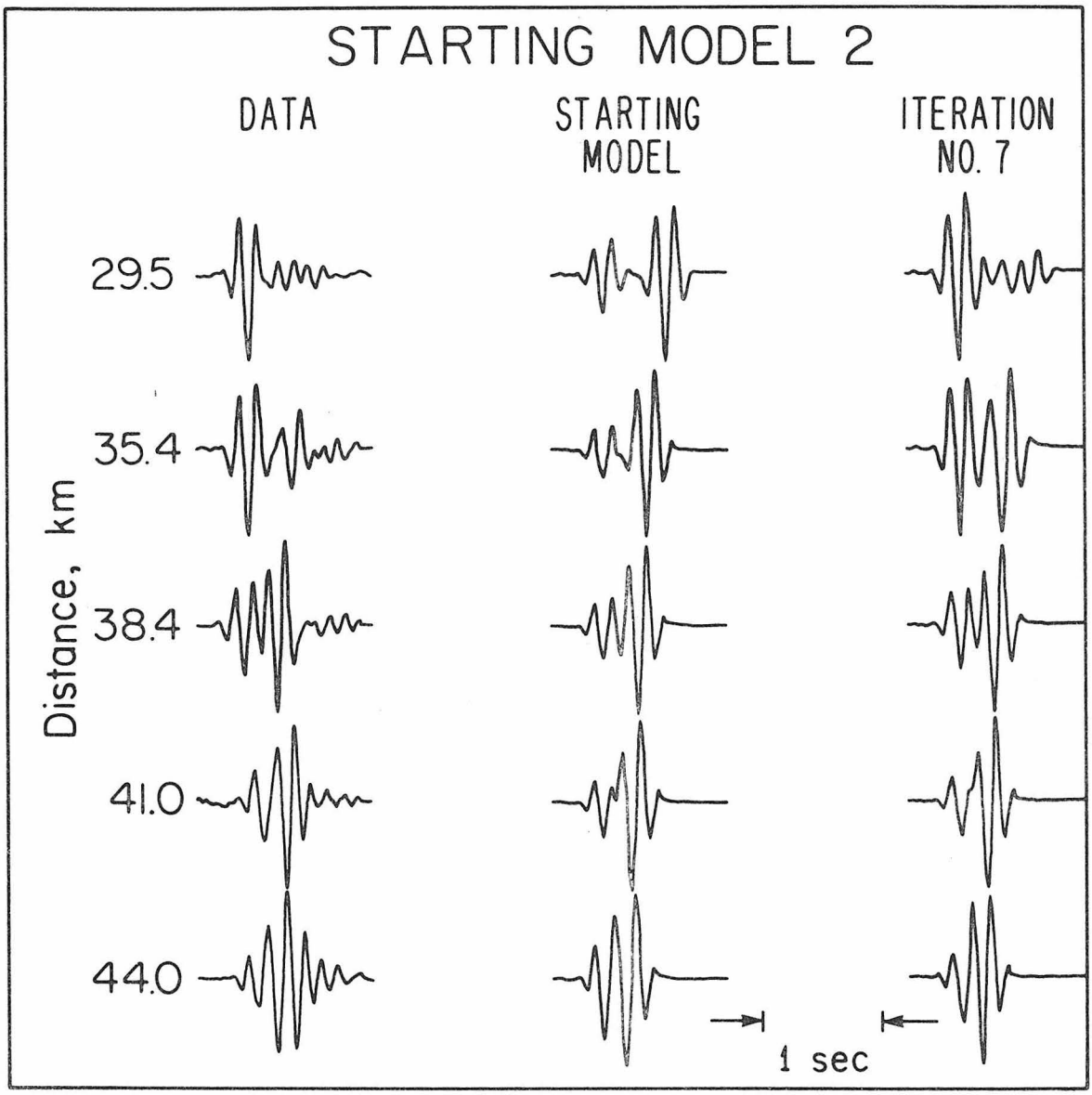

Figure 4.8. A comparison of the data, starting and final models for starting model 2. All seismograms are independently scaled to unit maximum amplitude.

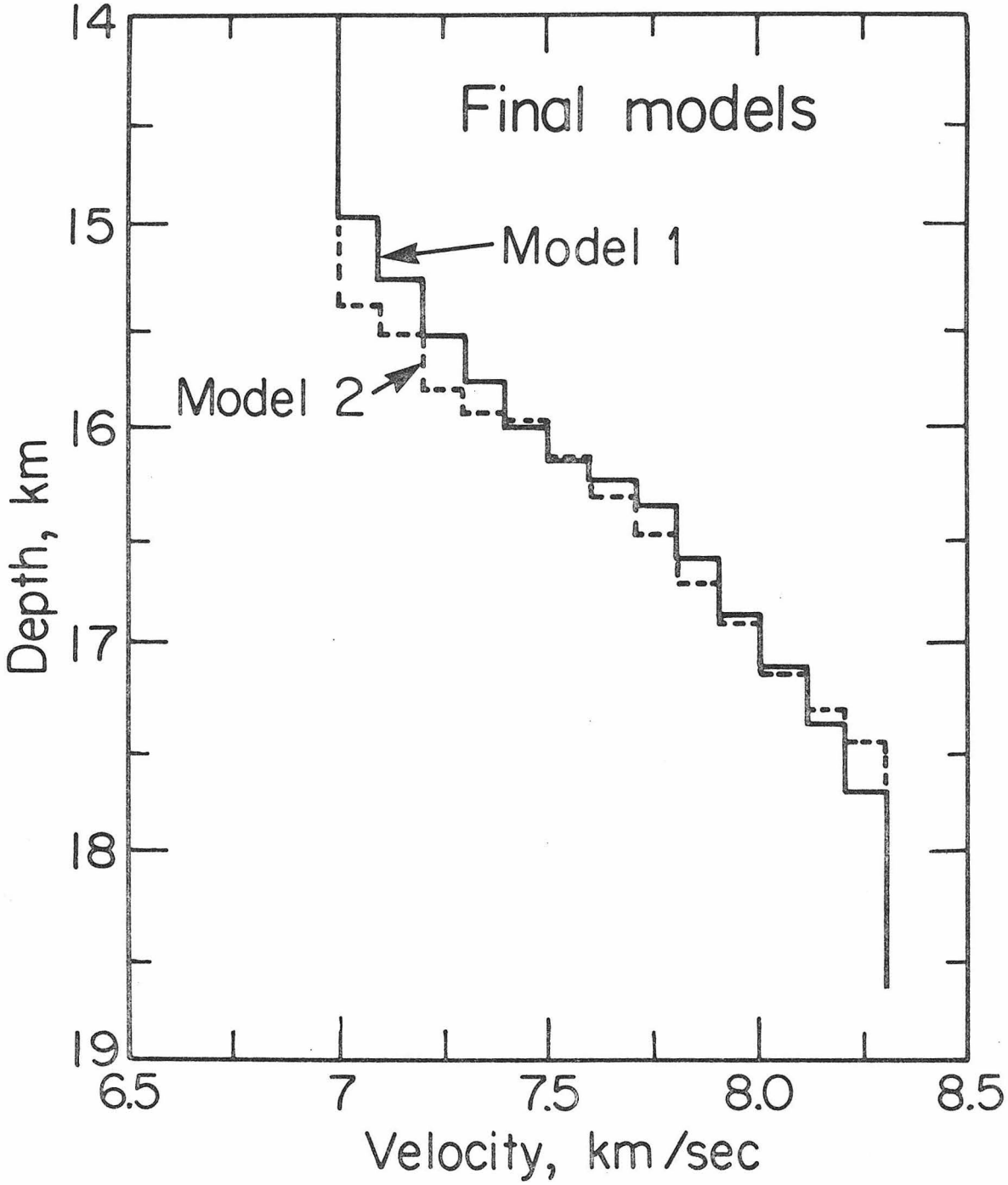

Figure 4.9. A comparison of the final models obtained through inversion starting from starting models 1 and 2. The close agreement obtained suggests that the model is closely constrained by the waveform data.

shown in Figure 4.6, contains a .6 km transition zone. The depth of the transition zone in this second model was chosen to make model 2 as close as possible to the model RTT1 in Figure 4.1. This model was taken from Helmberger (1976) and was determined solely on the basis of travel times. In both starting models, the transition region was divided into 12 layers, and in both cases all non-linear terms in equation (3.5) were used in the inversion.

In the case of starting model 1 an acceptable model was reached in just two iterations. A comparison of the data with the starting and final waveforms for model 1 is given in Figure 4.7. The second arrivals, clearly too small in the starting model, have increased in size in the final model. This was accomplished, as shown in Figure 4.5, by a slight decrease in the overall thickness of the transition region.

In the case of starting model 2, it took seven iterations to produce an acceptable model. A comparison of the data with the starting and final synthetic seismograms for model 2 is given in Figure 4.8. The second arrivals, clearly far too large relative to the first arrivals for the starting model, have been considerable reduced in size. This was accomplished by an increase in the thickness of the transition region, as shown in Figure 4.6.

It is interesting to compare the final models obtained from the two starting models. This is done in Figure 4.9. Despite the rather large difference in the starting models, the final models are quite similar. It is also interesting to note that for the distances used, that is, for the onset of the triplication, the amplitude of the

second arrival is least sensitive to the structure of the top portion of the transition region. This is precisely where the largest disagreement between the two models occurs. Thus, while it does not provide a proof, the closeness of the two models certainly suggests that the waveform data tightly constrain the thickness of the transition region.

For two significantly different starting models, we might expect that waveform errors in the final models would be significantly different. Indeed, in final model 2 the second arrivals are too large compared to the first arrival, as they were in the starting model. For model 1, the second arrival at 38.4 km and 41.0 km is very slightly too small realtive to the first arrival, as it was for the starting model. At 35.4 km, however, the second arrival is too large though still considerable smaller than in model 2. This suggests that either there is a systematic bias in the inversion procedure or that the seismogram at 35.4 km is inconsistant with the other data. Despite a considerable number of inverse and forward calculations, no model has yet been found that simultaneously fits the 35.4 km record and the 38.4 km and 41.0 km records. This supports the hypothesis that the 35.4 km record is somehow inconsistent with the other data, possibly due to the presence of lateral heterogeneity. This hypothesis is also supported by the 32.4 km record, which has a second arrival larger than the one at 35.4 km. This record was not included in the inversion due to the fact that the shot was clearly smaller than others in the series but still provides some indication that the second arrival at 35.4 km is too small.

No model tried has as yet been able to produce the extra cycle of ringing in the 44.0 km record either. Once again there is some indication that the record may be anomalous. The spacing between time marks on this record changes by about a factor of two while the seismogram is being recorded. Even though a correction was applied to remove this time compression, it is not known whether conditions causing the change in time scale caused other anomalies as well.

Despite the errors at these two ranges, the inversion procedure has, on the average, done a good job in fitting the waveform data. This once again points out the advantages and disadvantages of a least squares, as opposed to an exact, inversion. It is never possible, using a least squares method, to prove that a datum is inconsistent. The method will, however, often produce a reasonable model that gives a good average fit to the data, rather than a wildly improbable model which may fit the data exactly.

It should be noted that the examples that have been presented are cases in which the inversion method has succeeded. As with most iterative methods, this inversion procedure fails if the starting model is sufficiently bad. Experience has shown that failure can occur if a major arrival has an arrival time that is consistently more than instrument period in error. This condition can sometimes be corrected simply by low pass filtering the data and synthetics, thus effectively providing a longer period instrument. This works best with broad band data. Alternatively, one may pick starting models that satisfy the relative travel times of the data. This can usually be done quite simply.

The necessity of having reasonably good travel times in the starting model suggests a possible means of using the waveform inversion. We choose starting models from extremal models generated through travel time inversion (Bessonova et al., 1974). Waveform inversion may then be used to refine the bounds determined by the travel time inversion. This assures us of having starting models that are sufficiently close, and further provides a means of finding starting models that bracket the actual solution.

CONCLUSION

We have developed an iterative method for the determination of earth structure by the inversion of bodywave waveforms. This method makes use of the inherent non-linearities of the problem to stabilize each iteration. Through the selection of several starting models, it is possible to not only find a model which fits the waveform data, but to explore the resolution of specific model features.

The inversion appears to be particularly well suited to the study of the fine structure of regions which control the onset of triplications. We have therefore used it to study the fine structure of the crust-mantle transition using a Bering Sea refraction profile. The results demonstrate that very good resolution of such transition regions may be obtained using a combination of travel time and waveform data, even when such data are both sparse and noisy.

Chapter 5

DETERMINATION OF SOURCE PARAMETERS BY INVERSION ON BODY-WAVE WAVEFORMS

INTRODUCTION

The body-wave propagation problem discussed in Chapter 2 is an example of a situation in which synthetic seismograms may be expressed as a convolution of smooth functions with a sum of highly localized "rays". When the functional dependence of the amplitude and arrival times of these rays on the model parameters is sufficiently simple, the inversion procedure developed in Chpater 3 becomes applicable. Another example of such a situation is the estimation of earthquake source parameters for shallow earthquakes using long period teleseismic body-wave seismograms.

The forward problem of modeling shallow earthquakes using point shear dislocations in a layered halfspace has been treated by Langston and Helmberger (1975). We shall use their results for the forward problem in order to express changes in an error function in terms of changes in model parameters, much as was done in Chapter 3 for the structure inversion problem. We may then use the apparatus developed in Chapter 3 to develop an iterative procedure for the estimation of source parameters.

THE SOURCE INVERSION

For simplicity, we consider the case of a p-wave arrival for a single point source. Langston and Helmberger (1975) show that a synthetic seismogram $s_i(t)$ may be written as

$$s_i(t) = \frac{M_0}{4\pi\rho} \sum_j R_j(p_i) \sum_{k=1}^{3} A_k(\theta,\lambda,\delta)\, C_k(p_i)\, \delta(t-t_i^0-t_{ij}) \qquad (5.1)$$

$$* \; Q(t) * I_i(t)$$

where the j summation is over all near source reflections and mode conversions that arrive within the designated time window, p_i is the direct wave ray parameter, $R_j(p_i)$ is the product of transmission and reflection coefficients appropriate for that ray, together with the geometric spreading corrections for the converted rays, t_i^0 is the arrival time of the direct ray, and t_{ij} is the additional travel time for the reflected and converted rays. The functions A_k (θ,λ,δ) and C_k are given in Langston and Helmberger (1975), and are reproduced in Appendix 1 for convenience. The function Q(t) is the far-field source time function and $I_i(t)$ is the effective instrument function, which contains all receiver effects, propagation effects and attenuation effects as well as the instrumental transfer function. If Q(t) has unit area, then M_0 is the seismic moment.

We have used the approximation in equation (5.1) that all rays have the same ray parameter. This proves to be a very good approximation for shallow sources at teleseismic distances. We further assume that there is no change in ray parameter for a change in source depth. Then, as long as the source is not moved across a layer boundary, we see that the amplitude of a ray is dependent only on the strike, rake and dip (θ,λ,δ) of the fault. The travel time of a ray is dependent only on the source depth, h. This is somewhat different than in the structure problem, where both amplitudes and travel times were dependent on layer thickness.

The other difference between the source and structure inversion problems is the far-field time function Q(t). For the source inversion this function is one of the model variables. There is no analogous variable in the structure problem. Rather than perturbing the continuous function Q(t), we will consider the discretely sampled version of the perturbation, $\delta Q(m\Delta t)$ where Δt is the time spacing used in the digital synthetic seismogram and m is an integer. Thus, we now have a finite number of model parameters $\delta Q_m \equiv \delta Q(m\Delta t)$. Depending on the time spacing used and the length of the far field time function needed, this may result in a quite large number of model variables. In practice it is usually preferable to specify some parametric form for Q(t). In this case, it is a fairly easy matter to calculate changes induced by changes in a time function parameter from knowledge of change induced by the δQ_m's.

We wish to determine the relationship between changes in the source parameters and changes in the error function d_i defined by equation (3.2). Using equation (3.7), we see that this reduces to evaluating

$$\delta I = \left(x \star \delta s_i\right)(0) \tag{5.2}$$

for arbitrary x(t).

From (5.1) we have

$$\left(s+\delta s\right)\left(t+t_i^0+\delta t_i^0\right) \approx \frac{m_0}{4\pi\rho} \sum_j R_j(p_i) \left[\sum_{k=1}^{3} A_k(\theta,\lambda,\delta) + \sum_{m-1}^{3} \frac{\partial A_k}{\partial \theta_m} \delta\theta_m\right] \cdot$$

$$\delta(t-t_{ij}-\delta t_{ij}) * \left(Q(t)+\delta Q(t)\right) * I_i(t) \tag{5.3}$$

where we have used $(\theta_1,\theta_2,\theta_3) = (\theta,\lambda,\delta)$ for convenience.

Since the travel time is of no consequence for source inversion,

we use t_i^0 as a reference time. That is, we realign the perturbed seismogram so that the direct arrival aligns with the direct arrival of the unperturbed seismogram. The time shift parameter, τ_i, from Chapter 3 now refers to shifts relative to the direct arrival time, rather than shifts in absolute travel time. If no layer boundaries are crossed, we may write

$$\delta t_{ij} = \gamma_{ij}\ \delta h \tag{5.4}$$

where γ_{ij} is a function of the vertical component of slowness. For example, if the source is located in the top layer, with p-wave velocity c_α and s-wave velocity c_β, then for the phase pP, we have

$$\delta t_{ij} = \gamma_{ij}\ \delta h = 2\eta_\alpha(p_i)\ \delta h$$

with

$$\eta_\alpha = \left(\frac{1}{c_\alpha^2} - p^2\right)^{1/2}$$

For the phase sP we have

$$\delta t_{ij} = [\eta_\alpha(p_i) + \eta_\beta(p_i)]\ \delta h.$$

Using equations (5.1), (5.3) and (5.4) we find, to first order

$$\begin{aligned}\left(x \star \delta s_i\right)(0) \approx \frac{M_0}{4\pi\rho} \sum_j R_j(p_i) \Bigg[&\left(\left(Q*I_i\right) \star x\right)(t_{ij}+t_i^0) \cdot \sum_{k,m} \frac{\partial A_k}{\partial \theta_m}\,\delta\theta_m \\ &+ \left(\left(Q*I_i\right) \star \frac{\partial x}{\partial t}\right)(t_{ij}+t_i^0) \cdot \sum_k A_k \gamma_{ij}\,\delta h \\ &\sum_k A_k \sum_m \delta Q_m\ I_i * Q\ (t_i^0+t_{ij}+m\Delta t)\Bigg]\end{aligned} \tag{5.5}$$

As in Chapter 3, we use terms in $(\delta t_{ij})^2$ to provide stability in the inverse problem. Including these terms, we find

$$\begin{aligned}
\left(x * \delta s_i \right)(0) \approx \frac{M_0}{4\pi\rho} \sum R_j(p_i) \quad & \left(\left(Q * I_i \right) * x \right) (t_{ij}+t_i^0) \cdot \sum_{k,m} \frac{\partial A_k}{\partial \theta_m} \delta\theta_m \\
+ & \left(\left(Q * I_i \right) * x \right) (t_{ij}+t_i^0) \cdot \sum_k A_k \gamma_{ij} \, \delta h + \\
1/2 & \left(\left(Q * I_i \right) * \frac{\partial^2 x}{\partial t^2} \right) (t_{ij}+t_i^0) \cdot \sum_k A_k \gamma_{ij}^2 \, \delta h^2 + \\
& \sum_k A_k \sum_m \left(I_i * x \right) (t_i^0+t_{ij}+m\Delta t) \, \delta Q_m
\end{aligned} \tag{5.6}$$

where we include terms in δh^2 only if they increase the error function. We note that δt_{ij}^2 terms affect only δh and no other model parameters. Stabilization of other model parameters must come from the $(\delta s * \delta s)$ term in equation (3.7) or from an imposed model correlation function.

Substituting (5.6) into (3.7) we find

$$\begin{aligned}
\delta d_i \approx \frac{M_0}{4\pi\rho} \sum_j R_j(p_i) \Bigg[& -F_i(t_{ij}) \sum_{k,m} \frac{\partial A_k}{\partial \theta_m} \partial\theta_m - \frac{\partial F_i}{\partial t} (t_{ij}) \sum_k A_k \gamma_{ij} \delta h \\
& -1/2 \, \frac{\partial^2 F_i}{\partial t^2} (t_{ij}) \sum_k A_k \gamma_{ij}^2 \delta h^2 - \sum_m \sum_k A_k G_i \, (t_i^0+t_{ij}+m\Delta t) \, \delta Q_m + \\
& + J_i (t_{ij}) \sum_{k,m} \frac{\partial A_k}{\partial \theta_m} \delta\theta_m \, \delta\tau_i + \frac{\partial J_i}{\partial t} (t_{ij}) \sum_k A_k \gamma_{ij} \delta h \, \delta\tau_i \\
& + \sum_m \sum_k A_k K_i \, (t_i^0+t_{ij}+m\Delta t) \, \delta Q_m \delta\tau_i + \frac{c_i M_0}{8\pi\rho} \sum_q R_q(p_i) \\
\Bigg(& \sum_{k,m} \sum_{r,s} \frac{\partial A_k}{\partial \theta_m} \frac{\partial A_r}{\partial \theta_s} M_i \, (t_{ij}-t_{iq}) \, \delta\theta_m \, \delta\theta_s + \\
& \sum_{k,m} \sum_{r,s} A_k A_r N_i \, (t_{ij}-t_{iq}+\Delta t(m-s)) \, \delta Q_m \delta Q_s +
\end{aligned} \tag{5.7}$$

$$2\sum_{k,m}\sum_{r,s}\frac{\partial A_k}{\partial\theta_m}A_r\,O_i\,(t_{ij}-t_{iq}-s\Delta t)\,\delta\theta_m\delta Q_s + \sum_k\sum_r A_k\,A_r\,\gamma_{ij}\,\gamma_{iq}\,\frac{\partial^2 M_i}{\partial t^2}\,(t_{ij}-t_{iq})\,\delta h^2\Big)\Big]$$

$$-1/2\,\frac{\partial}{\partial t^2}\left(\hat{f}_i(t-\tau_i) - c_i\,\hat{s}_i(t)\right)(0)\,\delta\tau_i^2$$

with

$$F_i(t) = \frac{(Q*I_i)\star\left(\hat{f}_i(t-\tau_i) - c_i\hat{s}_i(t)\right)}{\left((s_i*s_i)(0)\right)^{1/2}}$$

$$G_i(t) = \frac{I_i\star\left(\hat{f}_i(t-\tau_i)-c_i\hat{s}_i(t)\right)}{\left((s_i*s_i)(0)\right)^{1/2}}$$

$$J_i(t) = \frac{Q*I_i\star\left(\frac{\partial\hat{f}_i}{\partial t}*\hat{s}_i\right)}{\left((s_i*s_i)(0)\right)^{1/2}}$$

$$K_i(t) = \frac{I_i\star(\frac{\partial\hat{f}_i}{\partial t}*\hat{s}_i)}{\left((s_i*s_i)(0)\right)^{1/2}}$$

$$M_i(t) = \frac{(Q*I_i)\star(Q*I_i)}{s_i*s_i(0)}$$

$$N_i(t) = \frac{I_i\star I_i}{s_i*s_i\,(0)}$$

$$O_i(t) = N_i * Q$$

Equation (5.7) is of the same form as equation (3.32). It may therefore be inverted in the same manner.

DISCUSSION

While we have formulated the source inversion for a single source,

the inclusion of additional sources is straightforward, if somewhat tedious. This may be done by introducing a second set of source parameters, with additional new parameters describing the location of the additional source and its starting time relative to the first source. If source time functions are described parametrically, then parameters representing the relative amplitudes of the time functions must be included. Interaction between sources occurs through the $\delta s * \delta s$ term in (3.7) only.

The possible multiplicity of sources in fact represents the major uncertainty in the source inversion procedure. It is in fact often not possible to discriminate between near source structural effects and multiple sources using only far-field bodywave data. Thus, in the absence of near-field data or near source crustal studies, complications in the later portion of the data seismograms may be explained either by crustal structure or source multiplicity. Both possibilities must often be explored.

It should be noted that the major non-linearity in the source inversion is caused not by the double couple representation used in this inversion method, but rather by the fact that source parameters control both the arrival time and amplitude of arrivals. Thus, while use of a moment tensor formulation allows a linear inversion to be done (Stump and Johnson, 1977), it does so only at the expense of having to assume the source depth and source time function. Due to the major role played by source depth in the seismograms of shallow earthquakes, this is probably not a satisfactory approach. It is possible, however, that an iterative approach based on this method

which allows for determination of source depth and time function will prove both stable and efficient.

As may be seen from equation (5.7), the inclusion of even the low order non-linear terms leads to a rather complicated expression. Since the forward source problem is computationally much faster and simpler than the forward structure problem, we no longer have a situation where it is advantageous to compute large numbers of second derivatives in order to minimize the number of error function evaluations necessary. Instead, it may be possible to obtain adequate stability through use of a simplified version of the $\delta s \star \delta s$ term in (5.7), particularly when a parametric form of the source time function is used. The rather poor convergence properties and the stability problems encountered in attempting to use only the linear equations given in (5.6), however, indicate that some use of non-linear terms to provide stability is still highly advantageous. Exactly which form of inversion yields the best results is unknown at this time, but it appears that even use of the full form of equation (5.7) is preferable to a linear partial step method.

Chapter 6

APPLICATION - THE BORREGO MOUNTAIN EARTHQUAKE

INTRODUCTION

Since the introduction of simple theoretical fault models, many investigators have attempted to infer details of earthquake faulting by comparing far-field bodywave recordings with model predictions. They have found that most deep and intermediate events have simple wave shapes which can be easily explained with smooth dislocation models (Mikumo, 1971a, b; Teng and Ben Menahem, 1965; Burdick and Helmberger, 1974) but that shallow earthquakes have very complex wave forms. Until recently, this was interpreted to mean that shallow events have fundamentally more complex fault surfaces and time histories. By determining the response of a layered half-space to a shallow double-couple point source, Helmberger (1974), Fukao (1971), and Hudson (1969), among others, have shown that this interpretation is not entirely correct because much of the wave-form complexity is caused by the interaction of the source with the free surface. Thus, it will once again be worthwhile to address the question of whether or not a smooth dislocation is appropriate for shallow earthquakes. This time, however, the free-surface interaction should be included in the analysis.

Many of the previous investigators of body waves from shallow events have focused their attention on the Fourier transform of the entire body-wave pulse. They employed a technique which enabled them to determine important source parameters such as seismic moment, stress drop and source dimensions from the rough characteristics of the amplitude

spectrum (Hanks and Wyss, 1972; Wyss and Hanks, 1972a,b; Molnar and Wyss, 1972; Molnar et al., 1973). Since the reflected or converted phases such as pP, sP or sS can affect both the long-period level and the shape of the amplitude spectrum, it will be important to see if the results change when the free surface is correctly accounted for.

Langston and Helmberger (1975) have outlined a simple procedure for including the surface interaction in the computation of a synthetic seismogram for a model of a shallow dislocation source. In other words, they have presented a tractable solution to the forward problem of computing the data given the model. We have demonstrated in Chapter 5 that the existence of a solution to the forward problem along with a quantitative method for comparing the synthetic to the actual data make it possible to solve the inverse problem; that is, an optimal fault model can be determined from the data by an iterative inverse technique. We present here the result of the application of the inversion technique to the Borrego Mountain earthquake of April 9, 1968. We present a final model which accurately predicts all of the observed wave forms. We then use the model to identify a single, strong arrival in the record, and finally we interpret the shape of this basic seismic pulse in terms of a smooth dislocation model.

THE BORREGO MOUNTAIN EARTHQUAKE

The Borrego Mountain event was a magnitude 6.4 strike-slip earthquake which occurred at 02:29 GMT April 9, 1968 on the Coyote Creek fault in southern California. Figure 6.1 shows the location of the main shock as well as many of the aftershocks and the trace of ground

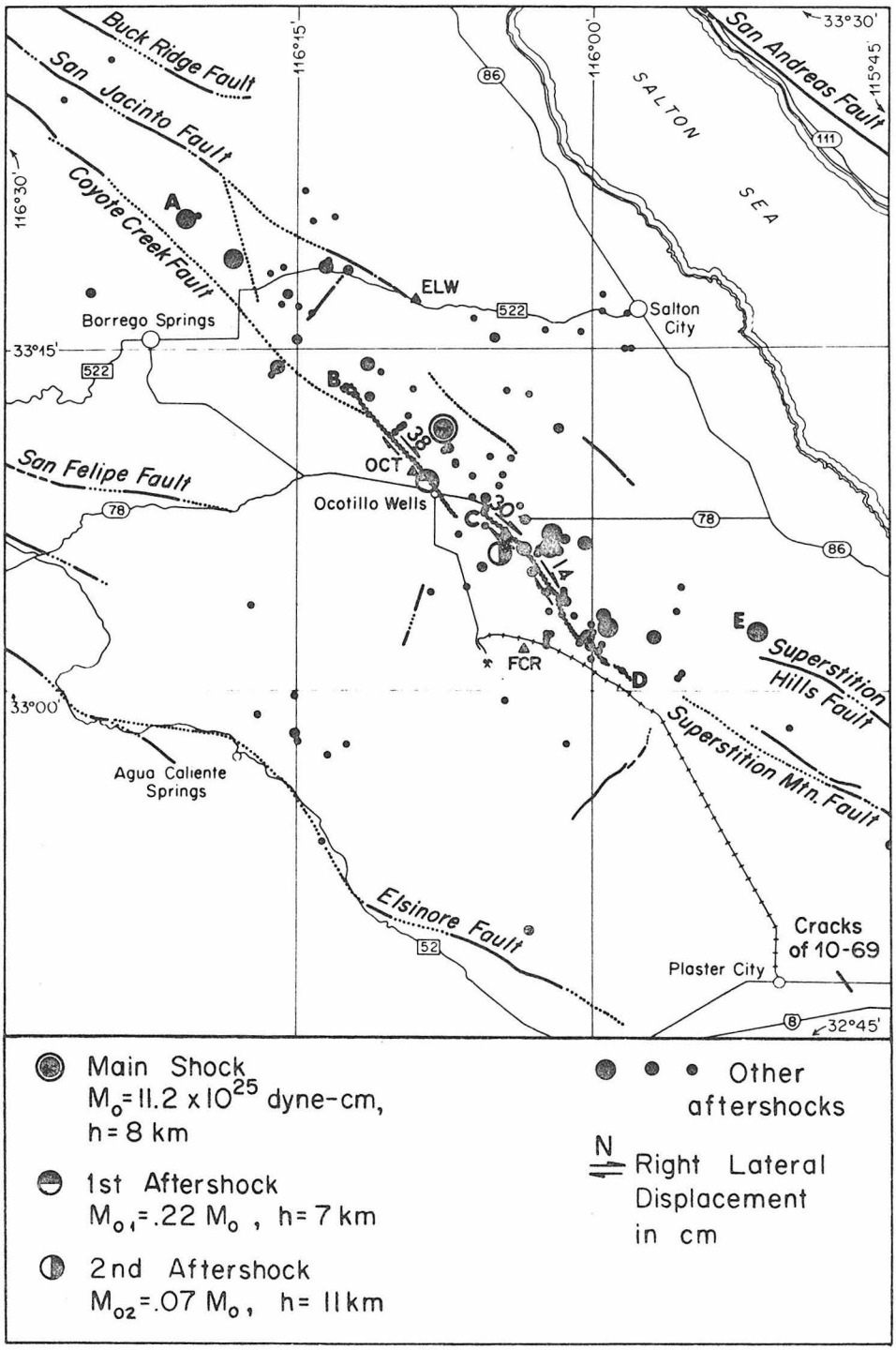

Figure 6.1. The Borrego Mountain Tectonic Zone: Segment AE∿55 km marks the extent of the aftershock zone and BD∿31 km the total rupture length. Segment BC radiated most of the energy in the main shock. The length of this segment plus the 8 km depth of the main shock motivated the choice of a circular fault model with radius 8 km. Segment CD∿17 km was probably due to a swarm type event. (Figures 1 and 2 modified from Allen and Nordquist, 1972).

breakage. After the event, both the California Institute of Technology and the U.S.G.S. undertook a thorough study of all major types of postseismic phenomena. From their observations, we can draw two important conclusions which bear heavily on our interpretation of what happened during the earthquake. The first is that even though the ground breakage appears simple, the pattern of stress release was probably very complex. This can be inferred from the following points: (1) In the Imperial Valley, the San Andreas fault splays out into a number of closely interrelated faults. Each nearby zone of weakness contributes to the complexity of the stress pattern near the Coyote Creek fault (Sharp, 1972). (2) Surface offsets were observed on the Imperial, Superstition Hills and San Andreas faults as well as the Coyote Creek fault (Allen et al., 1972). (3) The aftershocks had a very diffuse spatial pattern. It defined only a broad three-dimensional region of stress release instead of a single plane of failure (Allen and Nordquist, 1972; Hamilton, 1972). This complex prestress pattern seems to manifest itself in some unusual aftershocks occurring immediately after the main shock.

The second conclusion which can be made from the postseismic observations is that there was a clear difference in the behavior of the north break (segment BC in Figure 6.1) and the south break (segment CD in Figure 6.1). The north break had a large initial surface offset, relatively few aftershocks and very little postseismic creep. The south segment had a small initial offset, more aftershocks, and as much postseismic as coseismic displacement (Allen and Nordquist, 1972; Clark, 1972; Burford, 1972). Evidence in the body waves shows that

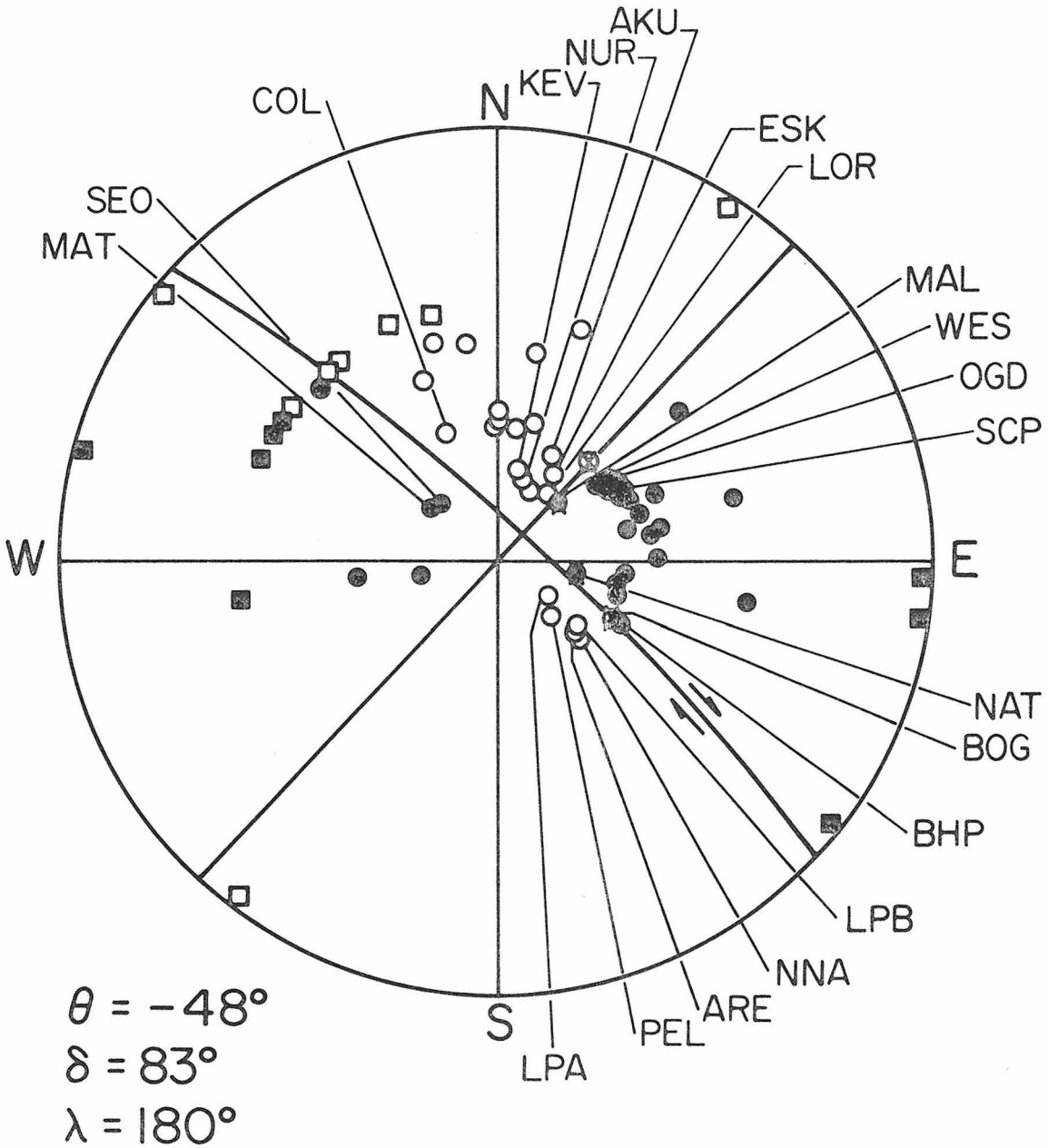

Figure 6.2. The stations used in this study as they distribute with respect to the fault plane solution determined by Allen and Nordquist (1972). Unlabeled points are other stations which they used in their first motion study. θ is the fault strike, δ the dip and λ the rake.

these variations reflect different behaviors deep in the Earth.

THE DATA SET

The data set used in the inversion procedure was selected from the P and SH body-wave forms recorded at stations in the World Wide Seismograph Station Network. Recordings made outside the epicentral range of 30 to 90° were excluded to circumvent problems with upper mantle or core structure, and recordings with a signal-to-noise ratio of less than 5:1 were excluded to reduce difficulty with background noise. Processing noise was kept to a minimum by digitizing each record ten times and averaging the results. The names and locations of the stations which had records of acceptable quality are listed in Table 6.1 and their azimuthal spread shown in Figure 6.2. The stations are plotted along with the first motion data and the fault planes determined by Allen and Nordquist (1972). It is regrettable that no high-quality wave-form data were available to the southwest of the event but there was sufficient coverage to impose some heavy constraints on the allowable source mechanism. The observed waveforms are the top traces shown in Figure 6.5.

MODEL PARAMETERIZATION AND INVERSION

The first step in applying linear inversion theory to a problem is to formulate a technique for computing theoretical values for the observed data from a finite number of model parameters. In the Langston and Helmberger (1975) procedure for computing synthetic seismograms for a point dislocation source, the basic parameters are a time function, source depth, and the three fault orientation

Table 6.1

STATION LOCATION AND AMPLITUDE DATA

Stn.	Azimuth from North	Wave Type	Moment $\times 10^{-25}$ dyne-cm	ϕ	Relative Deviation of M_o from Average
MAT	309°	P	17.2	6°	.53
SEO	315°	p	16.0	0°	.42
COL	338°	P	12.3	23°	.09
KEV	13°	P	12.1	58°	.08
KEV	13°	SH	9.5	58°	- .15
NUR	18°	P	13.6	63°	.21
UME	18°	SH	11.2	63°	.00
AKU	27°	SH	10.5	72°	- .06
ESK	33°	SH	10.4	78°	- .07
LOR	36°	SH	10.2	81°	- .09
MAL	48°	SH	10.3	87°	- .09
WES	62°	P	12.3	73°	.09
WES	62°	SH	9.8	73°	- .13
OGD	64°	P	9.9	71°	- .12
OGD	64°	SH	9.3	71°	- .17
SCP	65°	P	11.1	70°	- .01
SCP	65°	SH	8.3	70°	- .26
NAT	100°	P	11.8	35°	.05
BOG	117°	P	18.4	18°	.64
BHP	117°	P	10.0	18°	- .11
LPB	129°	P	11.6	6°	.03
LPB	129°	SH	9.0	6°	- .20

Table 6.1 - continued

Stn.	Azimuth from North	Wave Type	Moment x 10^{-25} dyne-cm	ϕ	Relative Deviation of M_o from Average
ARE	132°	P	15.0	3°	.34
ARE	132°	SH	7.1	3°	- .37
NNA	133°	P	12.9	2°	.15
NNA	133°	SH	6.4	2°	- .43
LPA	136°	SH	9.5	1°	- .16
PEL	142°	SH	8.8	7°	- . 22

Av = 11.2

σ = 2.8

parameters. If the source is to be considered as a sum of point sources, the same parameters as well as a relative size, time and location must be specified for each additional source. The origin time and epicentral location of the primary source are assumed to be known quantities, and its absolute size need not be specified if only relative wave shapes are considered. In order to obtain an adequate fit to the Borrego Mountain data, it was necessary to use a sum of three sources. This made a total of 20 parameters and three time functions which had to be specified to compute the synthetics.

The problem of parameterizing a time function can be approached in two ways. The first is to directly parameterize some pulse-like function and assume that it is independent of azimuth. The second is to use a finite source model. The free parameters in a finite source are usually the rupture velocity and average dislocation time on a failure surface with some assumed geometry. The time pulse for such a model is a function of both azimuth and takeoff angle (Fukao, 1971; Savage, 1966). The approach used in this study was to begin with a simple, azimuthally independent pulse. After an optimal model was obtained, the synthetics were compared with the data to test for any evidence which might justify an azimuthally dependent model. The azimuthally independent pulse shape chosen was a triangular pulse requiring only two parameters: a zero-to-peak time and a peak-to-zero time.

It was also necessary at the outset of the inversion procedure to choose a near-source and near-receiver earth structure. Again the decision was made to start with the simplest possible assumptions,

but to continuously test for any features in the data which would justify a more complex model. More specifically, at the beginning only the rays P, pP and sP (or S and sS) were computed. At several points, however, the strongest rays generated by the near-source structure proposed by Hamilton (1972) and the near-receiver structure discussed by Burdick and Helmberger (1974) were also included. No effects which could be unambiguously attributed to layered structure near the source or receiver were ever identified, so throughout this study only the five basic rays were used to compute the synthetics.

The inversion method used differs somewhat from the method described in Chapter 5. Rather than using analytic derivatives, finite difference estimates of the derivatives were used. For better accuracy, symmetric differences were used. Only linear terms were included. Stability was provided by eigenvalue damping and by use of a partial step method. A one-dimensional search was used to minimize the error function along the direction of the iterative solution.

In point of time, the Borrego Mountain inversion preceded the structure inversion. In fact, it was largely through experience with the linearized source inversion that the need for inclusion of non-linear terms became apparent, even though, through use of differences some non-linear effects were taken into account.

The initial attempts at inversion were made using a single point source model. The top two traces of Figure 6.3 illustrate the results for a typical seismogram. It was clear that, although the model was adequate for the first few seconds, there was much more structure

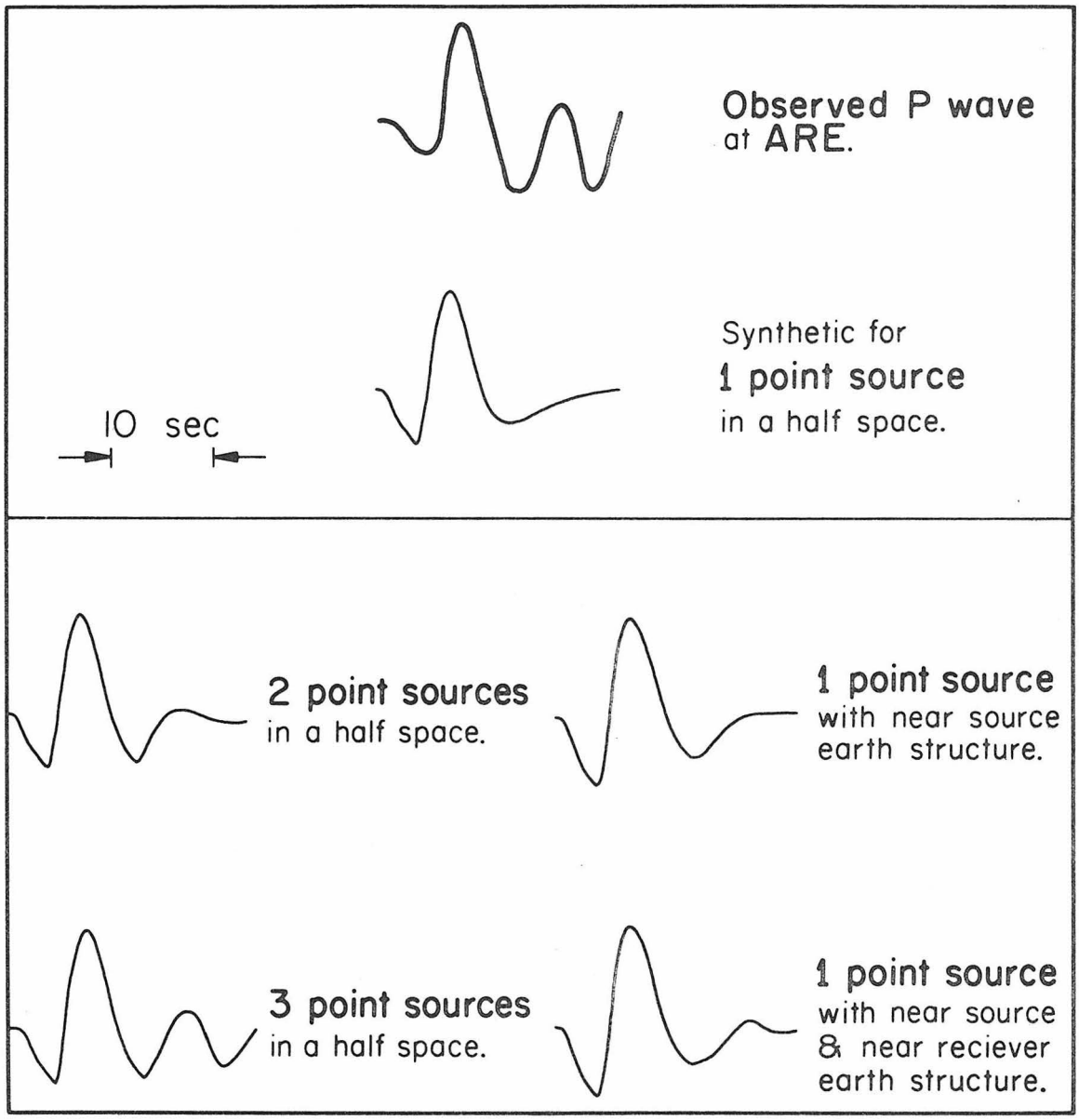

Figure 6.3. The top of the figure shows that a single point source can not account for the structure late in the seismogram. The left column shows that it is possible to obtain a better fit by adding in additional point sources while the right shows that inclusion of the rays generated by the near source crustal structure (Hamilton, 1972) and an appropriate near receiver structure does not.

present in the later portion of the seismogram than was predicted by the synthetic. This could have been the result of either a complicated earth structure or a more complicated source mechanism. On the right in the third row of Figure 6.3 is shown the synthetic including the effects of assuming that the Hamilton (1972) crust model exists near the source, and on the left is the result of including a second point source. In the lowest row, the result of including three point sources is shown as opposed to including both the near-source and near-receiver crustal effects (see Table 6.2). The effects of introducing appropriate earth structure were always too small to explain the discrepancies between the synthetics for a one source model and the observations. We concluded that the structure late in the waveforms was probably caused by the first large aftershocks. We attempted to model the first two with additional point sources.

The previously published mechanism for the Borrego main shock was used as a starting model for the single point-source inversion runs. When it became apparent that a multiple point-source model would be necessary, the seismograms were examined to determine the time when the data first began to diverge from its predicted behavior. A new point source was postulated to have occurred at that time. It was intiially presumed to have had the same location as the main shock. The space of possible fault plane solutions for the second source was then explored by trial and error using a crude spacing between models. Synthetics were computed for only a few key observations. When a roughly satisfactory model had been determined, the inversion procedure was used to iterate in on a more refined model for the location, time,

Table 6.2

VELOCITY MODELS

Half Space Model

Layer	V_p $(\frac{km}{s})$	V_s $(\frac{km}{s})$	ρ $(\frac{g}{cc})$	Th (km)	$(\frac{T}{Q_\alpha})$ av	$(\frac{T}{Q_\beta})$ av
1	6.1	3.5	2.7	∞	1.3	5.2

Hamilton Crustal Model

1	2.5	1.6	1.4	.4
2	5.1	3.0	2.3	2.5
3	6.0	3.5	2.7	11.1
4	7.1	4.2	3.2	11.0
5	7.9	4.6	3.6	∞

Near Receiver Crustal Model

1	6.28	3.63	2.87	37
2	7.96	4.60	3.37	∞

time function and fault-plane solution of the shock. The same procedure was used on the second aftershock. We stress that there can be no way of insuring that the models found by this method are in any way unique. However, as we shall show, they do predict the fine details of the observed waveforms very closely. Also, we can state that in our rough search of the model space we did not find any other model which came nearly as close to predicting the data as the one presented in the following section.

THE FINAL MODEL

In the second row of Figure 6.5 are the synthetic wave forms for the final model. Those arrivals which are marked are the direct arrivals and the primary reflections from the main shock. The later complications in the waveform are caused by the later shocks. The wide variety in the appearance of the secondary structure provides an additional indication that it is a manifestation of source and not crustal complexity. A strong arrival from a sharp layer always arrives at nearly the same point on the record and generally varies slowly as a function of azimuth; but a secondary source predicts three arrivals, P, pP and sP whose interaction can vary rapidly with azimuth. The final source locations, time functions and fault planes used in computing the synthetics are shown in Figures 6.1 and 6.4.

Given that structure-generated arrivals on the order of those shown in Figure 6.3 have been neglected, the fit to the data appears most satisfactory. For each peak in the data, there is a corresponding peak of the right duration and sign in the synthetics. The worst fits both

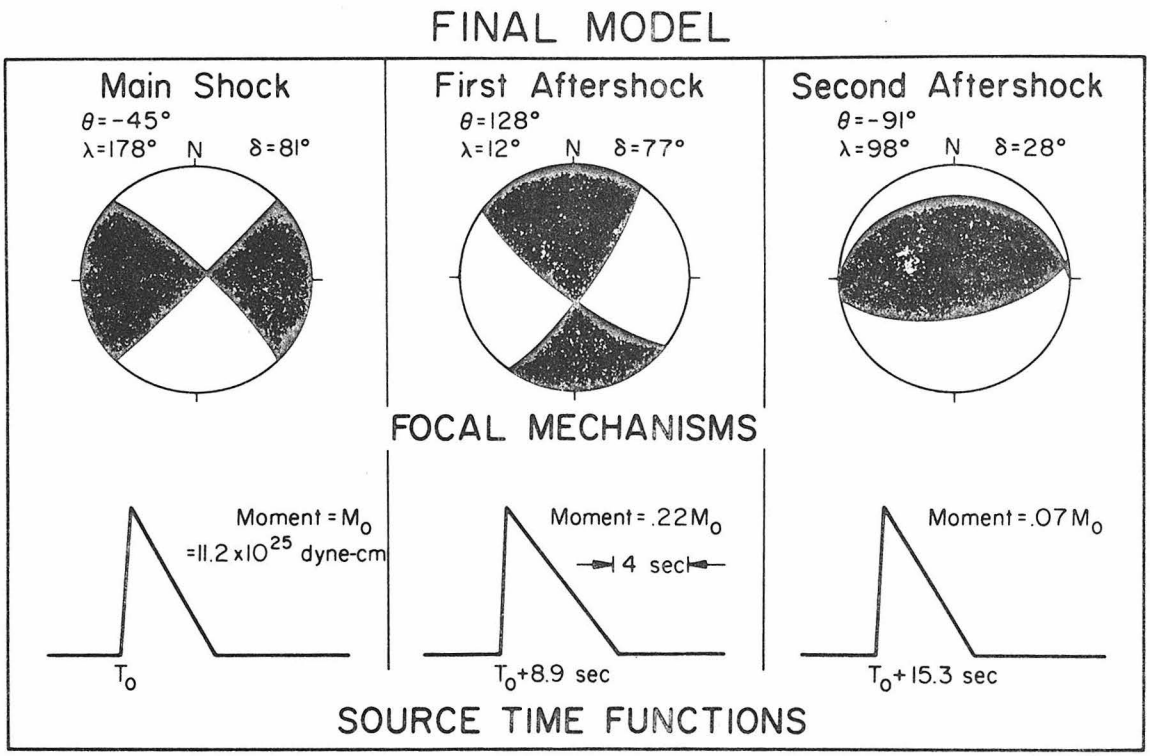

Figure 6.4. The fault plane solutions and the time functions of the main shock and the first two aftershocks. The shaded portions of the circles represent the compressional quadrants. The fault orientation parameters have been defined in Langston and Helmberger (1975).

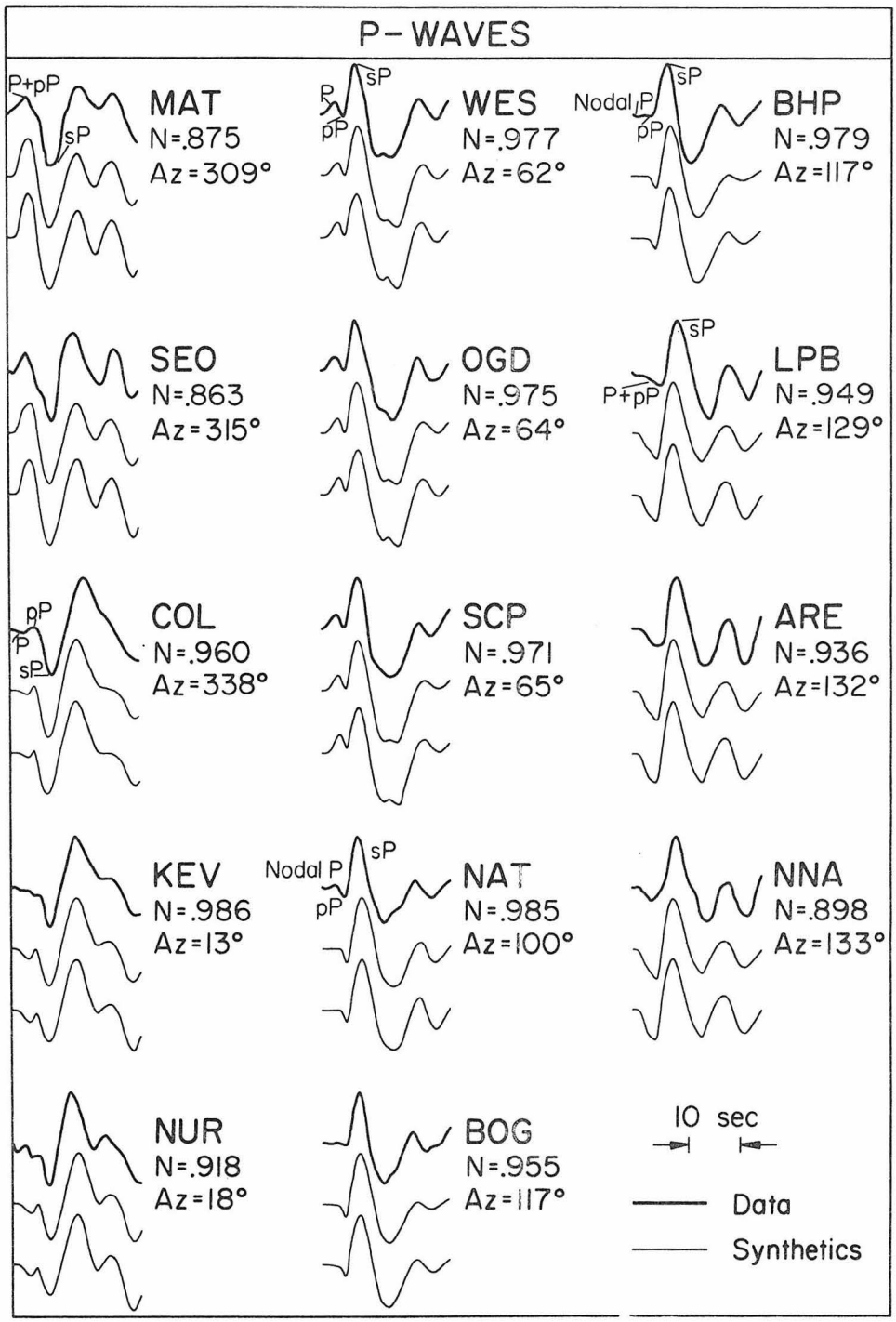

Figure 6.5a. The observed P waves (top) predicted by the final (3 point sources with azimuthally independent time functions) model (middle) and the synthetics predicted by the same model with the main shock represented by a finite (azimuthally dependent time function) source model (bottom). The quantity N_i is the normalized correlation operator which uniquely approaches 1 as the synthetic approaches the data. The azimuths are measured from North.

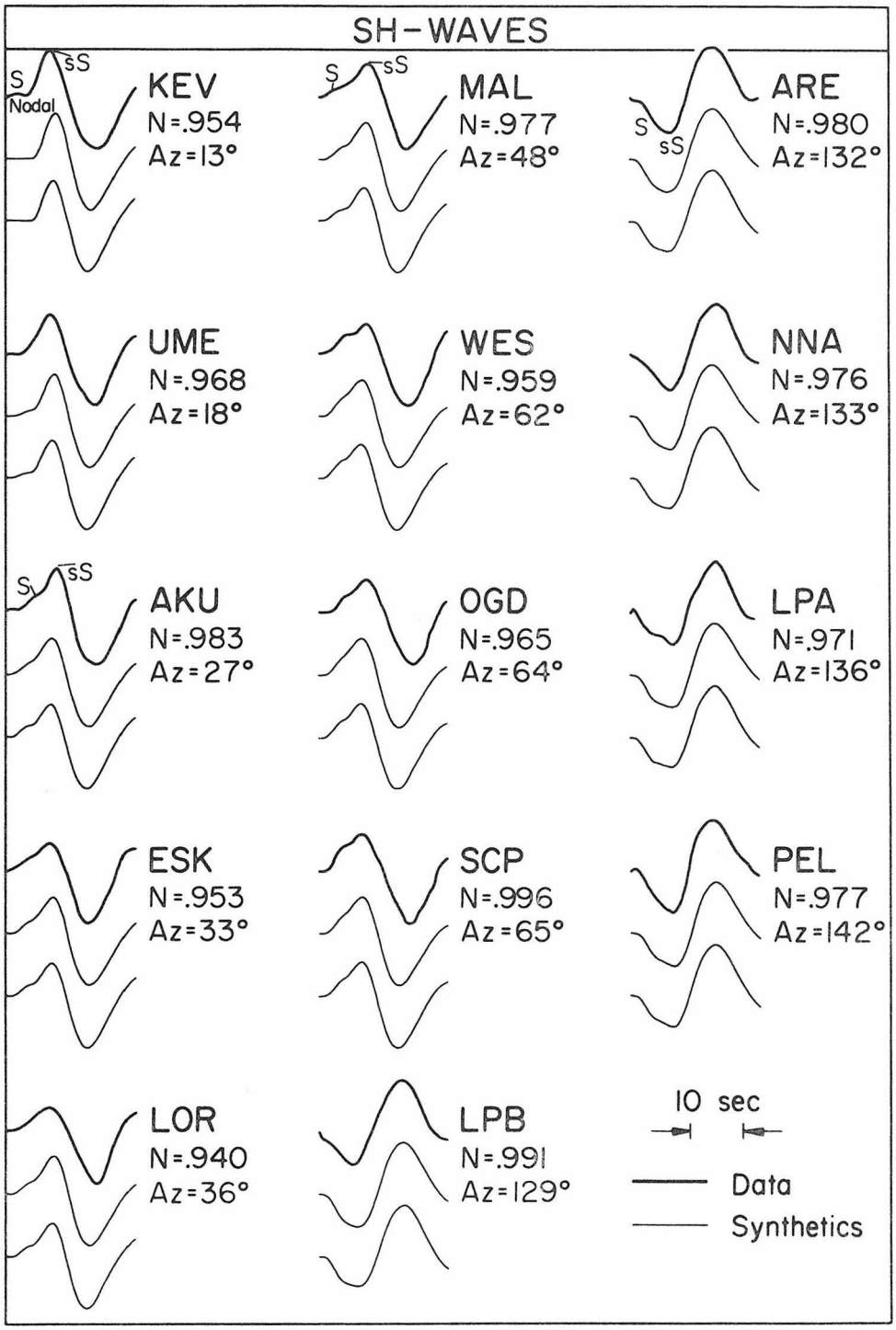

Figure 6.5b. The observed SH waves (top) predicted by the final model (middle) and the synthetics predicted by the same model with the main shock replaced by a finite source model. The labeled arrivals in both Figure 6.5a and 6.5b are from the main shock. In both figures, the stations are shown in order of increasing azimuthal deviation from the NW extension of the fault trace (see Figure 6.2).

in terms of visual appearance and the correlation N_1 occur for the P waveforms at stations where P and pP arrive with the same polarity. These include MAT, SEO, LPB, ARE and NNA. Their common feature is that they lie off the very ends of the fault trace. They are composed of rays which travel directly along the fault plane (see Figure 6.2). As Figure 6.5 shows, the difficulty is that the predicted ratio of the peaks sP/(p+pP) is too small with respect to the observed values. There is no way to determine whether this occurs because of anomalously large S or anomalously small (P+pP) without the use of absolute amplitude measurements.

A value for M_o, the seismic moment of the first source, can be determined from a measurement of the absolute amplitude at each station by use of the formula

$$M_o = \frac{A_{observed}}{A_1}$$

$A_{observed}$ is the observed amplitude of either the sP or the S+sP peak and A_1 is the theoretical amplitude of the same peak for an event with moment one. The moment values determined from the 28 observations used in the inversion are listed in Table 6.1. They have an average value of 11.2×10^{25} dyne-cm and a standard deviation of 2.8×10^{25} dyne-cm. The relative errors between the amplitude computed assuming the average moment and the observed amplitude are plotted against an azimuthal angle in Figure 6.6. This angle is defined to be zero for stations directly off either end of the fault and to have a maximal value of 90 for stations in a direction perpendicular to the fault. The observed values of sP tend to be too large and the observed values

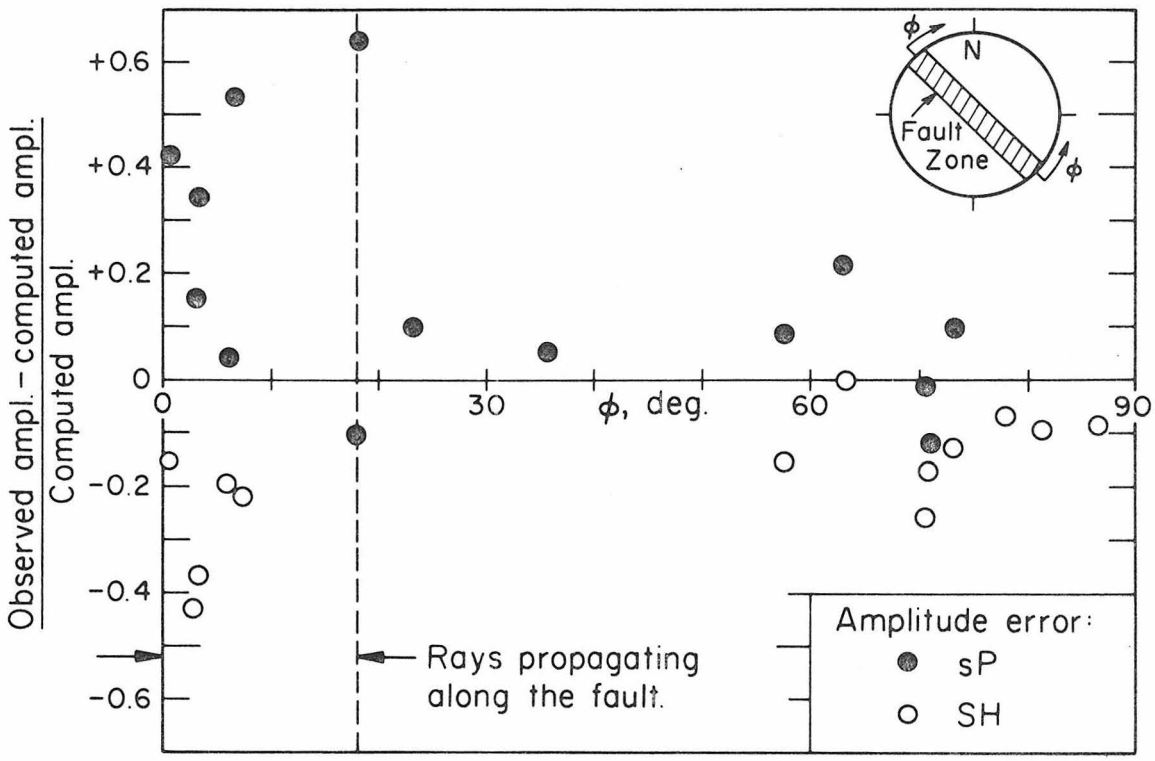

Figure 6.6. The dependence of the scatter in the amplitude data on the azimuthal angle ϕ which is defined so that it becomes small whenever rays propagate along the fault zone. The final model can predict observed amplitudes to within 25% except at stations with low values of ϕ.

of S+sS too low whenever those rays travel directly along the fault zone. It is important to note that most of the tectonic features in the region also trend parallel to the fault. The implication is that the ratio of the amplitudes of SV to SH is sensitive to the lateral variations induced by the fault itself or by some other tectonic feature. Since the sP phase is often the dominant one in the far-field P wave form, this instability may be responsible for anomalies in P-wave shape and amplitude as well as in the S.

The fault plane determined for the main shock (Figure 6.4) is virtually identical to the one determined from the first-motion data by Allen and Nordquist (1974). The strike of the northwest-trending plane corresponds closely with the strike of ground breakage, and the motion indicated by the conjugate plane corresponds with most of the observed offsets. There can be little doubt that the northwest plane is highly representative of the actual plane of failure. Because of the information in the body waves about the separation of P, sP and pP, the depth can be constrained to be between 7 and 9 km.

The second shock was apparently a left-lateral, strike-slip event occurring 9 sec after the first. The location is very poorly constrained, since it did not occur far enough away from the main shock to cause obvious azimuthal dependence in its arrival time (Figure 6.1). As shown in Figure 6.4, it seems to have released a stress nearly reversed to that of the main shock. There are several indications from other types of data that such an event might have occurred. First, there were observations of ground displacement near point B with a left lateral component which was clearly not of the

Reidel type (Clark, 1972). Second, there are the previously cited lines of evidence which suggest complex prestress and stress release patterns in which reversed stresses might easily have developed. Sharp (1972) mentions several instances where left-lateral strain buildup had been reported in the region in the past. Finally, studies by Burridge (1969) and Madariaga (1976) have shown that it is theoretically possible for reversed or overshoot-type stresses to develop even in relatively simple cases.

The third shock which occurred approximately 15 sec after the first was a thrust event (Figure 6.4). This mechanism is consistent with the stress pattern which induced the first event in that the major axis of compression is roughly similar. The location is again very poorly constrained by the far-field data, but it appears that the shock occurred near point C in Figure 6.1. The surface break takes a sudden step to the left and shows an abrupt decrease in total offset at this point. Also, one of the later aftershocks which occurred there was a thrust event with a mechanism similar to this one (Hamilton, 1972). These are the first of several correlations that were found between details of the postseismic observations and the final source model. The second shock had a moment only a quarter as large as the first, and the third less than a tenth of the first. Since they were much smaller, they had a relatively minor effect on the waveform and on the surface break. In effect, they are nothing more than the first and second aftershocks. The first event which radiated the most energy determined the first motions and the gross features of both the waveforms and the ground breakage.

A FINITE SOURCE MODEL

We return now to the initial question of what type of finite source model is appropriate for shallow earthquakes. We will attempt to model the first source since it was the largest. Figure 6.5 shows that it would be difficult to separate the direct P pulse from the pP or the S from the sS. The sP, however, is strong enough to be relatively clear on the record. We present here an attempt to determine a model which fits the characteristics of that one phase. Then we use the model to compute the complete seismograms for comparisons with the data and the inversion result.

Several different techniques were used to attempt to find azimuthal dependence in the duration of the sP pulse as was done for P waves from deep earthquakes by Mikumo (1971a,b). No clear azimuthal pattern was resolved by any of these means. The effect is apparently too small to be seen over the noise level. Any inferences to be made about the finiteness of the source will have to come from the shape or frequency content of the time function. This type of analysis requires a better estimate of the shape of the source-time function than the crude result from the inversion. A much better determination was obtained by making use of the high quality recording from WES. At this station, both the long- and short-period recordings were strong, clear and virtually free of noise. As illustrated in Figure 6.7, a time function was obtained by a simultaneous deconvolution technique which could be reconvolved with either the short- or long-period instrument to reproduce the data. The deconvolution technique consists of transforming equivalent segments of the long-period and short-period records into the frequency domain,

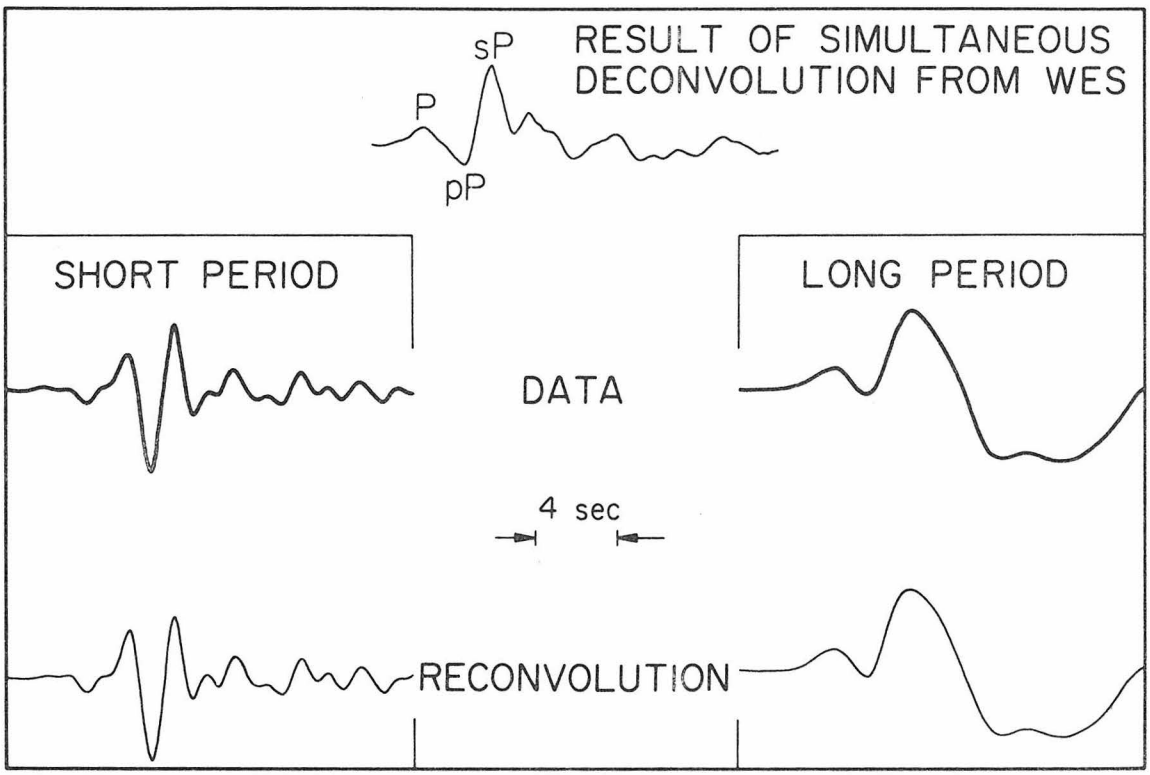

Figure 6.7. (Top) A time function which is compatible with both the long period and short period records from WES. It was obtained by Fourier transforming both records (middle traces), dividing out the instrument and Q filter from each, taking a weighted average of the results and inverse transforming. When the top trace is reconvolved with the appropriate instrument and Q filter from each, taking a weighted average of the results and inverse transforming. When the top trace is reconvolved with the appropriate instrument and Q it produces the bottom traces.

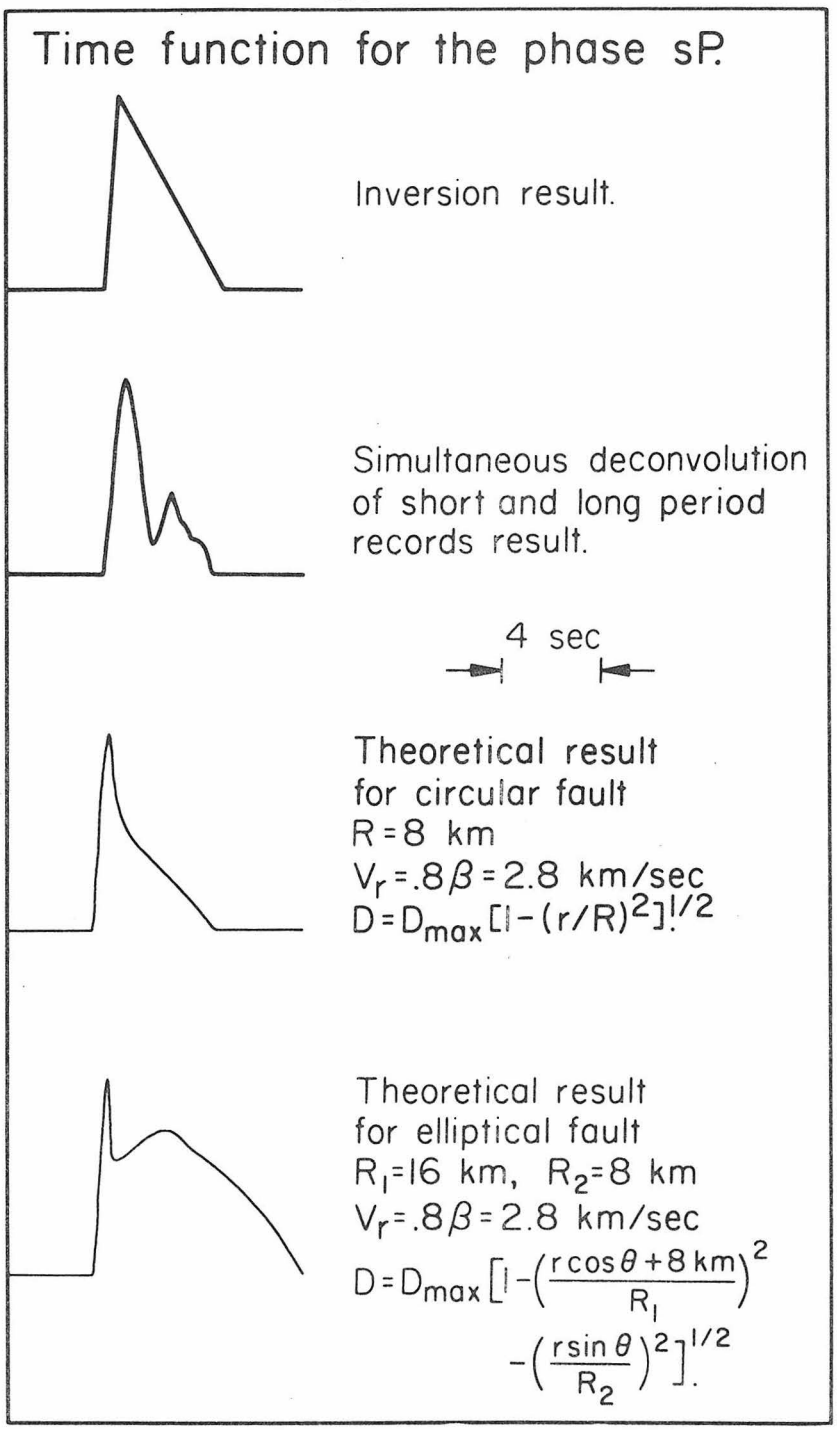

Figure 6.8. sP time functions for the station WES obtained from inversion and simultaneous short period-long period deconvolution as opposed to theoretical results for a circular fault large enough to extend over segment BC in Figure 1 and on elliptical fault large enough to cover BD. D_{max} is the maximum displacement, and r and θ are cylindrical coordinates on the fault surface. The average time history for the theoretical models is a step function.

dividing each by the appropriate instrument and Q responses, weighting, averaging, and inverse transforming. The weighting function for the long-period instrument was equal to one for frequencies less than 0.25 Hz, and it fell off linearly from that frequency to zero at 0.5 Hz. The short-period weighting function was just one minus the long-period function. A correction was made for any difference in reference time between the two record segments by solving for the pure phase delay which made the long-period record's phase curve most like that of the short-period in the crossband of 0.25 to 0.50 Hz. The portion of the deconvolved time function which is dominated by the first source sP is compared with the inversion result in Figure 6.8.

The deconvolution result bears a strong resemblance to the time function for a circular fault published by Savage (1966). The third trace in Figure 6.8 is the theoretical time function for a circular rupture propagating on the fault plane at 2.8 km/sec (0.8 β) to a final radius of 8 km. The dislocation-time history is assumed to be a step and the final offset is assumed to die off as $(1-(r/R)^2)^{1/2}$. Figure 6.1 shows that this would correspond to a rupture beginning at the hypocenter, propagating up to the surface, and downward by an equal amount, northwest to point B and southeast only to point C. The time function for an ellipsoidal fault surface extending all the way down to point D is too long in duration to be compatible with the inversion or deconvolution result as shown at the bottom of Figure 6.8. The implication is that segment CD did not contribute significantly to the energy in the body-wave pulse. If the rupture velocity had been assumed to be β instead of 0.8 β, the fault radius would only have had

to be increased to 9 km to keep the pulse duration the same. Therefore, this result is not dependent on the assumed rupture velocity. There is abundant evidence in the postseismic observations that the two segments behaved in different fashions. The more southern segment showed a much smaller initial offset, extensive postseismic creep, and a higher level of aftershocks. We infer that the southern segment initially absorbed most of the stress load induced by the brittle failure of the north segment but then released it slowly. Some failure must have occurred sometime in the first few hours to account for the initial surface offset observations, but the creep movement extended over a period of months. It seems as though the southern portion of the Borrego event was very similar to the nearby Brawley swarm event studied by Johnson and Hadley (1976).

It should be noted that we are not including in our calculations the correction for the fact that the two sides of the fault have a finite slip velocity. One approximate way to do this would be to convolve a boxcar of roughly the same duration as the average slip time with the theoretical pulses. The total rupture time would have to be decreased by a corresponding amount to keep the total duration of the pulse consistent with the observations. This would mean that the estimated radius would be even smaller. In this sense, the value of 8 km should be considered as an upper bound.

The complete synthetic seismograms predicted by the finite source model are the bottom traces in Figure 6.5. They appear to fit just as well as the ones computed from the point source model. The predicted azimuthal dependence of pulse duration is very slight which explains

why this effect was so difficult to observe in the data.

Assuming that the first shock had a moment of 11.2×10^{25} dyne-cm and a radius of about 8 km, and if μ was approximately 3.4×10^{11} gm/cm sec^2 then the average displacement must have been

$$D_{av} = \frac{M_o}{\mu \pi R^2} = 164 \text{ cm.}$$

This value is four times as large as the observed surface offsets implying that the displacements decreased as the rupture propagated upward. Since for the theoretical model considered here, displacement varies along the fault as $D = D_{max} (1-(r/R)^2)^{1/2}$, the largest displacement was

$$D_{max} \sim 3/2 \; D_{av} = 246 \text{ cm.}$$

Keilis-Borok (1959) has formulated an expression for the stress-drop from a dislocation of this type.

$$\Delta\sigma = \frac{7\pi}{24} \frac{D_{max}}{R} \mu$$

assuming that $\lambda = \mu$. This gives a stress drop of $\Delta\sigma = 96$ bars. Kanamori and Anderson (1975) have compiled a list of stress-drop determinations for a large number of earthquakes. The values scatter between 10 and 100 bars, so the Borrego Mountain earthquake falls within the range of previous determinations. However, they have noted that most interplate earthquakes fall toward the low end of the range. In this sense, the event is somewhat anomalous. It remains to be seen whether other earthquakes also give higher values of $\Delta\sigma$ when analyzed using the techniques used in this study.

CONCLUSIONS

The purpose of this study was twofold. The first was to identify and characterize all of the different elements which control the shape of the body waves from a shallow earthquake. The second was to isolate an arrival which was not strongly contaminated by other arrivals and to model this single arrival with a finite dislocation source. In pursuing the first of these, we found that reflections from the free surface play a dominant role in shaping the pulse, but also that arrivals from the first large aftershocks could be observed in the wave form. This result is not too remarkable since there is no reason to expect a long delay between the termination of the main shock and the initiation of the aftershock sequence. In pursuing the second goal, we decided to construct a model for the sP phase from the main shock. A smooth dislocation proved to be adequate to model the pulse just as in the case of most deep earthquakes.

The fault parameters of the Borrego Mountain event were previously determined using the spectral characteristics technique by Hanks and Wyss (1972) and by Wyss and Hanks (1972a). They analyzed the P and S data separately which gave two different values for each parameter. Their moment values of $M_o(P) = 10 \times 10^{25}$ dyne-cm and $M_o(S) = 6.6 \times 10^{25}$ dyne-cm compare favorably with the value from this study of 11.2×10^{25} dyne-cm. However, this agreement is probably fortuitous, since the moments they determined were based on the long-period level Ω_o of the amplitude spectrum of the entire P or S waveforms. This means that they interpreted the sum $\Omega_o(P) + \Omega_o(pP) + \Omega_o(sP)$ as though it were only $\Omega_o(P)$ and the sum $\Omega_o(S) + \Omega_o(sS) + \Omega_o(pS)$ as though it were

only $\Omega_o(S)$. Their values for the fault radius, R(P) = 14 km and R(s) = 23 km are significantly larger than the R = 8 km result of this study. Therefore, they computed a stress drop $\Delta\sigma$ of only 6 bars as compared to the $\Delta\sigma$ = 96 bars result obtained here. It is encouraging that when the free surface is properly accounted for, it is not necessary to use different source parameters for S and P.

The relatively small value of R = 8 km was chosen to give an appropriate fit to the shape and duration of the observed sP pulse. As we have discussed, an 8-km fault radius does not conflict with the postseismic observations, if the CD segment of the fault is assumed to be a creep or swarm event. If this analysis is correct, it means that it is necessary to be cautious about inferring fault dimensions from rupture lengths or aftershock zones.

Finally, we have demonstrated the adequacy of a shallow double-couple point-source model in predicting wave shapes. The only breakdowns occur when observations are made near nodes. One of the mechanisms of breakdown is apparently instability in the polarization of the S motion induced by lateral structure. Since sP sometimes dominates the P wave form, this can cause anomalies in the P waves as well as the S waves.

REFERENCES

Allen, C. R. and Nordquist, J. M. (1972). Foreshock, main shock and larger aftershocks of the Borrego Mountain earthquake, U. S. Geol. Survey Prof. Paper 787, 16-23.

Allen, C. R. et al. (1972). Displacements on the Imperial, Superstition Hills and San Andreas faults triggered by the Borrego Mountain earthquake, U. S. Geol. Survey Prof. Paper 787, 87-104.

Backus, G. and Gilbert, F. (1967). Numerical applications of a formalism for geophysical inverse problems, Geophys. J. R. astr. Soc., 13, 247-276.

Bessonova, E. N., Fishman, V. M., Ryaboyi, V. Z. and Sitnikova, G. A. (1974). The tau method for inversion of travel times, Geophys. J. R. astr. Soc., 36, 377-398.

Burdick, L. J. and Helmberger, D. V. (1974). Time functions appropriate for deep earthquakes, Bull. Seism. Soc. Am., 64, 5, 1419-1428.

Burdick, L. J. and Mellman, G. R. (1976). Inversion of the body waves from the Borrego Mountain earthquake to the source mechanism, Bull. Seism. Soc. Am., 66, 1485-1499.

Burford, R. O. (1972). Continued slip on the Coyote Creek Fault after the Borrego Mountain earthquake, U. S. Geol. Survey Prof. Paper 787, 105-111.

Burridge, R. (1969). The numerical solution of certain integral equations with nonintegrable kernels arising in the theory of crack propagation and elastic wave diffraction, Phil. Trans. Roy. Soc. (London) Ser. A. 265, 353-381.

Chapman, C. H. (1973). The earth flattening approximation in body wave theory, Geophys. J. R. astr. Soc., 35, 55-70.

Chapman, C. H. (1974). Generalized ray theory for an inhomogeneous medium, Geophys. J. R. astr. Soc., 36, 673-704.

Chapman, C. H. (1976). Exact and approximate generalized ray theory in vertically inhomogeneous media, Geophys. J. R. astr. Soc., 46, 201-234.

Clark, M. M.,(1972). Surface ruptures along the Coyote Creek Fault, U. S. Geol. Survey Prof. Paper 787, 55-86.

Davies, M. and Whitting, I. J. (1972). A modified form of Levenberg's correction, in Numerical Methods for Non-Linear Optimization, F. A. Lootsma (ed.), Academic Press, New York.

de Hoop, A. T. (1960). A modification of Cagniard's method for solving seismic pulse problems, Appl. Sci. Res. B., 8, 349-356.

Fuchs, K. and Muller, G. (1971). Computation of synthetic seismograms with the reflectivity method and comparison with observations, Geophys. J. R. astr. Soc., 23, 417-433.

Fukao, Y. (1971). Seismic body waves from surface faults, J. Phys. Earth, 19, 4, 271-281.

Futterman, W. I. (1962). Dispersive body waves, J. Geophys. Res., 67, 5279-5291.

Gilbert, F. and Knopoff, L. (1961). The directivity problem for a buried line source, Geophysics, 26, 626-634.

Hamilton, R. M. (1972). Aftershocks of the Borrego Mountain earthquake from April 12 to June 12, 1968, U. S. Geol. Survey Prof. Paper 787, 31-54.

Hanks, T. C. and Wyss, M. (1972). The use of body-wave spectra in the determinationof seismic-source parameters, Bull. Seism. Soc. Am., 62, 2, 561-589.

Helmberger, D. V. (1968). The crust mantle transition in the Bering Sea, Bull. Seism. Soc. Am., 58, 179-214.

Helmberger, D. V. (1973). Numerical seismograms of long period body waves from seventeen to forty degrees, Bull. Seism. Soc. Am., 63, 633-646.

Helmberger, D. V. (1974). Generalized ray theory for shear dislocations, Bull. Seism. Soc. Am., 64, 1, 45-64.

Helmberger, D. V. (1976). Fine structure of an Aleutian crustal section, Geophys. J. R. astr. Soc., 48, 81-90.

Hudson, J. A. (1969). A quantitative evaluation of seismic signals at teleseismic distances. I. Radiation from point sources, Geophys. J. R. astr. Soc., 18, 233-249.

Johnson, C. E. and Hadley, D. M. (1976). Tectonic implications of the Brawley earthquake swarm, Imperial Valley, California, January 1975, Bull. Seism. Soc. Am., 66, 1133-1144.

Johnson, L. E. and Gilbert, F. (1972). Inversion and inference for teleseismic ray data; in Methods of Computational Physics, 12, Seismology: Body Waves and Sources, B. Adler et al. (eds.) Academic Press, New York.

Jordan, T. H. and Franklin, J. N. (1971). Optimal solution to a linear inverse problem in geophysics, Proc. Nat. Acad. Sci., 68, 291.

Kanamori, H. and Anderson, D. L. (1975). Theoretical basis of some emp empirical relations in seismology, Bull. Seism. Soc. Am., 65, 5, 1073-1095.

Keilis-Borok, V. (1959). On estimation of displacement in an earthquake source and of source dimensions, Ann. Geofis. (Rome), 12, 205-214.

Langston, C. A. and Helmberger, D. V. (1975). A procedure for modeling shallow dislocation sources, Geophys. J. R. astr. Soc., 42, 117-130.

Levenberg, K. (1944). A method for the solution of certain non-linear problems in least squares, Q. appl. Math., 2, 164-168.

Madariaga, R. (1976). Dynamics of an expanding circular fault, Bull. Seism. Soc. Am., 66, 639-666.

Mellman, G. R. and Helmberger, D. V. (1978). A modified first motion approximation for the synthesis of body wave seismograms, Geophys. J. R. astr. Soc., 54, 129-140.

Mikumo, T. (1971a). Source processes of deep and intermediate depth earthquakes as inferred from long period P and S waveforms, I, J. Phys. Earth, 19, 1, 1-19.

Mikumo, T. (1971b). Source processes of deep and intermediate earthquakes as inferred from long period P and S waveforms II, J. Phys. Earth, 19, 303-320.

Minster, J. B., Jordan, T., Molnar, P. and Haines, E. (1974). Numerical modeling of instantaneous plate tectonics, Geophys. J. R. astr. Soc., 36, 541-576.

Molnar, P. and Wyss, M. (1972). Moments, source dimensions and stress drops of shallow focus earthquakes in the Tonga-Kermadec Arc, Phys. Earth Planet. Int., 6, 263-278.

Molnar, P., Tucker, B. E. and Brune, J. N. (1973). Corner frequencies of P and S waves and models of earthquake sources, Bull. Seism. Soc. Am., 63, 6, 2091-2104.

Osborne, M. R. (1972). Some aspects of non-linear least squares calculations, in Numerical Methods for Non-linear Optimization, F. A. Lootsma (ed.), Academic Press, New York.

Parker, R. L. (1970). The inverse problem of electrical conductivity in the mantle, Geophys. J. R. astr. Soc., 32, 121-138.

Roberts, S. M. and Livers, H. I. (1961). The gradient method in process control, Indust. and Eng. Chem., 53, 877-882.

Savage, J. C. (1966). Radiation from a realistic model of faulting, Bull. Seism. Soc. Am., 56, 2, 577-592.

Sharp, R. V. (1972). Tectonic setting of the Salton Trough, U. S. Geol. Survey Prof. Paper 787, 3-15.

Shor, G., Jr. (1964). Structure of the Bering Sea and the Aleutian Ridge, Marine Geol., 1, 213-219.

Stump, B. and Johnson, L. R. (1977). The determination of source properties by the linear inversion of seismograms, Bull. Seism. Soc. Am., 67, 6, 1489-1502.

Teng, T. L. and Ben-Menahem, A. (1965). Mechanism of deep earthquakes from spectrums of isolated body wave signals, J. Geophys. Res., 70, 20, 5157-5170.

Wiggins, R. A. and Helmberger, D. V. (1973). Upper mantle structure of the western United States, J. Geophys. Res., 78, 1870-1880.

Wiggins, R. A. (1976). Body wave amplitude calculations II, Geophys. J. R. astr. Soc., 46, 1-10.

Wyss, M. and Hanks, T. C. (1972a). The source parameters of the San Fernando earthquake inferred from teleseismic body waves, Bull. Seism. Soc. Am., 62, 2.

Wyss, M. and Hanks, T. C. (1972b). Source parameters of the Borrego Mountain earthquake, U. S. Geol. Survey Prof. Paper 787, 24-30.

APPENDIX

For ease of reference, we quote a result from Langston and Helmberger (1975). They show that, in the first motion approximation, the displacement potentials for a shear dislocation are given by

$$\phi = \frac{M_o}{4\pi\rho} \sum_{j=1}^{3} A_j\ (\theta,\lambda,\delta) C_j \frac{H(t-R/\alpha)}{R}$$

$$\Omega = \frac{M_o}{4\pi\rho} \sum_{j=1}^{3} A_j\ (\theta,\lambda,\delta)\ SV_j \frac{H(t-R/\beta)}{R}$$

$$\chi = \frac{M_o}{4\pi\rho} \sum_{j=1}^{2} A_{j+3}\ (\theta,\lambda,\delta)\ SH_j \frac{H(t-R/\beta)}{R}$$

$C_1 = -p^2$ $\qquad$ $SV_1 = \varepsilon p \eta_\beta$ $\qquad$ $SH_1 = 1/\beta^2$

$C_2 = 2\varepsilon p \eta_\alpha$ $\qquad$ $SV_2 = \eta_\beta^2 - p^2$ $\qquad$ $SH_2 = -\varepsilon/\beta^2\ \eta_\beta/p$

$C_3 = p^2 - 2\eta_\alpha^2$ $\qquad$ $SV_3 = 3\varepsilon p \eta_\beta$

$\varepsilon = +1 \quad z > h$

$\varepsilon = -1 \quad z < h$

$A_1 = \sin 2\theta \cos\lambda \sin\delta + 1/2 \cos 2\theta \sin\lambda \sin 2\delta$

$A_2 = \cos\theta \cos\lambda \cos\delta - \sin\theta \cos\lambda \cos 2\delta$

$A_3 = 1/2 \sin\lambda \cos 2\delta$

$A_4 = \cos\theta \cos\lambda \sin\delta - 1/2 \sin 2\theta \sin\lambda \sin 2\delta$

$A_5 = -\sin\theta \cos\lambda \cos\delta - \cos\theta \sin\lambda \cos 2\delta$

and

θ = strike angle from end of fault

λ = rake angle

δ = dip angle

α = p-wave velocity at source

β = s-wave velocity at source

ρ = density at source

M_o = seismic moment

p = ray parameter

$$H(t) = \begin{cases} +1 & t > 0 \\ 0 & t < 0 \end{cases}$$